Quarterly Reviews of Biophysics **36**, 4 (2004), pp. 373–427. © 2004 Cambridge University Press
DOI: 10.1017/S0033583504003932 Printed in the United Kingdom

Metal ion effects on ion channel gating

Fredrik Elinder and Peter Århem*

Department of Neuroscience, The Nobel Institute for Neurophysiology, Karolinska Institutet, Retzius väg 8, SE-171 77 Stockholm, Sweden

Abstract. Metal ions affect ion channels either by blocking the current or by modifying the gating. In the present review we analyse the effects on the gating of voltage-gated channels. We show that the effects can be understood in terms of three main mechanisms. Mechanism A assumes screening of fixed surface charges. Mechanism B assumes binding to fixed charges and an associated electrostatic modification of the voltage sensor. Mechanism C assumes binding and an associated non-electrostatic modification of the gating. To quantify the non-electrostatic effect we introduced a slowing factor, *A*. A fourth mechanism (D) is binding to the pore with a consequent pore block, and could be a special case of Mechanisms B or C. A further classification considers whether the metal ion affects a single site or multiple sites. Analysing the properties of these mechanisms and the vast number of studies of metal ion effects on different voltage-gated ion channels we conclude that group 2 ions mainly affect channels by classical screening (a version of Mechanism A). The transition metals and the Zn group ions mainly bind to the channel and electrostatically modify the gating (Mechanism B), causing larger shifts of the steady-state parameters than the group 2 ions, but also different shifts of activation and deactivation curves. The lanthanides mainly bind to the channel and both electrostatically and non-electrostatically modify the gating (Mechanisms B and C). With the exception of the ether-à-go-go-like channels, most channel types show remarkably similar ion-specific sensitivities.

* Author to whom correspondence should be addressed.
Tel.: +46-8-524 869 03; Fax: +46-8-34 95 44; E-mail: peter.arhem@neuro.ki.se

1. Introduction

Metal ions were early recognized to play fundamental roles in life processes (Ringer, 1883; Loeb, 1901); acting as cofactors in enzymes, as osmotic regulators, as current carriers and consequently as factors in information processing, and as integrators and stabilizers of proteins and lipids (see Fraústo da Silva & Williams, 2001). At least 10 metal ions have been classified as essential, implying that they occur in most biological tissues and that they cause reproducible physiological abnormalities at their exclusion (Fig. 1, Table 1). The four most abundant metals have been called bulk metals (Na, Mg, K, Ca), in spite of comprising less than 0·9% of the vertebrate body weight. The remaining six metals are described as trace elements (Mn, Fe, Co, Cu, Zn, Mo), implying that they occur in lower concentrations in most organisms. Furthermore, four elements are classified as beneficial (V, Cr, Ni, Sn), being necessary for normal life in certain organisms. Concerning the functional role of trace and beneficial metals only fragmentary knowledge is

https://doi.org/10.1017/S0033583504003932 Published online by Cambridge University Press

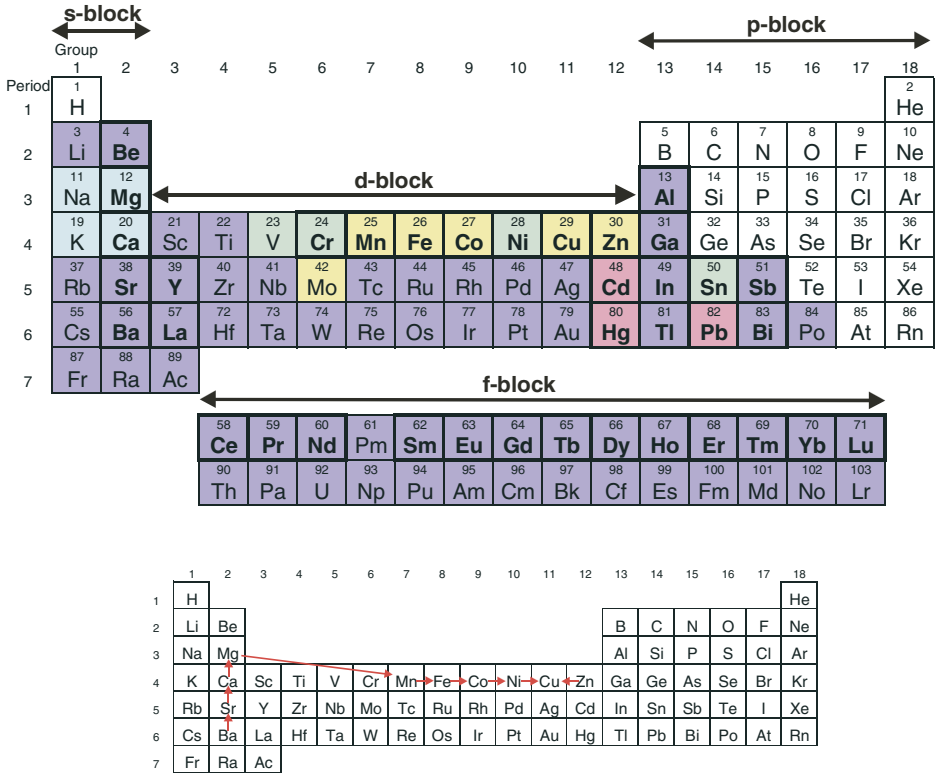

Fig. 1. The periodic table. The metals are colour coded; bulk metals (light blue), trace metals (yellow), beneficial metals (green), toxic metals (pink), and other metals (violet). Metals considered in the present review are in bold fount. The inset shows the order in the Irving–Williams series.

available (see Fraústo da Silva & Williams, 2001). A number of heavier metal ions (e.g. Cd, Hg, Pb) show toxic effects in most organisms (Kiss & Osipenko, 1994), with more or less well-known environmental consequences (Kinter & Pritchard, 1977; Tarras-Wahlberg *et al.* 2001). Excessive exposure makes all metals toxic for humans (Friberg *et al.* 1986a, b). For instance, aggregation of the human Alzheimer's disease amyloid peptide is significantly enhanced by Zn^{2+} (Bush *et al.* 1994).

Considering their central roles in various life processes, it is not surprising that metal ions also have found their places, more or less successfully and more or less transitory, in medical therapies. Historically well known is the use of Hg. It was an early ingredient in ointments against skin parasites and eczema. Around A.D. 650, an Hg alloy (amalgam) was introduced in Chinese dentistry and during the last 150 years it has been widely used in combination with a number of different metals (Ag, Sn, Cu, Zn). In Europe, Hg was introduced against syphilis in 1495, during the French warfare against Naples (Goldwater, 1972). Later on, Paracelsus (1493–1541) introduced internally applied Hg for treatment of syphilis and anaemia. Also well known is the use of Li^+ as a mood stabilizer in the treatment of bipolar affective disorder (Cade, 1949). Mg^{2+} has been successfully used against cerebral ischaemia, seizures, and eclampsia (Goldman & Finkbeiner, 1988; Eclampsia Trial Collaborative Group, 1995). Lanthanides have been used in the treatment of tuberculosis, as anticoagulant agents, and as anti-nausea agents (Haley, 1965; Venugopal & Luckey, 1978). Bismuth (Bi^{2+}) has recently been introduced as an inhibitor of

https://doi.org/10.1017/S0033583504003932 Published online by Cambridge University Press

Table 1. *Properties of the metal ions considered in the present review*

Element	Biological classification	Concentration log (M) Sea	Concentration log (M) Serum	Complexing property	Preferred ligand	Radius (pm)	Electron shell configuration 4s3d4p	5s4d5p	6s4f5d
s-block elements									
Group 1									
11. Na^+	Bulk	−0·3	−0·8		O	98			
19. K^+	Bulk	−2·0	−2·4		O	133			
Group 2									
4. Be^{2+}		−11		Hard		34			
12. Mg^{2+}	Bulk	−1·3	−3·2	Hard	O	78			
20. Ca^{2+}	Bulk	−2·0	−2·9	Hard	O	106			
38. Sr^{2+}		−5·0		Hard		127	2 10 6		
56. Ba^{2+}		−6·9		Hard		143	2 10 6	2 10 6	
d-block elements									
Groups 3–11									
24. Cr^{2+}	Beneficial	−8·4		Hard		84	0 4		
25. Mn^{2+}	Essential	−9·3		Hard	O	91	0 5		
26. Fe^{2+}	Essential	−9·0	−4·7	Borderline	O	82	0 6		
27. Co^{2+}	Essential	−11		Borderline	N/S	82	0 7		
28. Ni^{2+}	Beneficial	−8·1		Borderline	N/S	78	0 8		
29. Cu^{2+}	Essential	−8·4	−4·8	Borderline	N/S	72	0 9		
Group 12									
30. Zn^{2+}	Essential	−8·1	−4·8	Borderline	S/N	83	0 10		
48. Cd^{2+}	Toxic	−9·0		Soft		103	2 10 6	0 10	
80. Hg^{2+}	Toxic	−11		Soft		112	2 10 6	2 10 6	0 14 10
p-block elements									
Group 13									
13. Al^{3+}		−7·7		Hard		57			
31. Ga^{3+}		−10				62	0 10		
49. In^{3+}		−12				92	2 10 6	0 10	
81. Tl^{3+}		−10				105	2 10 6	2 10 6	0 14 10

Group 14								
50.	Sn^{2+}	Beneficial	−11	Borderline	93	2 10 6	2 10	
82.	Pb^{2+}	Toxic	−11	Borderline	132	2 10 6	2 10 6	2 14 10
Group 15								
51.	Sb^{3+}		−9		89	2 10 6	2 10	
83.	Bi^{3+}		< −12		96	2 10 6	2 10 6	2 14 10
f-block elements								
Lanthanides								
39.	Y^{3+}		−10		106	2 10 6		
57.	La^{3+}		−11		122	2 10 6	2 10 6	
58.	Ce^{3+}		−11		107	2 10 6	2 10 6	0 1
59.	Pr^{3+}		−11		106	2 10 6	2 10 6	0 2
60.	Nd^{3+}		−11		104	2 10 6	2 10 6	0 3
62.	Sm^{3+}		−11		100	2 10 6	2 10 6	0 4
63.	Eu^{3+}		−12		98	2 10 6	2 10 6	0 6
64.	Gd^{3+}		−11		97	2 10 6	2 10 6	0 7
65.	Tb^{3+}		−12		93	2 10 6	2 10 6	0 8
66.	Dy^{3+}		−11		91	2 10 6	2 10 6	0 9
67.	Ho^{3+}		−12		89	2 10 6	2 10 6	0 10
68.	Er^{3+}		−11		89	2 10 6	2 10 6	0 11
69.	Tm^{3+}		−12		87	2 10 6	2 10 6	0 12
70.	Yb^{3+}		−11		86	2 10 6	2 10 6	0 13
71.	Lu^{3+}		−12		85	2 10 6	2 10 6	0 14

Although not treated in the present review, Na^+ and K^+ are included in the table for comparison. The concentrations of the elements in sea water and in human serum given are total concentrations. The propensity for complexing is indicated by the hard/borderline/soft scale. The ligand preference is denoted O for oxygen (threonine, serine, tyrosine, aspartate, glutamate, aspargine, glutamine), N for nitrogen (lysine, arginine, histidine, tryptophan), and S for sulphur (cysteine, methionine). The electron configurations are given for the elements in ionic form. Note that the d-block elements Y^{3+} and La^{3+} here are combined together with the f-block elements due to their chemical similarities (data from Larsen, 1965; Bruland, 1983; Cox, 1989, 1995; Evans, 1990; Emsley, 1991; Housecroft, 1999; McCleverty, 1999; Fraústo da Silva & Williams, 2001).

Helicobacter pylori, assumed to cause gastric ulcers. No doubt, further knowledge of the physiological mechanisms of metals will increase their clinical applications.

Metal ions have also proven instrumental in analysing biological structures and functions: they are simple, have well-characterized atomic structures, and show small size differences, which is important for probing permeability mechanisms. Perhaps most conspicuous are their use as tools when analysing structure and function in ion channels. For instance, the divalent cation Ba^{2+} can be used as a K^+ substitute in K channels (Armstrong & Taylor, 1980), and the transition elements Co^{2+}, Ni^{2+} and Cd^{2+} substitute for Ca^{2+} in Ca channels (e.g. Winegar *et al.* 1991). La^{3+} and other lanthanides can be used as 'super calcium' because of their Ca^{2+}-like sizes and chemistries (Lettvin *et al.* 1964; Takata *et al.* 1966; Martin & Richardson, 1979). Gd^{3+} blocks stretch-activated ion channels (Yang & Sachs, 1989; Hamill & McBride, 1996).

The present review attempts to summarize and analyse our knowledge of the action of metal ions on a central aspect of nervous function: the gating of voltage-gated ion channels. More specifically, we will (1) summarize proposed mechanisms of action, (2) summarize reported experimental data for extracellular polyvalent metal ion effects, and (3) discuss the effects with reference to recent findings on molecular channel structure (e.g. Doyle *et al.* 1998; Jiang *et al.* 2003a, b). The amount of literature on the subject covered by this review is considerable. An indication is given by the result of a Medline search for the transition metals Mn, Co, Ni, Zn, Cd in combination with the word 'channel*', yielding almost 4000 papers (2400 from the last 10 years).

This review will not cover effects of all metal ions. (1) We will not discuss monovalent ions. Due to their role as main current carriers in the nervous system and in addition having regulatory effects on ion channels the number of articles is immense and would require a review in itself. (2) We will not discuss very rare metal ions, since they are unavailable for studies. An extreme case is francium (Fr), element number 87. It has been estimated that in the whole of Earth at any one time there are only about seventeen atoms of francium (Atkins, 1995). (3) We will not discuss radioactive metals, since, if available at all, they are unattractive to work with. In addition to element number 43, technetium (Tc), and element number 61, promethium (Pm), all elements with higher atom number than 83, bismuth (Bi), are radioactive. (4) We will not discuss metal ions that are impossible to dissolve in physiological solutions (pH 7–8 and ionic strength of approximately 0·1 M). This means that we are left with 37 ions to consider (Table 1).

2. Metals in biology

The biologically interesting metals form a distinct pattern in the periodic system (Fig. 1), revealing the importance of their evolutionary history. The essential elements (blue and yellow in Fig. 1) are all relatively light, presumably reflecting the fact that life mainly is a surface phenomenon in Earth terms. The metal composition of extracellular fluid in most organisms still shows close similarity with the composition of sea water (Table 1). Heavier metals are found in the deeper layers of Earth and are consequently involved later in the evolutionary process. The toxic character of heavier metal ions probably reflects this fact. Thus the bulk metals (Na, K, Mg, Ca) belong to the lower periods of groups 1 and 2 and most trace metals (Mn, Fe, Co, Cu, Zn) belong to the first transition series (period 4) while the heavier metals Cd and Hg are toxic. That the evolution of metals in biology is an ongoing process is exemplified by cases where normally toxic metal ions may be essential for certain organisms. For instance, marine diatoms have been shown to express a Cd^{2+}-specific carbonic anhydrase that can replace

https://doi.org/10.1017/S0033583504003932 Published online by Cambridge University Press

a Zn^{2+}-specific enzyme under Zn^{2+} restrictions (Lane & Morel, 2000). It is likely that presently toxic ions will find metabolic roles in future organisms. Another observation understandable in an evolutionary perspective is that essential metals in many cases can be functionally replaced by other metals, illustrating the fact that the periodic system, viewed in evolutionary terms, is a system of redundancy; the role of these ions in organisms to a large extent reflects their abundance in sea water rather than their unique chemical properties. For instance, Na^+ can be replaced by the smaller Li^+, and K^+ can be replaced by the larger Rb^+, but Na^+ and K^+ cannot replace each other. In a similar way, Ca^{2+} can be replaced by the biologically rare Ba^{2+}.

The position of the biometals in the periodic system determines relevant chemical characteristics such as valence, tendency to be in ionic form, and tendency to form complexes. The important chemical characteristics in our context are associated with the properties of metal ions in aqueous solution. All metals are electron donors and therefore capable of interacting with ligands such as –OH, –SH, $–NH_2$, –COOH, and $–PO_3H_2$ (Passow *et al.* 1961; Sillén & Martell, 1971). A measure of the tendency to form complexes is given by the Irving–Williams series of stability; for a given ligand the formation constants of a complex with a divalent metal ion are in the order shown in the inset in Fig. 1. The order of the series depends on parameters such as the charge to radius ratio and, in the case of the transition metal ions, on ligand field stabilization energy.

The Irving–Williams series is related to another attempt to classify complex forming tendencies of metal ions, namely what Pearson (1963) called the hard–soft characteristics of metal ions. A hard metal ion is one which preferably retains its valence electrons and which is not readily polarized. Ions of small size and high charge are hard. A soft ion is relatively large, does not firmly bind its valence electrons, and is easily polarized. Hard metal ions preferably complex with hard bases such as oxygen (e.g. water), nitrogen (e.g. amines, ammonia), or fluorine while soft ions complex rather with soft bases such as phosphor, arsenic, or sulphur (Table 1). The bonding in hard–hard complexes is largely electrostatic whereas in soft–soft complexes it is more covalent. Examples of hard metal ions discussed in the present biological context are Mg^{2+}, Ca^{2+}, Mn^{2+}, while among the relatively fewer relevant soft ions we only find Cd^{2+} and Hg^{2+}. The border between hard and soft ions is not sharp and a number of relevant ions fall in between: Zn^{2+}, Cu^{2+}, Ni^{2+}.

Summarizing the chemical profiles of the character of the discussed metal ions we find that the *group 2* metals (s-block elements), including the bulk elements Mg^{2+} and Ca^{2+} are all well described in equilibrium ionic-model chemistry. They easily form complexes and their complex binding ligands are likely to possess one or two carboxylates and several carbonyl donor groups (Table 1). They have flexible coordination numbers and form predominantly ionic complexes that minimize the steric requirements of the ligand (Moeller *et al.* 1965; Sinha, 1976). Specific combinations of the negatively charged residues aspartate and glutamate are found in specific Ca^{2+}-binding proteins, such as calmodulin (Means *et al.* 1982), or in specific Ca^{2+}-binding sequences, such as EF-hands (Kretsinger, 1972).

The first *transition series* metals (d-block elements) Mn^{2+}, Fe^{2+}, Co^{2+}, and Cu^{2+} are all redox reactive, the reactivity increasing with atomic number, and even more than the groups 1 and 2 metals they are prone to complex formation. The transition elements preferably bind to nitrogen donor groups (Martin, 1988), suggesting that the transition metal complexation sites are made up of rings of nitrogens. The strong complex-forming tendency decreases the probability of the metal to exist in physiological solution and thus to have a physiological regulatory role. However, Mn^{2+}, Fe^{2+} and Co^{2+} show a relatively high degree of ionization (50–60%).

https://doi.org/10.1017/S0033583504003932 Published online by Cambridge University Press

The *group 12* (or Zn group; d-block elements) metals differ from those of the transition series in not being redox reactive. However, they are strong electron acceptors, thus strong Lewis acids, and therefore prone to complex formation, preferably to ligands containing sulphur. Nevertheless, Zn is mainly in ionized form in physiological solutions, suggesting a functional role for the regulation of ion channels. Zn^{2+} show both catalytic and structural binding in biological systems. Zn^{2+} demonstrates high affinity to the active site (usually with a dissociation constant in the nanomolar range) in catalytic binding. The site is often located in β-sheet structures, the rigidity of which contributes to the tight binding and prevents exchange of metal ions. The structural role of Zn^{2+} is exemplified by zinc-finger peptides (Miller *et al.* 1985) and insulin. Many of these binding sites have α-helical structures, the non-rigid or flexible nature of which makes the binding affinity of Zn^{2+} lower (see Berg & Godwin, 1997). High-affinity binding sites for Zn^{2+} in proteins are generally formed by near-tetrahedral coordination by various combinations of cysteine, histidine, glutamate, and aspartate residues (Christianson & Alexander, 1989).

The *lanthanides* (f-block elements), like Ca^{2+}, have flexible coordination numbers and predominantly form ionic complexes that minimize the steric requirements of the ligand (Moeller *et al.* 1965; Sinha, 1976). Since the ionic radius increases with coordination number, a change in coordination number could help the smaller ions maintain optimal lengths with pore ligands (Martin & Richardson, 1979). The well-known magnetic properties of the lanthanides (Evans, 1990) are determined by the occupancy of the strongly localized 4f electronic shells, and do not involve the outer s–d electrons, determining the bonding and other electronic properties, which are a focus of the present review (Skriver, 1983).

3. The target molecules: structure and function of ion channels

The target molecules for the metal ion effects in the present study are a very specific group of membrane proteins, the voltage-gated ion channels. To give a background we will briefly discuss the structure, function, and evolution of these molecules.

Voltage-gated ion channels form a diverse class, comprising the classical Na, K and Ca channels as well as Ca^{2+}-activated, cyclic nucleotide-gated and hyperpolarization-activated channels. They are essential for conduction of nervous impulses, muscular contraction, and synaptic transition among several functions (see Hille, 2001, for a review). Figure 2*a* shows the functional structure (e.g. Armstrong & Hille, 1998; Armstrong, 2003). At the extracellular side the pore comprises the selectivity filter, a narrow pathway that determines which ion will pass the pore. At the intracellular end of the pore, a gating mechanism is located, opening and closing the ion-conducting pathway. The gate is coupled to a voltage sensor responding to changes in the membrane electric field. Most channels open at positive voltages. Some, however, are activated by negative voltages. The difference is caused by different coupling mechanisms rather than different voltage sensor movements (Männikkö *et al.* 2002).

Cloning has revealed two main types of ion channel subunits: one consists of two transmembrane α-helices (2TM) and one of six (6TM) (Fig. 2*b*). The α-helices are labelled M1 and M2 in the 2TM channels, and S1–S6 in the 6TM channels. M1 and M2 are homologous to S5 and S6. Four equal or similar subunits pack together, creating an ion- conducting pore in the centre (Fig. 2*b*). The crystallographic structure has been determined for 2TM channels in closed (Doyle *et al.* 1998) and open (Jiang *et al.* 2002) states (Fig. 2*b*). The K channels are structurally simpler than Na and Ca channels in being formed by four separate subunits. Na and Ca channels are larger molecules and consist of four linked domains. The combined segments S1–S4 form the

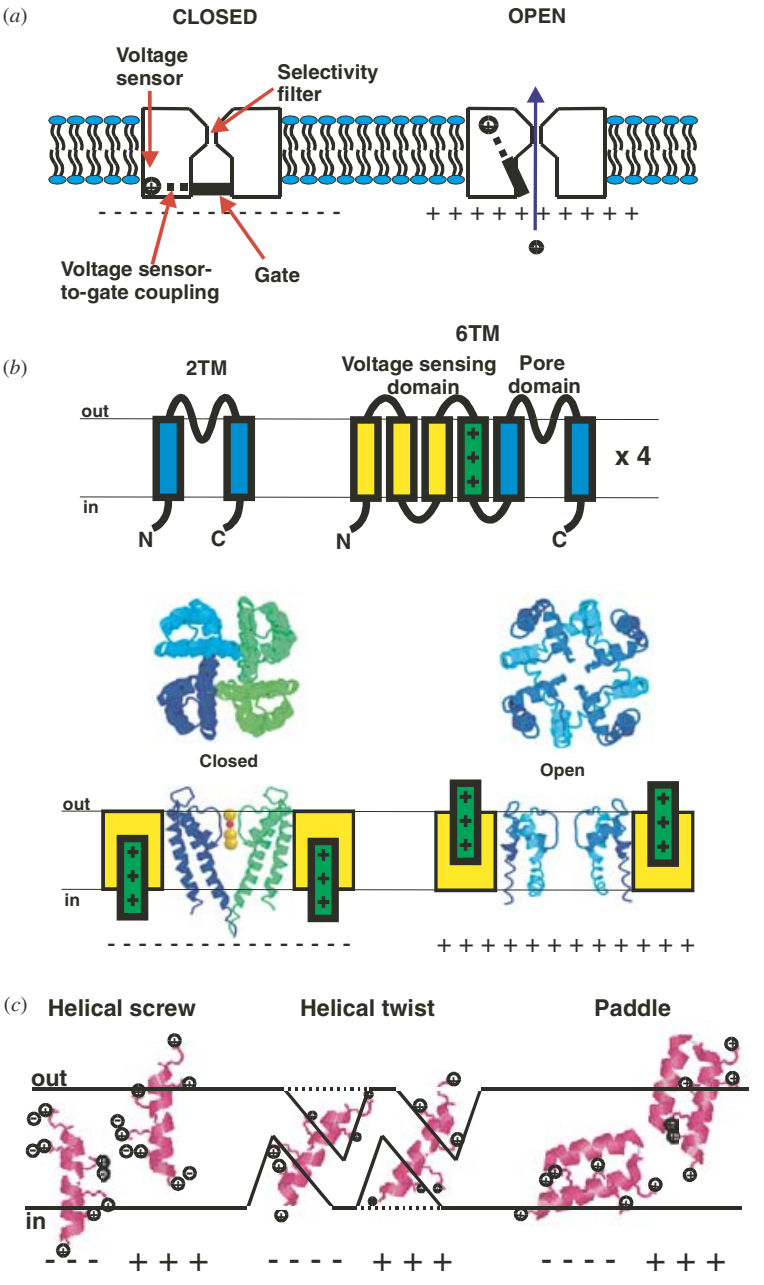

Fig. 2. Structure of voltage-gated ion channels. (*a*) A functional model of an ion channel in closed and open states. At negative membrane voltages the positively charged voltage sensor is attracted to the intracellular end of the channel and the gate is closed. At positive voltages the gate is open. (*b*) Structural models (see text for explanation). (*c*) Models for voltage sensor movements discussed in the literature (see text for description).

voltage-sensing domain, while S5–S6 form the ion-conducting (or pore) domain. Between S5 and S6 there is a loop, forming the narrow ion selective part of the channel, the selectivity filter. S4, with highly conserved positive charges in every third position, has been identified as the

https://doi.org/10.1017/S0033583504003932 Published online by Cambridge University Press

voltage sensor (see Yellen, 1998). At depolarization S4 moves in an outward direction, which leads (in most cases, see above) to the opening of the activation gate, located at the inner end of the pore (Fig. 2*b*). The walls of the inner vestibule are lined with S6 residues.

Recently, a 3D structural model of a voltage-gated K channel, based on X-ray crystallography, was presented together with a suggestion of how S4 moves at gating (Jiang *et al.* 2003a, b). This novel mechanism has not been generally accepted, rather opposition to it has increased (Cohen *et al.* 2003; Miller, 2003). At present we have three alternative gating models at the centre of the debate (Fig. 2*c*).

(i) The *helical screw* motion was proposed soon after the cloning of the first voltage-gated ion channel (e.g. Catterall, 1986; Guy & Seetharamulu, 1986; Keynes & Elinder, 1999; Gandhi & Isacoff, 2002; Lecar *et al.* 2003; Silverman *et al.* 2003). In this model, positive charges in S4 pair with negative conserved charges in S2 and S3. Upon activation, S4 moves in steps to new stable positions by rotating 60° and translating 4·5 Å per step. Up to three steps have been suggested.

(ii) The *helical twist* motion only involves a 180° rotation with no translational movement (Papazian & Bezanilla, 1997; Cha *et al.* 1999). Narrow, water-filled crevices make it possible for a net transfer of charges during gating.

(iii) The *paddle model* is the suggestion of Jiang *et al.* (2003b), mentioned above. It assumes that the C-terminal part of S3 (S3b) is tightly packed against S4 to form a hydrophobic cation that moves from the intracellular side of the lipid bilayer to the extracellular side during gating.

The evolution of ion channels (Wei *et al.* 1996; Coetzee *et al.* 1999) parallels the evolution of metal involvement in life processes (discussed above). Thus, K channels are evolutionarily older than Ca and Na channels (Hille, 2001). It took time before the toxic elements Na and Ca could be used by the nerve cell. Thus K channels are, as mentioned above, structurally simpler and have a more general and less specialized function in the cellular life, involved in regulating and modifying impulse pattern and setting the resting potential. Presumably, the K protochannel was structurally similar to the pore-forming S5–P–S6 motif (2TM) in extant K channels. Such 2TM channels are found among prokaryotes, and presumably originated before 1400 million years ago, but are also present in higher organisms in the shape of the inward rectifiers (Kir). 6TM channels probably originated in protists between 1400 and 700 millions years ago. In one scenario, 2TM subunits associated with highly charged 4TM proteins (corresponding to S1–S4), functioning as potential sensitive transporters in the mitochondrial membrane (Hille, 2001).

4. General effects of metal ions on channels

4.1 Three types of general effect

It was recognized early that K^+ played a major role for nerve cell activity in being instrumental for membrane electricity. The resting potential was explained by a K^+-dependent mechanism, using classical thermodynamic theory (the Nernst equation). In 1902 Overton found experimental evidence for the importance of the Na^+ ion for nerve cell activity, a view that was firmly established by Hodgkin & Katz (1949). Together such facts suggest a generalization: univalent alkali metal ions mainly function as current carriers, while divalent alkali earth (group 2) metal ions function as regulators of nerve activity (Brink, 1954).

https://doi.org/10.1017/S0033583504003932 Published online by Cambridge University Press

In summary, we can outline three main roles for metal ions in normal ion channel physiology:

(i) The function as *current carriers* is perhaps the most conspicuous, and only concern group 1 and 2 ions (Na^+, K^+ and Ca^{2+}). As mentioned above, we will not discuss effects of univalent ions further in the present review.

(ii) The function as *stabilizers* of channel proteins means that the ion is important for the integrity of the channel protein. An old idea is that Ca^{2+} plays such a role in membrane function. Frankenhaeuser (1957) demonstrated the important role for the action potential in myelinated axons. In line with this, a stabilizing role has been assigned to Ca^{2+} in the pore of Na and K channels (Armstrong & Lopez-Barneo, 1987; Armstrong & Miller, 1990), and to Zn^{2+} in the tetramerization domain T1 in K channels (Bixby *et al.* 1999).

(iii) The function as *regulators* mainly comprises modifying the voltage dependence of gating and concerns a large number of polyvalent ions but also the univalent K^+ and Na^+ ions. This regulatory role for polyvalent metal ions will be the main theme of the present review. However, channel-permeable univalent metal ions also affect channel gating, i.e. there is a coupling of permeation and gating (e.g. Van Helden *et al.* 1977; Århem, 1980a; Swenson & Armstrong, 1981; see also Horn, 1999). For instance, raising the concentration of either permeant or pore-blocking ions inhibits the gates from closing, either activation or inactivation gates. This foot-in-the door mechanism was first described by Armstrong (1966, 1971) to explain the effects of intracellular pore blockers on potassium-channel gating. In contrast, many of the effects described in the present paper are related to a slowed opening of the channel and a faster closing. Furthermore, many metal ions seem to cause gate effects without blocking the channel.

4.2 The main regulators

The main physiological regulators of nerve cell activity are the *group 2* ions Ca^{2+} and Mg^{2+}, and the group 12 ion Zn^{2+}. Ca^{2+} is important for a wide variety of biological functions (Kostyuk, 1992), including firing properties of nerve cells (Katz, 1936; Huxley, 1959), muscle contraction (Heilbrunn & Wiercinski, 1947), transmission (Katz, 1969) and plastic changes (i.e. LTP, long-term potentiation; Bliss & Collingridge, 1993) at the synapse, and cell death (Zimmerman & Hulsmann, 1966; Berridge *et al.* 1998). For instance, lowering extracellular Ca^{2+} concentration (e.g. caused by hypoparathyroid disease, or anxiety-induced hyperventilation), reduces the current needed to evoke an action potential, increases the spontaneous nervous activity and blood pressure, and induces tetany and epilepsy (Loeb, 1901; Gordon & Welsh, 1948). Raising the Ca^{2+} concentration has the opposite effects and also increases the resting membrane resistance (reviewed by Brink, 1954; Elinder & Århem, 1991). Similarly, Zn^{2+} is also important for a wide variety of biological functions (Vallee & Falchuk, 1993; Choi & Koh, 1998; Koh, 2001).

Ca^{2+} was early considered to be important for 'ion channel gating'. In 1948, Hodgkin & Huxley suggested that Na^+ is transported through the membrane by the use of a carrier molecule. The carrier molecule was voltage dependent and Ca^{2+} was suggested to bind in the 'closed state' to prevent Na^+ shuttling (described in Hodgkin, 1976). In 1957, Frankenhaeuser & Hodgkin described specific effects on ion channel gating (see below) and based on these observations, Huxley (1959) could quantitatively explain the effect of extracellular Ca^{2+} affecting

https://doi.org/10.1017/S0033583504003932 Published online by Cambridge University Press

a number of electrophysiological parameters, such as resting potential, damping of oscillations, generation of spikes, and propagated responses. Intracellular Ca^{2+} also has important and specific effects on ion channels, such as activation of Ca^{2+}-activated K channels (Gárdos, 1958), inactivation of L-type Ca channels (Brehm & Eckert, 1978), and modulation of expression of Na channels (Sherman *et al.* 1985).

Extracellular Mg^{2+} normally gate NMDA receptor channels (Mayer *et al.* 1984; Nowak *et al.* 1984), and is thus important for LTP. Intracellular Mg^{2+} gates Kir channels (Matsuda *et al.* 1987), and have more speculative roles in regulating ATP binding to K_{ATP} channels (Deutsch *et al.* 1994), dephosphorylation of a cardiac K channel (Duchatelle-Gourdon *et al.* 1989; Tarr *et al.* 1989), and gating of Ca^{2+}-activated K channels (McLarnon & Sawyer, 1993).

The group 12 ion Zn^{2+} is widely distributed throughout the vertebrate CNS (Frederickson, 1989) and may reach considerable levels in synaptic clefts (Assaf & Chung, 1984). It is believed to be an endogenous neuromodulator by affecting several types of ligand-gated ion channels (Peters *et al.* 1987; Westbrook & Mayer, 1987; Xie & Smart, 1991; Li *et al.* 1993; Smart *et al.* 1994; Zheng *et al.* 2001). Also voltage-gated ion channels could be affected by physiological concentrations of Zn^{2+}. Zn^{2+} markedly potentiates a transient K current in hippocampal CA1 neurons and modulates the electrical activity of suprachiasmatic nucleus neurons through effects on a transient K current. The reported modulatory effects on gating of hKv1.4 may well be of physiological significance, in view of the localization of this channel in mossy fibre terminals in the hippocampus, where Zn^{2+} is found in abundance (Harrison *et al.* 1993a, b; Huang *et al.* 1993). In addition, low concentrations of the transition metal ion Ni^{2+} dramatically prolong the action potential (Spyropoulus & Brady, 1959), and increase the response of rod channels to both cAMP and cGMP (Karpen *et al.* 1993; Gordon & Zagotta, 1995).

5. Effects on gating: mechanisms and models

Since the dawn of excitable-membrane physics with the classical studies by Hodgkin & Huxley (1952), it has been a bedrock principle to separate the permeation process from the gating process (Horn, 1999). Most models of metal–ion effects maintain this principle, although some coupling between permeation and gating was found early in studies of monovalent metal ion effects (Århem, 1980a; Swenson & Armstrong, 1981). A causal relationship between the pore and the gating machinery has been invoked to explain the effects of Ca^{2+} in several recent studies (Armstrong & Cota, 1991; Armstrong, 1999; Gomez-Lagunas *et al.* 2003).

The classical starting point for an analysis of metal ion effects on channels is the study by Frankenhaeuser & Hodgkin (1957) on the effects of extracellular Ca^{2+} on squid giant axons (Fig. 3). They showed that Ca^{2+} primarily shifts voltage-dependent parameters of both Na and K channels along the voltage axis; conductance *versus* voltage, $G(V)$, steady-state inactivation *versus* prepulse voltage, $G(V_{PP})$, and time constant *versus* voltage, $\tau(V)$, curves were shifted in a positive direction along the voltage axis. These findings have been confirmed in a number of studies (see Hille, 2001). However, some studies also complicate the picture. The effects vary quantitatively for different metal ions, for different preparations and cell types, and for different parameters. For instance, the opening rate is in many cases more affected than the closing rate. Furthermore, the shifts are accompanied by voltage-dependent block of the ion-conducting pore. To explain the effects, a variety of models have been suggested.

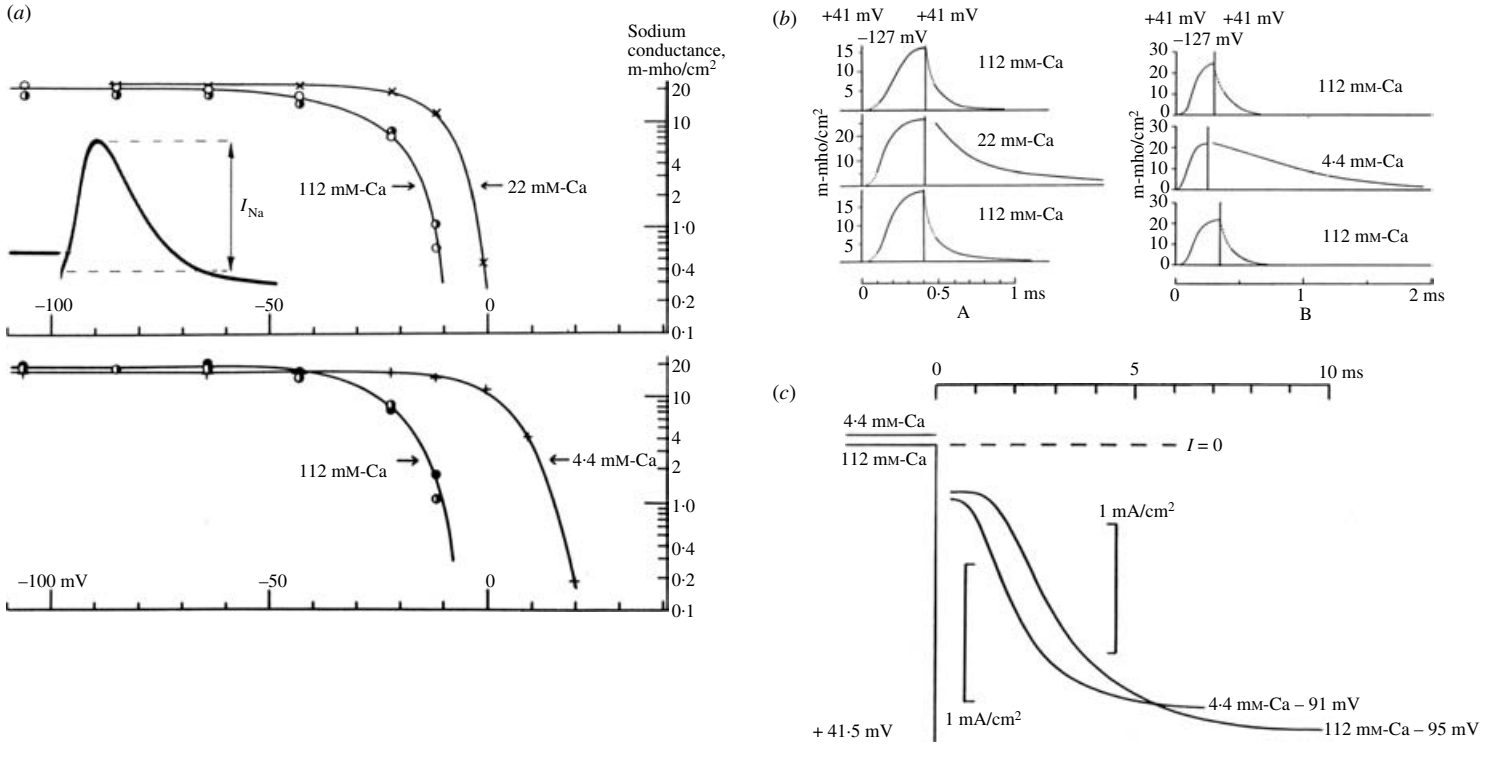

Fig. 3. Effects of Ca^{2+} on Na and K currents in the squid giant axon (reproduced from Frankenhaeuser & Hodgkin, 1957). Note that the convention of voltage polarity for the experiments was opposite to that current at the time of publication of the data. (*a*) Decrease of extracellular Ca^{2+} concentration from 112 to 22 mM or to 4·4 mM shifts the $G(V)$ curve along the voltage axis. The shift along the voltage axis is in a positive direction according to the convention used. With current convention the shift is in a negative direction along the voltage axis. The effects are clearly reversible. (*b*) The opening time-course becomes slightly faster in low Ca^{2+}, while the closing is clearly slower. (*c*) The K-current activation is faster in low Ca^{2+}.

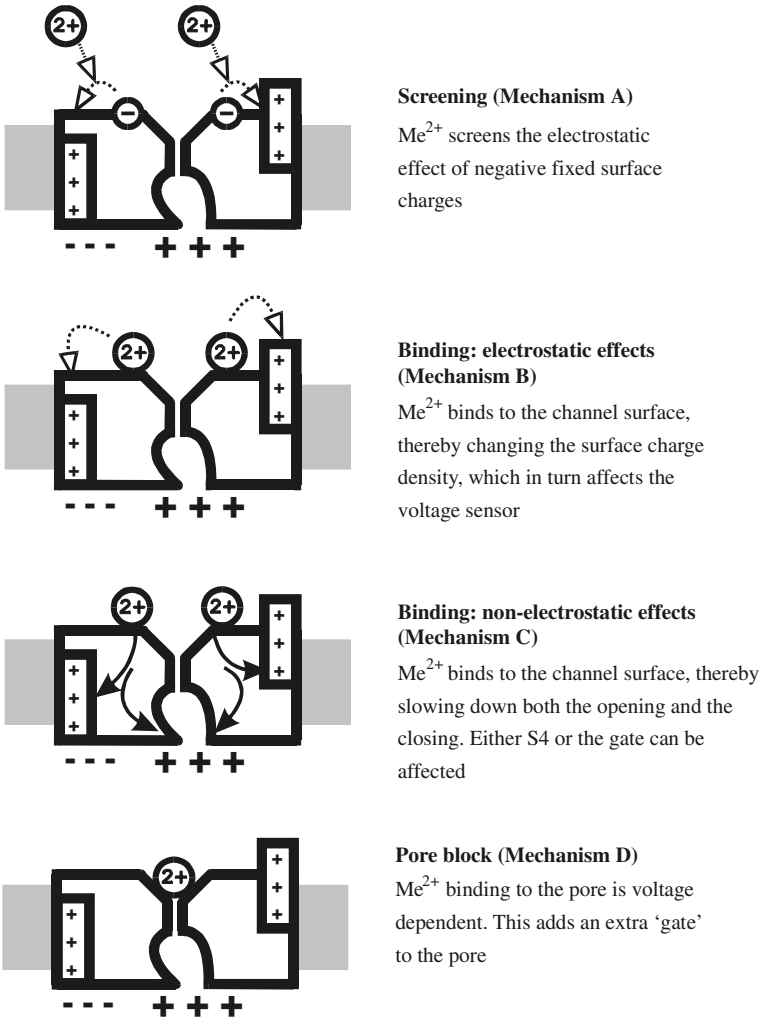

Fig. 4. The four basic mechanisms of metal ion action. The left part of the channel is in a closed state and the right in an open state.

We will here discuss the different suggested models in terms of four basic mechanisms, schematically diagrammed in Fig. 4. The classical approach is to assume that metal ions electrostatically screen fixed surface charges, thereby modifying the electric field sensed by the voltage sensor (Mechanism A). For some ions, binding to fixed charges and a consequent modification of the field at the voltage sensor due to electrostatics has been assumed (Mechanism B). In some cases, binding to a site has been assumed to cause a direct non-electrostatic effect on the gating mechanism (Mechanism C). Finally, binding to and blocking the ion-conducting pore also affects gating; a special case of historical interest is when the metal ion blocks the pore voltage-dependently, thus introducing an extra gate (Mechanism D). All of these mechanisms can be further subclassified according to how many charges/binding sites are affected per channel. For simplicity only one-site mechanisms are depicted in Fig. 4. As will be evident below, and summarized in Table 2, many models discussed in the literature comprise

https://doi.org/10.1017/S0033583504003932 Published online by Cambridge University Press

Table 2. *Summary of characterizing features of the models discussed in the text*

	Eq., Scheme	Mechanism	Number of sites	Change in rate		$\Delta V_{\alpha/\beta}$	Ion
				Opening	Closing		
Screening							
Classical screening	1	A	Multiple	↓	↑	$\alpha=\beta$	Mg^{2+}, Sr^{2+}
Binding/electrostatic effects							
Binding and screening	1, 4, 5	B + A	Multiple	↓	↑	$\alpha=\beta$	Ca^{2+}?
State-dependent binding	8, 9	B	Single	↓	↑	$\alpha\neq\beta$	
Only binding to resting channel	12, 13	B	Single	↓	→	$\alpha\neq\beta$	Zn^{2+}, Ni^{2+}, Cd^{2+}
Binding/non-electrostatic effects							
State-dependent binding + slowing	14	C + B	Single	↓	↓/↑	$\alpha\neq\beta$	Gd^{3+}, La^{3+}
Pore block							
Voltage-dependent pore block	15	D	Single	→	→	$\alpha=\beta$	
State-dependent block	16	D + B	Single	↓	↑	$\alpha\neq\beta$	Ca^{2+}
Only binding to open channel	17, 19	D + B	Single	→	↑	$\alpha\neq\beta$	Ca^{2+}
Extended model	19, 20	D + C	Single	↓	↑	$\alpha\neq\beta$	Ca^{2+}, Ba^{2+}

The models are classified according to underlying mechanisms described in the main text. The majority of models are hybrid models, using combinations of mechanisms (see Section 5.5 for a summary of the mechanisms). The induced change in rate is described by arrows, denoting faster (↑), slower (↓), or intact (→) rates. $\Delta V_{\alpha/\beta}$ shows whether the activation (α) and deactivation (β) rates are equally shifted along the voltage axis or not. The ion column lists the ions applicable to the different models.

combinations of the four mechanisms. For instance, a pore-blocking metal ion (D) may electrostatically affect the voltage sensor (B).

5.1 Screening surface charges (Mechanism A)

5.1.1 The classical approach

Since the first report on Ca^{2+}-induced shifts of $G(V)$ and $G(V_{PP})$ of Na and K currents by Frankenhaeuser & Hodgkin in 1957 (Fig. 3), a shift effect has been observed for most polyvalent metal ions and a variety of preparations. The shift effect was originally explained by an adsorption of the positively charged Ca^{2+} ion to the membrane, thereby changing the membrane electric field (after a suggestion by A. F. Huxley in Frankenhaeuser & Hodgkin, 1957), and was early associated with surface-charge theory (Chandler *et al.* 1965; Gilbert & Ehrenstein, 1969; McLaughlin *et al.* 1971; Brismar, 1973). The underlying physical theory had been developed by Gouy (1910) and Chapman (1913) (see e.g. McLaughlin, 1989) and has been extensively dealt with, both in general terms (Verwey & Overbeek, 1948; Teorell, 1953; Bokris & Reddy, 1970; McLaughlin, 1977) and in specific membrane biology terms (Honig *et al.* 1986; McLaughlin, 1989; Cevc, 1990), or in ion channel physiology terms (Gilbert, 1971; Gilbert & Ehrenstein, 1984; Green & Andersen, 1991; Hille, 2001).

The classical approach assumes infinitely many point charges, making infinitely small contributions to the field at the voltage sensor. In effect this implies a homogenous smeared

https://doi.org/10.1017/S0033583504003932 Published online by Cambridge University Press

charge field at the surface of the membrane and consequently at the voltage sensor. Using this approach, a very useful equation, describing the relation between the surface-charge density (σ) and the surface potential (ψ; relative bulk potential), was developed by Grahame (1947):

$$\sigma^2 = 2\varepsilon_r \varepsilon_0 RT \sum_i c_i [\exp(-z_i F \psi R^{-1} T^{-1}) - 1], \quad (1)$$

where ε_r is the dielectric constant of the medium (80 in water), ε_0 the permitivity of free space ($8{\cdot}85 \times 10^{-12}$ F m^{-1}), R the gas constant (8·31 J mol^{-1} K^{-1}), T the absolute temperature (293 K in most experimental situations), c_i and z_i the bulk concentration and the valence respectively, of the ith ionic species in the (extracellular) solution, and F Faraday's constant (96 500 C mol^{-1}). The assumption of a uniformly smeared charge is itself a problem, since at the level of macromolecules, such as ion channels, the charges are discrete. However, several investigations have paid attention to this problem (Cole, 1969; Brown, 1974; Nelson & McQuarrie, 1975; Sauve & Ohki, 1979; Enos & McQuarrie, 1981; Gilbert & Ehrenstein, 1984; Winiski *et al.* 1986; Mathias *et al.* 1992). A general conclusion is that the smeared charge assumption is valid if the charge density is high enough. In a molecular dynamics study, Peitzsch *et al.* (1995) concluded that charge densities down to (−)0·17 elementary charges per nm^2, in a 100 mM monovalent solution, can be regarded as homogenously smeared. This density corresponds to a distance between the charges of 2·6 nm (hexagonal packing). Applying this value to voltage-gated channels, it means about 3 charges per subunit (surface area about 4×4 nm^2). Most K channels seem to have larger densities (Elinder *et al.* 1998) suggesting that Eq. (1) can be a useful tool in the analysis.

5.1.1.1 Applying the Grahame equation

Figure 5*a* shows the relation between the surface potential and the surface-charge density for a frog Ringer's solution as described by Eq. (1). The large square indicates the range of surface-charge densities from published studies. To estimate the surface potential (and the surface-charge density) the ionic composition is varied during the experiment. This will change the surface potential and consequently the transmembrane potential felt by the ion channel. The change in membrane electric field at the voltage sensor is most easily probed by a shift of the $G(V)$ curve along the voltage axis (e.g. Fig. 3*a*), which is directly related to the change in the surface potential close to the voltage sensor for the activation gate of the ion channel.

Figure 5*b* shows the surface potential for the addition of different concentrations of divalent metal ions (Me^{2+}), assuming that the corresponding anions of the salt are monovalent, and for different surface-charge densities. Figure 5*c* shows the same curves where the effects are plotted as shifts instead of absolute values. All curves start at different surface potentials (see Fig. 5*a*) and all approach 0 mV at high concentrations. To shift 10 mV (dashed line in Fig. 5*c*) approximately 5 mM Me^{2+} is needed for a surface-charge density of $-1{\cdot}0e_0$ nm^{-2}, whereas approximately 40 mM is needed for a density of $-0{\cdot}125e_0$ nm^{-2}. For the following examples we will use a charge density of $-0{\cdot}5e_0$ nm^{-2}, which is close to what has been found for several channels (Hille *et al.* 1975; Gilbert & Ehrenstein, 1984; Elinder & Århem, 1994b; Elinder *et al.* 1996).

Not only the surface-charge density, but also the valence of the added metal ion has a large impact on the effects. Figure 5*d* shows that to shift the $G(V)$ curve 10 mV by a trivalent ion, only 0·9 mM is needed, whereas to shift the curve equally as much with divalent and monovalent ions 9 and 100 mM respectively, are needed. Furthermore, the maximum slope of the shift *versus* concentration curve also depends on the valence; being (per 10-fold concentration change)

https://doi.org/10.1017/S0033583504003932 Published online by Cambridge University Press

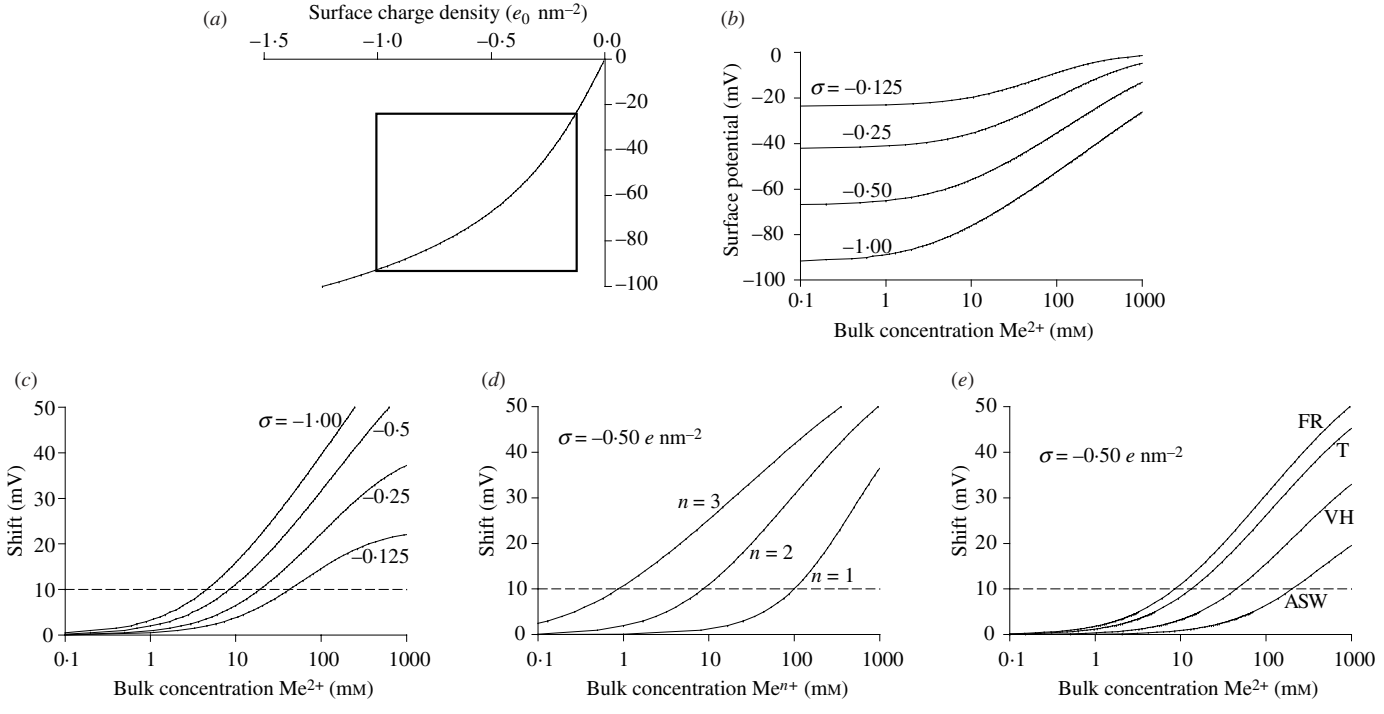

Fig. 5. The surface-charge hypothesis. (*a*) The relation between smeared surface-charge density and surface potential in frog Ringer's solution (118 mM, 1+; 2 mM, 2+; 122 mM, 1−) according to the Grahame equation [(Eq. (1)]. The square indicates the surface-charge densities found in most channels. (*b*) The relation between surface potential and concentration of Me^{2+} (+2 An^-) added to frog Ringer's solution for four different surface-charge densities (indicated). All curves approach 0 mV at infinite concentration. (*c*) The same as in (*b*) but the curves are shifted to 0 mV in control solution. For different surface-charge densities different concentrations of divalent cations are needed to change the surface potential with 10 mV (dashed line). (*d*) Effects of salts with different valencies at a surface-charge density of $-0{\cdot}50e$ nm^{-2}. (*e*) Effects of a divalent salt added to different background solutions at a surface- charge density of $-0{\cdot}50e$ nm^{-2}. FR, Frog Ringer's solution (118 MM, 1+; 2 mM, 2+; 122 mM, 1−); T, Tyrode's solution (150 mM, 1+; 3 mM, 2+; 156 mM, 1−); VH, Van Harrevald's solution (210 mM, 1+; 16 mM, 2+; 242 mM, 1−), and ASW, artificial sea water (440 mM, 1+; 60 mM, 2+; 560 mM, 1−).

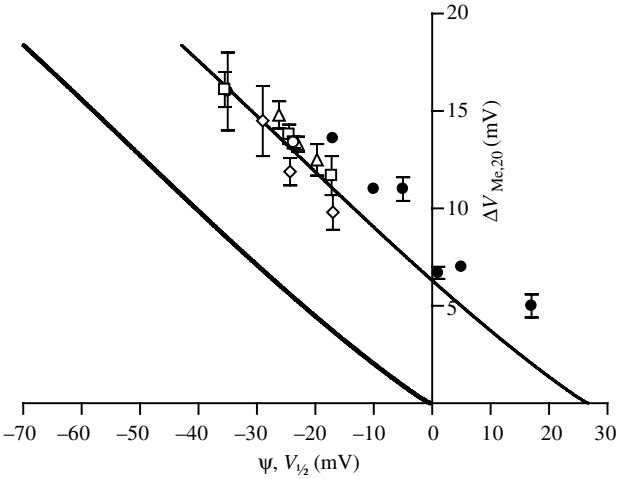

Fig. 6. Metal-ion induced shift of $G(V)$ curves *versus* midpoint values of the $G(V)$ curves in control solution. Open symbols for Shaker K channel: wild type (circles), 419C (squares), 451C (diamonds), and 452C (triangles). The four symbols represent unmodified channels (middle), channels modified with the negatively charged cysteine-specific reagent MTSES, and channels modified with the positively charged cysteine-specific reagent MTSET. 20 mM Mg^{2+} was used to shift the $G(V)$ curves for the Shaker mutants. The closed symbols represent seven different K-channel clones (Kv1.1, Kv1.5, Kv1.6, Kv2.1, Kv3.4, Shaker and xKv1.1). 20 mM Sr^{2+} was used to shift the $G(V)$ curves for the other K-channel clones. The thick line is the solution of Eq. (1) (for frog Ringer's solution) if ψ is denoted on the *x*-axis. Note that no parameters were free. The thin line is the thick curve shifted +27 mV along the voltage axis [data from Elinder *et al.* (1996, 1998) and from Elinder & Århem (1998) for the K-channel clones, and from Elinder *et al.* (2001a) for the Shaker mutants].

16 mV for Me^{3+}, 21 mV for Me^{2+}, and 29 mV for Me^{+} (see also Gilbert & Ehrenstein, 1970). Thus, Eq. (1) can be used to predict effects of monovalent ions from the shift effects of divalent ions (Brismar, 1973).

The surface-charge hypothesis highlights the importance of the ionic strength of the surrounding electrolytes for evaluating and comparing shift effects. Figure 5*e* shows the effect of different physiological solutions (artificial sea water, ASW; Van Harrevald's, VH; Tyrode's, T; Frog Ringer's, FR). It is clear that we expect very different shift results from different preparations even though the surface-charge density is the same. To shift 10 mV, concentrations from 9 to 200 mM are needed in the different background solutions. This makes it difficult to directly compare experimental data. In the following, we will therefore not include data from ASW experiments (e.g. squid giant axons; reviewed in Gilbert, 1971; Lakshminarayanaiah, 1976, 1977; Gilbert & Ehrenstein, 1984) and from Van Harrevald experiments (e.g. crayfish). Data from Tyrode's (mammalian) and from Ringer's (amphibian) solutions will be treated as equal.

Equation (1) is not trivial to use – normally one has to solve it numerically and test it under different conditions to fully understand the relation between the parameters. However, the relation between the surface potential, ψ, and the experimentally measured shift of a voltage-dependent parameter caused by the application of 20 mM $MeCl_2$, $\Delta V_{Me,20}$, is surprisingly linear (see thick line in Fig. 6 for frog Ringer's solution). For frog Ringer's solution the relation can be approximated as

$$\psi = -3.8\,\Delta V_{Me,20}. \qquad (2)$$

https://doi.org/10.1017/S0033583504003932 Published online by Cambridge University Press

This equation predicts that if the surface potential around the voltage sensor S4 is changed by +10 mV then the Me^{2+}-induced $G(V)$ shift should change with −2·6 mV (−10/3·8). Even though single neutral point mutations in ion channels can have profound effects on channel gating [i.e. shifting $G(V)$; Papazian *et al.* 1991; Schoppa *et al.* 1992; Elinder *et al.* 2001a; in most cases without affecting the Me^{2+}-induced $G(V)$ shift] there is an striking correlation between the position of the $G(V)$ curves and the Me^{2+}-induced $G(V)$ shifts. In Fig. 6 we present data for the mid-point of the $G(V)$ curve, $V_{\frac{1}{2}}$, plotted *versus* the Mg^{2+}- or Sr^{2+}-induced $G(V)$ shift ($\Delta V_{Me,20}$; caused by 20 mM $MgCl_2$ or $SrCl_2$) from 17 different channels. The symbols falls surprisingly well on a straight line with the same slope as the thick line predicted by Eq. (1). If the thick-line curve is shifted 27 mV along the voltage axis it fits very well to the experimental data for the Shaker K channel (open symbols). Thus, we predict that when all extracellular surface charges are completely screened the midpoint of the $G(V)$ curve should be +27 mV. Taken together, these data suggest that the surface-charge theory [and Eq. (1)] could well explain the effects executed by Sr^{2+} and Mg^{2+}.

The surface-charge theory predicts relatively large negative surface potentials (−20 to −90 mV, from Fig. 5*a*). Such large magnitude of surface potentials (or changes in surface potential) in specific locations on ion channels have been measured through reactivity of cysteines by charged reagents. In acetylcholine receptor channels the electrostatic potential in the ion-conducting pore surrounded by four glutamates has been calculated as −230 mV by using such methods (Wilson *et al.* 2000). The summed potential is additive, each glutamate contributing −57 mV. In voltage-gated channels, we have measured changes up to 35 mV on the surface depending on the movement of the charged voltage sensor S4 (Elinder *et al.* 2001b), suggesting that a few charges greatly influences the surface potential.

5.1.2 A one-site approach

In the classical approach, just discussed, the number of charges was assumed to be infinite. As already pointed out, it is in many cases more realistic to assume discrete charges in the neighbourhood of the voltage sensor. In this case the following equation has proved useful. It describes the potential ψ_r at a distance r from an elementary charge e, assuming that the charge is located at the border between a low-dielectric (membrane) and a high-dielectric (water, $\varepsilon_r = 80$) medium (McLaughlin, 1989):

$$\psi_r = 2e \exp(-\kappa r)/(4\pi\varepsilon_0\varepsilon_r r), \tag{3}$$

where κ is the inverse of the Debye length (see Hille, 2001) in the aqueous phase. In frog Ringer's solution the Debye length is around 9 Å.

5.2 Binding and electrostatically modifying the voltage sensor (Mechanism B)

5.2.1 The classical model

The simple screening model cannot explain all experimental data. A major drawback is that different divalent cations induce different $G(V)$ shifts. To account for this, differential binding to the channel has been assumed. Further, the classical approach assumes infinitely many, small charges. The theory is an extension of the Gouy–Chapman model and was introduced by Stern (1924). Binding means that an ion (negative or positive) binds directly to the membrane or ion

https://doi.org/10.1017/S0033583504003932 Published online by Cambridge University Press

channel, thereby changing the surface-charge density. This change in density automatically leads to a change in the surface potential according to Eq. (1), and experimentally this can be seen as a shift of the $G(V)$ curve. However, the $G(V)$ shift caused by binding could be very difficult to differentiate from a shift caused by screening.

To quantitatively illustrate the shift effect of a divalent metal-ion (Me^{2+}) binding to the channel and thereby indirectly modifying the electric field, we assume that the fraction bound charges (σ_{bound}/σ) follow

$$\sigma_{bound}/\sigma = K_i[Me^{2+}]_{surf}/(1 + K_i[Me^{2+}]_{surf}), \tag{4}$$

where K_i is the intrinsic binding constant. This value is related to the dissociation constant, K_D, i.e. the concentration at which 50% of all binding sites are occupied, by $K_D = 1/K_i$. The concentration at the binding site (at the channel's surface, $[Me^{2+}]_{surf}$) is not necessarily equal to the bulk concentration of the extracellular solution. It depends on the surface potential (ψ) and the bulk concentration ($[Me^{2+}]_{bulk}$) following the Boltzmann relation

$$[Me^{2+}]_{surf} = [Me^{2+}]_{bulk} \exp(-z_{Me}\psi FR^{-1}T^{-1}), \tag{5}$$

where z_{Me} is the valence of the ion. Equations (1), (4) and (5) must be solved simultaneously. If we assume that the number of binding sites per nm^2 corresponds to σ ($-0{\cdot}5e\ nm^{-2}$) then 0·25 Me^{2+} can bind per nm^2 (i.e. 4 Me^{2+} per subunit if evenly distributed). Figure 7*a* shows how the $G(V)$ shifts for different Me^{2+} concentrations are affected by the K_D value. The result is a shift of the curve along the concentration axis. Now much lower concentrations are needed to shift 10 mV. It should also be noted that the apparent binding does not follow the normal Langmuir isotherm (dashed curve in Fig. 7*b*). The binding primarily occurs at the foot of the curves in Fig. 7*a*. At higher bulk concentrations the surface concentration is almost constant because of the accompanying change in surface potential. (Absorbed lanthanides impart a net positive charge to the membrane surface which makes the binding of further lanthanides increasingly more difficult; Lehrmann & Seelig, 1994.) In the calculations shown in Fig. 7 we assumed that the number of binding sites corresponds to the surface-charge density, but it should be noted that this is a simplification and could be different for different metal ions.

5.2.1.1 The classical model as state diagram – introducing basic channel kinetics

In the following we will relate the discussed classical screening and binding models to other models in terms of state diagrams. We will use the following simple two-state model:

$$C \underset{\beta}{\overset{\alpha}{\rightleftharpoons}} O, \tag{Scheme 6}$$

where C and O are closed and open states, and α and β are voltage-dependent rate constants expressed in terms of the transition-state theory (Glasstone *et al.* 1941):

$$\alpha = k_{eq} \exp((V - V_{eq})z_\alpha FR^{-1}T^{-1}), \tag{6a}$$

$$\beta = k_{eq} \exp(-(V - V_{eq})z_\beta FR^{-1}T^{-1}), \tag{6b}$$

where k_{eq} is the rate constant of α and β when $\alpha = \beta$, V the absolute membrane voltage, V_{eq} the membrane voltage when $\alpha = \beta$, z_α the gating valence for α and z_β the gating valence for β,

https://doi.org/10.1017/S0033583504003932 Published online by Cambridge University Press

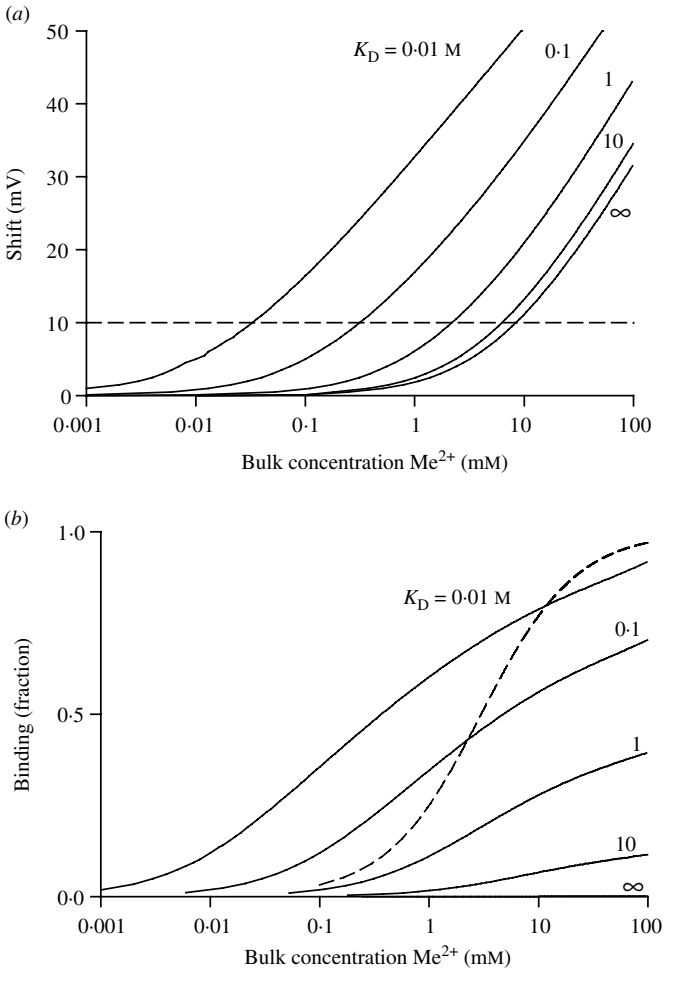

Fig. 7. (*a*) Effects of a divalent salt on the surface potential (measured as shifts) if Me^{2+} binds to the membrane. Calculated from Eqs. (1)–(3) for a surface-charge density of $-0{\cdot}50e\,\mathrm{nm}^{-2}$. K_D values as indicated. (*b*) Fraction of binding from (*a*). The dashed line indicates a Langmuir isotherm.

and F, R, and T have their normal thermodynamic significances. In the screening and binding models described above the channel in Me^{n+} is modelled as

$$C \underset{\beta_{Me}}{\overset{\alpha_{Me}}{\rightleftharpoons}} O, \qquad \text{(Scheme 7)}$$

where α_{Me} and β_{Me} are the rate constants, described by

$$\alpha_{Me} = k_{eq} \exp((V - V_{eq} - \Delta V_{Me})z_\alpha FR^{-1}T^{-1}), \qquad (7a)$$

$$\beta_{Me} = k_{eq} \exp(-(V - V_{eq} - \Delta V_{Me})z_\beta FR^{-1}T^{-1}), \qquad (7b)$$

where ΔV_{Me} is the Me^{n+}-induced shift of the parameter. Figure 8*a* shows resulting curves in control (continuous lines) and Me^{n+} solutions (dashed lines for $\Delta V_{Me} = 20$ mV).

https://doi.org/10.1017/S0033583504003932 Published online by Cambridge University Press

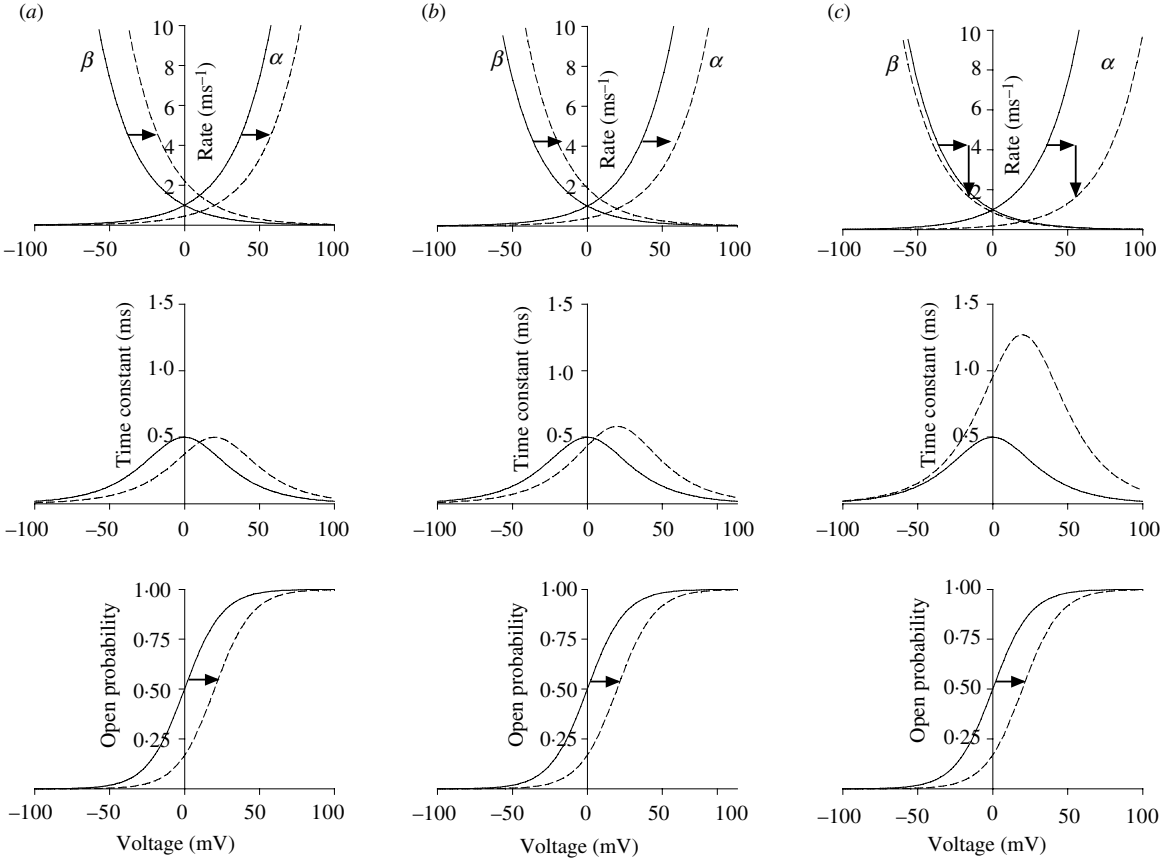

Fig. 8. Effects of a divalent metal ion on rate constants, time constants and open probability for three different models described in the text. The rate constants are calculated from Eq. (6) with $z_\alpha = z_\beta = 1$, $k_{eq} = 1$, $V_{eq} = 0$ mV. The time constant, τ, is $1/(\alpha+\beta)$. The open probability [$\approx G(V)$] is $\alpha/(\alpha+\beta)$. (*a*) Classical screening (Mechanism A) or multi-site binding (Mechanism B) according to Eq. (7). α and β are shifted 20 mV ($= \Delta V_{Me}$) along the voltage axis. (*b*) Single-site binding (Mechanism B) according to Eq. (9). $K_C[Me] = 0$ (continuous lines) and $K_C[Me] = 7$ (dashed lines). $\Delta V^*_{Me} = 30$ mV (*c*) Single-site binding with slowing of opening and closing (Mechanism C) according to Eq. (A 7) in the Appendix. The length of the horizontal arrows is 20 mV. The two vertical arrows represent a division with 2·5.

Characteristically for multi-site screening or binding models, the shift of $\tau(V)$ and $G(V)$ curves are equal. Thus, the opening rate is slower and the closing rate is faster.

5.2.2 A one-site approach

Binding models using one or a few binding sites predict results that deviate from those of the smeared surface-charge models just described. This will be clear from exploring a simple discrete binding model, where a metal ion is assumed to bind to one charge (or other site), electrostatically changing the rate constants α and β to α^*_{Me} and β^*_{Me}:

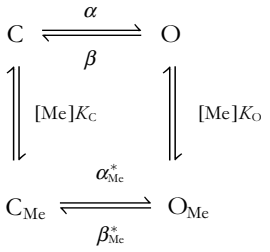

(Scheme 8)

K_C and K_O are binding constants and [Me] is the metal ion concentration. The rate constants are described by Eqs. (6)–(7). In Eq. (7), $\alpha_{\mathrm{Me}} = \alpha^*_{\mathrm{Me}}$, $\beta_{\mathrm{Me}} = \beta^*_{\mathrm{Me}}$, and $\Delta V_{\mathrm{Me}} = \Delta V^*_{\mathrm{Me}}$, where ΔV^*_{Me} is the effect on the electric field induced by one bound Me ion. (A general summary of Scheme 8 and more elaborate equations describing the properties of the model is found in the Appendix.) If the model is in thermodynamic equilibrium and the metal-binding transition is much faster than the channel gating, then Scheme 8 can be reduced to

$$\{\mathrm{C}\} \underset{\beta_{\mathrm{Me}}}{\overset{\alpha_{\mathrm{Me}}}{\rightleftharpoons}} \{\mathrm{O}\}, \qquad \text{(Scheme 9)}$$

where {C} denotes all closed states and {O} all open states, and where

$$\alpha_{\mathrm{Me}} = \alpha(1 + K_C[\mathrm{Me}] \exp(-\Delta V^*_{\mathrm{Me}} z_\alpha F R^{-1} T^{-1}))/(1 + K_C[\mathrm{Me}]), \qquad (9a)$$

$$\beta_{\mathrm{Me}} = \beta(1 + K_C[\mathrm{Me}] \exp(-\Delta V^*_{\mathrm{Me}} z_\alpha F R^{-1} T^{-1}))/(1 + K_C[\mathrm{Me}] \exp(-\Delta V^*_{\mathrm{Me}} (z_\alpha + z_\beta) F R^{-1} T^{-1})). \qquad (9b)$$

See the Appendix for the derivations [Eqs. (A 7*a*, *b*) for $A^* = 1$]. In Fig. 8*b* the rate constants, the time constants, and the open probability [$\approx G(V)$] are plotted for two concentrations of Me^{n+} ($K_C[\mathrm{Me}] = 0$ and 7). ΔV^*_{Me} is set to 30 mV. The resulting shifts are all in a positive direction but, in contrast to those of the continuous model (Fig. 8*a*), not equal in magnitude [for $\alpha(V)$, $\beta(V)$, and G(V) being 24, 16, and 20 mV respectively]. The shifts can also be calculated directly from Eqs. (A 8*a–c*) for $A^* = 1$ in the Appendix.

5.2.2.1 Explaining state-dependent binding – a simple electrostatic mechanism

The resulting difference in apparent affinity for closed (K_C) and open states (K_O) can be explained by a simple physical mechanism. We assume that the binding constant is state independent but the local concentration of the metal ion at the binding site varies with the position of the

https://doi.org/10.1017/S0033583504003932 Published online by Cambridge University Press

voltage sensor S4. In the open state(s) the positively charged voltage sensor is moved in an outwards direction thereby repelling Me^{n+} ions and lowering the local Me^{n+} concentration according to the Boltzmann relation

$$K_O = K_C \exp(-z_{Me} F \Delta V_{S4} R^{-1} T^{-1}), \tag{10}$$

where z_{Me} is the valence of the metal ion, and ΔV_{S4} is the change in surface potential at the binding site caused by the outwards movement of S4. Combining Eqs. (A 3)–(A 5) with Eq. (10) gives

$$z_{Me} \Delta_{S4} = (z_\alpha + z_\beta) \Delta V^*_{Me}. \tag{11}$$

Both sides of the equation represent the extra work ($W = QV = z_{e0} V$) done by S4 when moving in the field with a bound metal ion, or the extra work for the positive metal ion to bind when S4 is in its upper, activated position. If $z_\alpha = z_\beta = 1$ as assumed above and $z_{Me} = 2$ as for a divalent cation then $\Delta V^*_{Me} = \Delta V_{S4}$. Thus, the change in the local potential at S4 caused by the bound metal ion is equal to the change in local potential at the binding site caused by S4.

5.2.2.2 The relation between models assuming binding to smeared and to discrete charges

The exploration of the two surface-charge binding models described above reveal their differences. In the smeared binding model, metal ions shift activation rate, $\alpha(V)$, and deactivation rate, $\beta(V)$, curves equally, while in the discrete one-site binding model they shift $\alpha(V)$ more than $\beta(V)$. In the smeared model the binding is state-independent, while in the discrete model the channel shows higher metal-ion affinity in the closed state than in the open state, because the voltage sensor S4 removes the metal ion from the channel in open state by an electrostatic knocking-off effect. Discrete models, assuming an increasing number of binding sites affecting the voltage sensor, show less difference between the shifts of $\alpha(V)$ and $\beta(V)$. For example, if the bound metal ion changes the voltage at the voltage sensor with 45 mV, $\alpha(V)$ can be shifted up to 9 mV more than $G(V)$, and $\beta(V)$ up to 9 mV less than $G(V)$ [calculated from Eqs. (A 8*a–c*) for $z_\alpha = z_\beta = 1$ and $A^* = 1$]. There are reasons to believe that in most cases more than one metal ion binds to the channel but at some distance away from the voltage sensor. We assume that three metal ions bind at the same distance from the voltage sensor. To cause a total effect of 45 mV at the voltage sensor each ion must contribute with 15 mV. Scheme 8 can easily be extended to incorporate three binding metal ions. The maximum difference between the shifts of $\alpha(V)$ and G(V), as well as the difference between $G(V)$ and $\beta(V)$, is reduced to 3 mV. Furthermore, assuming cooperativity between the bound metal ions (i.e. one metal ion affects the binding of a second and a third ion for electrostatic reasons), makes the difference even smaller. In summary, the binding of a single metal ion close to the voltage sensor is state-dependent and affects the activation and deactivation time constants differently. The binding of several metal ions is less state-dependent and yields smaller differences between the shifts of $\alpha(V)$ and $\beta(V)$.

5.2.2.3 The special case of Zn^{2+} – no binding in the open state

As just seen, a discrete model predicts differential shifts of voltage-dependent parameters. For instance, $\alpha(V)$ is shifted more than $G(V)$. Figure 9 shows that 60 μM of the lanthanide Gd^{3+} has profound effects on the opening of voltage-gated K channels (Elinder & Århem, 1994a). The opening time-constant curve is shifted ~100 mV, although the $G(V)$ curve is

https://doi.org/10.1017/S0033583504003932 Published online by Cambridge University Press

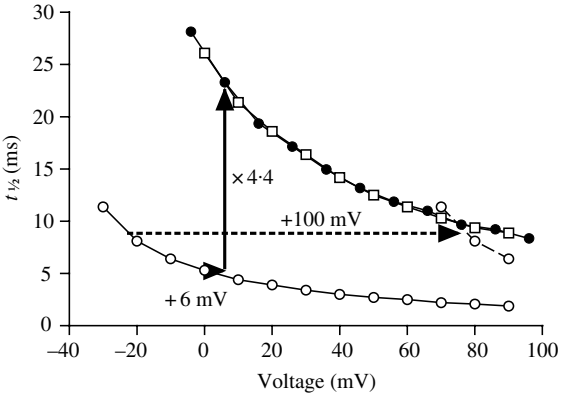

Fig. 9. Time to reach 50% of the steady-state K current in a myelinated axon of *Xenopus laevis*. Control (open circles), 60 μM Gd^{3+} (squares), shifted control data (open circles and dotted line; $\Delta V = 100$ mV), shift-and-scaled control data (closed circles; $\Delta V = +6$ mV, $A = 4{\cdot}4$) (data from Elinder & Århem, 1994a).

shifted only ~6 mV (Elinder & Århem, 1994a). This discrepancy has been observed for many ion species (Shrager, 1974; Stanfield, 1975; Gilly & Armstrong, 1982a, b; Schauf, 1983; Armstrong & Matteson, 1986; Armstrong & Cota, 1990; Cukierman & Krueger, 1990, 1991; Cukierman, 1993; Elinder & Århem, 1994a; Terlau *et al.* 1996; Tang *et al.* 2000). The largest discrepancy is found for Zn^{2+} and some of the lanthanides for the Kv channels (Stanfield, 1975; Gilly & Armstrong, 1982a, b; Armstrong & Cota, 1990; Elinder & Århem, 1994a), and for Mg^{2+} on ether-à-go-go (eag) channels (Terlau *et al.* 1996; Tang *et al.* 2000). As suggested from the shift of the $G(V)$ curve, the closing is often speeded up (e.g. Fig. 8*a*), but for some ions the closing is less affected than what is suggested from the shift of the $G(V)$ curve. Again the largest differences are found for Zn^{2+} and some of the lanthanides (Gilly & Armstrong, 1982a, b; Armstrong & Cota, 1990).

Zn^{2+}, at certain concentrations, slows down the opening while leaving the closing relatively unaffected (Gilly & Armstrong, 1982b). Gilly & Armstrong (1982a, b) suggested that Zn^{2+} binds directly to the voltage sensor exclusively in a closed state. In this state the positively charged voltage sensor is retracted into the channel and negative charges on the surface attract and bind Zn^{2+}, thereby obstructing the (outward) opening motion of the voltage sensor. In the open state the binding of Zn^{2+} is assumed to be prevented by the charged voltage sensor. Using the simple assumption of a binary state channel (Scheme 6), such a mechanism predicts that the opening is affected by Zn^{2+} but the closing is left unaffected, and can be described by the following kinetic scheme:

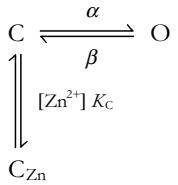

(Scheme 12)

where C_{Zn} is a Zn^{2+}-bound (closed) state and $[Zn^{2+}]$ is the bulk concentration of Zn^{2+}. This scheme can be seen as a special case of Scheme 8, where the rate constants describing the transitions to O_{Me} are zero. To make the point of a modified opening and an unmodified closing

https://doi.org/10.1017/S0033583504003932 Published online by Cambridge University Press

easier to grasp, we condense Scheme 12 to a binary state diagram, assuming that the Zn^{2+}-binding kinetics are much faster than the channel kinetics (α and β):

$$\{C\} \underset{\beta}{\overset{\alpha / (1 + [Zn^{2+}]K_C)}{\rightleftharpoons}} O, \qquad \text{(Scheme 13)}$$

where {C} is the set of the bound and unbound closed states. Using the fact that the scheme is a special case of Scheme 8, the rate constants are also directly obtained from Eqs. (9*a*, *b*), setting ΔV^* to infinity. Inspection of the experimental data presented by Gilly & Armstrong (1982b) to support Scheme 12, shows that the closing is not unaffected at all concentrations of Zn^{2+} (figs. 2b and 5a in Gilly & Armstrong, 1982b), suggesting that, in fact, the more general Scheme 8 better explains the discussed Zn^{2+} effects. This scheme also applies to intracellular Zn^{2+} effects on proton channels. These channels have many characteristics in common with the voltage-gated ion channels, including the effects of metal ions, although exerted at lower concentrations (Cherny & DeCoursey, 1999): intracellular Zn^{2+} does not affect the opening, but slows down the closing.

In conclusion, Scheme 8 explains the reported differences in metal-ion-induced opening and closing rates for a number of channel types and ion species. An alternative model, explaining similar data has been developed by Cukierman & Krueger (1990, 1991). This model combines state-dependent binding (Scheme 12) with screening [Eq. (1)], assuming an extracellular binding site that affects the opening, and an intracellular site that affects the closing. However, there are metal-ion effects that cannot be explained by any of these models. For instance, Cd^{2+} shows seemingly paradoxical effects on some hyperpolarization-activated K channels and trivalent ion species might shift opening and closing rate curves in opposite directions. This necessitates new models, possibly comprising non-electrostatic mechanisms. Such models will be treated below.

5.2.2.4 Opposing effects of Cd^{2+} on hyperpolarization-activated channels

In a hyperpolarization-activated ion channel (spHCN) the voltage-sensor movement is similar to that of depolarization-activated ion channels, but the coupling to the gate is different, making the gates in the two types of channels open at opposite voltages (Männikkö *et al.* 2002). Thus, an inward movement of the voltage sensor opens the channel and an outward movement closes the channel. For electrostatic reasons we would expect a faster opening and a slower closing at extracellular application of metal ions. This expectation holds for Mg^{2+}, for instance, when applied to cloned HCN channels (R. Männikkö & F. Elinder, unpublished results). However, opposite results have been reported for Cd^{2+} experiments on a hyperpolarization-activated K channel in crayfish opener muscle fibres (Araque *et al.* 1995). In this preparation Cd^{2+} slows the channel opening, while leaving the closing intact. This makes the electrostatic arguments, used in the Zn^{2+} case above, inapplicable. An alternative would be an electrostatically neutral, gate-dependent binding. These seemingly contradictory results clearly need further elucidation.

5.3 Binding and interacting non-electrostatically with the voltage sensor (Mechanism C)

As mentioned above, neither the Cukierman & Krueger model (1990, 1991), nor that of Scheme 8 can explain the findings that some trivalent ions can shift the opening and closing

https://doi.org/10.1017/S0033583504003932 Published online by Cambridge University Press

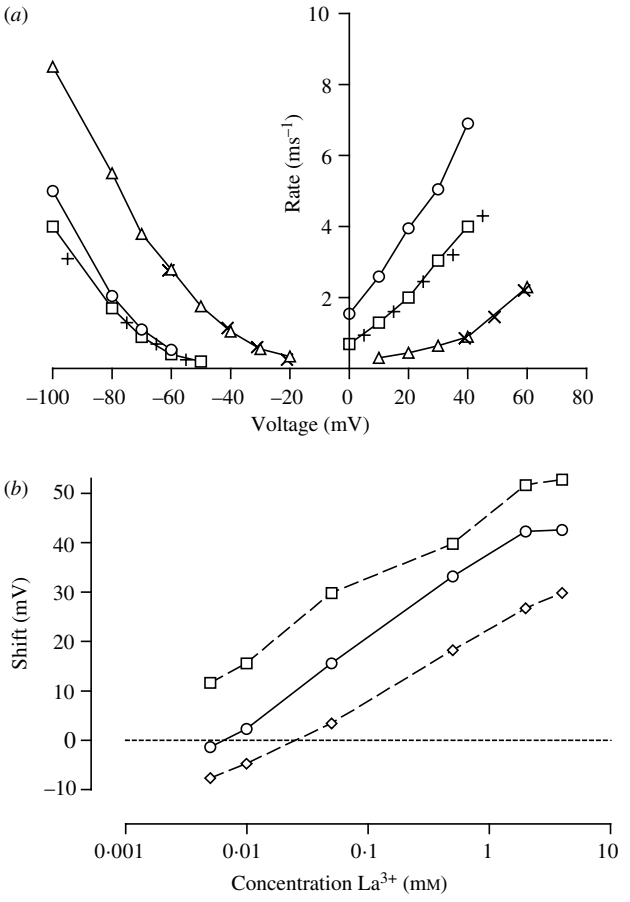

Fig. 10. Effects of La^{3+} on Na channels in GH3 cells (data from Armstrong & Cota, 1990). (*a*) Rate constants for opening (positive voltages) and closing (negative voltages). Control (circles), 10 μM La^{3+} (squares), 2 mM La^{2+} (triangles). Control data shifted and scaled with common values match experimental data very well, + ($\Delta V = 5$ mV, $A = 1{\cdot}6$), × ($\Delta V = 39$ mV, $A = 1{\cdot}8$). (*b*) Shifts of opening rate constants (squares), $G(V)$ (circles), and closing rate constants (diamonds). Note that the $G(V)$ shift is close to what is obtained from the shift-and-scaling analysis in (*a*).

rate curves in opposite directions. This applies for instance to the finding by Armstrong & Cota (1990) that extracellular La^{3+} can decrease the rate of Na-channel closing. Figure 10*a* shows the effects on opening and closing rates, and Fig. 10*b* summarizes the shift data of their study. The slopes of the curves in Fig. 10*b* are close to what is expected for Eq. (1) for a trivalent cation, suggesting that screening could be involved. Likewise, neither the Cukierman & Kreuger model (1990, 1991), nor Scheme 8 can explain the decreased rate of opening induced by intracellular Zn^{2+} and other divalent cations (Begenisich & Lynch, 1974; Fox *et al.* 1974), nor that the effect by Gd^{3+} on the activation time constant is impossible to describe as a simple shift of the time-constant curve (Fig. 9; Elinder & Århem, 1994a). Thus, we have to explore other models to explain these data. It is natural to search for models comprising non-electrostatic mechanisms.

https://doi.org/10.1017/S0033583504003932 Published online by Cambridge University Press

5.3.1 Combining mechanical slowing of opening and closing with electrostatic modification of the voltage sensor

In a study of Gd^{3+} we developed such a model. It can be shown to explain most of the effects induced by Zn^{2+}, Ca^{2+}, and La^{3+} discussed above (Elinder & Århem, 1994a, b). We combined screening/binding effects (Mechanisms A and B) with a bi-directional slowing of the voltage sensor motion, i.e. assuming that the metal ion acts as a brake on the gating mechanism (Mechanism C). The model is described by the basic Scheme 8, with rate constants for the metal-bound state transitions being

$$\alpha^*_{Me} = (A^*)^{-1} k_{eq} \exp((V - V_{eq} - \Delta V^*_{Me}) z_\alpha F R^{-1} T^{-1}), \tag{14a}$$

$$\beta^*_{Me} = (A^*)^{-1} k_{eq} \exp(-(V - V_{eq} - \Delta V^*_{Me}) z_\beta F R^{-1} T^{-1}). \tag{14b}$$

These expressions mean that the voltage dependence of the rate constants is shifted ΔV^*_{Me} in comparison to the rate constants in unbound conditions, and that the magnitude, in addition to the modification caused by the voltage shift, is reduced by a slowing factor A^* [corresponding to adding an energy barrier of $\Delta W = kT \ln(A^*)$]. The model and its mathematical derivations are described in the Appendix. Assuming that the metal-binding transition is much faster than the rate constants, the four-state Scheme 8 can be reduced to a two-state scheme, with rate constants given in the Appendix [Scheme A 6 and Eqs. (A 7*a*, *b*)].

Figure 8*c* illustrates the properties of the model. If $\Delta V^*_{Me} = +30$ mV and $A^* = 5$, changing K_C[Me] from 0 to 7 shifts the opening rate with 44 mV, while the closing rate is shifted -4 mV. The shift of the open probability curve ($+20$ mV) is identical to that of Fig. 8*a* where $A^* = 1$. These shifts could also be directly calculated from Eqs. (A 8*a–c*). In our experimental analysis we applied a shift-and-scaling procedure (Elinder & Århem, 1994a, b). That means that the metal-ion-induced effects on both the opening and the closing could be described as a combination of a common shift, ΔV, equal to the $G(V)$ shift, and a common scaling, A, of the time-constant curves. Applying this procedure to Scheme A 2 in the Appendix we obtain ΔV and A values directly from Eqs. (A 8*c*) and (A 10). It should be noted that the relation between this 'experimental' A value and the model A^* value is complex [Eq. (A 10)]. A shift-and-scaling analysis applied to the La^{3+} data by Armstrong & Cota (1990) gives slowing factors (A) of 1·6 and 1·8 at the two concentrations respectively (Fig. 10*a*). The analysis of the Gd^{3+} data on K channels in Fig. 9 gives $A = 4{\cdot}4$ and $\Delta V = 6$ mV [i.e. equal to the $G(V)$ shift].

In line with our proposal that a metal ion binds close to the voltage sensor, and thereby reduces both the forward and backward rates, Mg^{2+} can be assumed to affect the gating in Keag channels by slowing down early steps in the activation process; both in forward and backward direction (Terlau *et al.* 1996; Tang *et al.* 2000). In a gating model by Sigg & Bezanilla (2003), this was explained by assuming that Mg^{2+} binds to a site directly on or near a barrier particle, reducing its effective valence. Steric hindrance or mass effects might slow down fluctuations in the motion of the barrier particle–Mg^{2+} complex, leading to a reduction of rates across the first subunit transition.

5.4 Binding to the pore – a special case of one-site binding models (Mechanism D)

A special case of binding models is the group assuming binding to the pore. Due to their prominent roles in the discussion of metal ion effects, pore-binding models are here treated in

https://doi.org/10.1017/S0033583504003932 Published online by Cambridge University Press

a separate chapter. Historically, the pore block by Ca^{2+} is of special interest. It was through the pioneering work by Frankenhaeuser & Hodgkin (1957) on the effects of this ion species on the squid axon, and their discussion about a voltage-dependent block, that surface-charge thinking was introduced into nerve membrane physiology. Since then, a voltage-dependent block by Ca^{2+} has been described for Na and K channels in a number of studies (e.g. Woodhull, 1973; Yamamoto *et al.* 1984; Mozhayeva *et al.* 1985; Cukierman *et al.* 1988; Behrens *et al.* 1989; Gomez-Lagunas *et al.* 2003). The idea of a voltage-dependent block causing shift effects was revived by Armstrong & Cota (1990, 1991, 1999) and Armstrong (1999), who showed that the shifts of steady-state parameters are closely correlated with a pore block.

5.4.1 Voltage-dependent pore-block – adding extra gating

As mentioned, Frankenhaeuser & Hodgkin (1957) discussed a voltage-dependent block as a possible explanation to the effects of Ca^{2+} on Na and K channels. However, this alternative was rejected for reasons that will be discussed later. To quantitatively illustrate a simple voltage-dependent pore block, we use the simple binary-state model (Scheme 6):

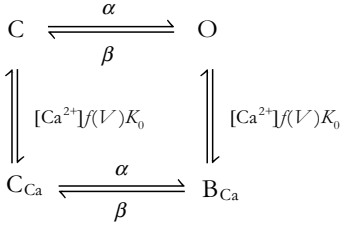

(Scheme 15)

where K_0 is the binding constant at $V = 0$ mV, B_{Ca} is the blocked state, and $f(V)$ is a function expressing the voltage dependence of the block as a Boltzmann relation:

$$f(V) = \exp(-z_{Ca} V \delta F R^{-1} T^{-1}), \tag{15a}$$

with z_{Ca} being the valence of the Ca^{2+} ion, and δ the fraction of the membrane voltage drop the ion traverses to reach the blocking site. Assuming that the voltage dependence of the activation and deactivation rate constants are described by Eqs. (6*a*, *b*) the open probability is

$$p_O = 1/[(1 + [Ca^{2+}]K_0 \exp(-V z_{Ca} \delta F R^{-1} T^{-1}))(1 + \exp(-(V - V_{eq})(z_\alpha + z_\beta) F R^{-1} T^{-1}))], \tag{15b}$$

$p_O(V)$ curves for different δ values (0·2, 0·5, and 1·0) are shown in Fig. 11. It is clear that the curves with a blocking distance of 0·2 (which is found experimentally for some ions, see Hanck & Sheets, 1992) deviate considerably from the normal S-shaped experimental curves. The bottom panel shows curves closer to the experimental ones, but the shifts are still too large. To get a shift of 21 mV at a 10-fold concentration increase of a divalent ion (found experimentally), we can calculate δ to be $\approx 1{\cdot}4$ [$\delta = \ln(10)\ RT/(Fz\Delta V)$]. Thus, a divalent cation has to traverse the entire membrane voltage drop plus 40%. This unacceptably large value was a major reason for Frankenhaeuser & Hodgkin (1957) to abandon the block mechanism to explain shifts as mentioned above. Another reason why this simple state-independent block mechanism does not hold is that the activation and deactivation time-courses are predicted to be unaffected by Ca^{2+} which clearly is not in agreement with the experimental findings. Furthermore, many

https://doi.org/10.1017/S0033583504003932 Published online by Cambridge University Press

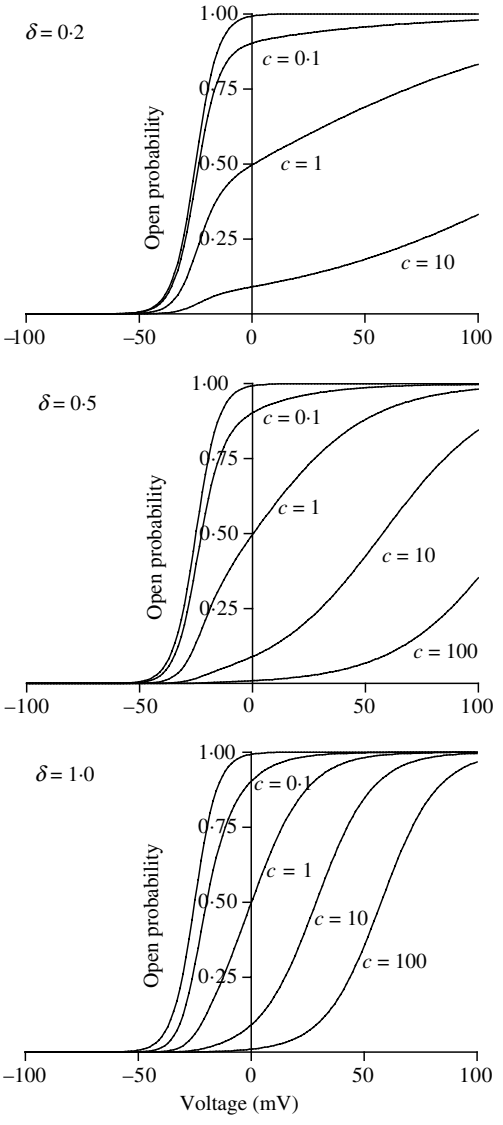

Fig. 11. Effect of a voltage-dependent pore block. Calculations based on Scheme 15 with $V_{eq} = -25$ mV, $z_{\alpha+\beta} = 5$ and where $c = K_0 \cdot [Ca^{2+}]$. The different curves correspond to solutions for different c and δ values as indicated in the figure.

investigations have found metal-induced shifts by measuring instantaneous tail-current amplitudes at a specific voltage – a procedure that automatically eliminates any voltage-dependent block.

5.4.2 Coupling pore block to gating

5.4.2.1 The basic model again

In spite of the implausibility of a simple pore-block model (see Section 5.4.1) as an explanation of the effects of Ca^{2+}, the close correlation between the induced block and the effects on the

https://doi.org/10.1017/S0033583504003932 Published online by Cambridge University Press

gating, and the assumed special role of Ca^{2+} in gating (e.g. Armstrong & Cota, 1991) have prompted a number of groups to explore different extended pore-binding models in which the block is associated with the gating; often thought of as changes in voltage-sensor motion. One of the more detailed models of this kind has been described by Boccaccio *et al.* (1998). Their study concerned Na channels and was based on the findings from TTX-binding experiments that Ca^{2+} shows state-dependent affinity, with better binding to closed states than to the open state ($K_C > K_O$). In state diagram terms it can be described as similar to Scheme 8:

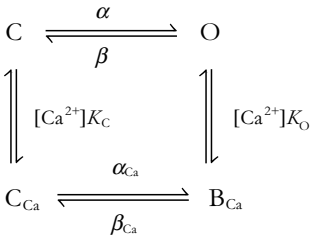

(Scheme 16)

The block can be voltage-dependent but does not necessarily have to be. An important property of this scheme (as well as for Schemes 8 and A 2) is that the magnitude of the shift depends on the slope of the $G(V)$ curve. Experimental support for this relation was found by Pusch (1990) in a study of Ca^{2+} on Na channels. The effect of Ca^{2+} on the wild-type channel closely follows the prediction of the Grahame equation [Eq. (1)], but the effect on a mutated channel (K226Q) deviates. This mutated channel is peculiar for two reasons: (i) Despite the fact that the mutation is located on the intracellular end of the voltage sensor S4, it has a relatively high effect on the Ca^{2+}-induced $G(V)$ shift, probably via a reduced slope of the $G(V)$ curve. (ii) The Ca^{2+}-induced shift is about 30 mV per 10-fold concentration increase and is consequently not explained by the Grahame equation (Fig. 5). However, it is well described by the pore-block model (Scheme 16) in combination with screening. Screening contributes with $\approx 1/3$ of the shift (Boccaccio *et al.* 1998). A similar kind of state-dependent pore-block effect on the voltage sensor has been described for the highly charged (+5) blocker of Na channels, conotoxin, which shifted $G(V)$ 6 mV (French *et al.* 1996).

5.4.2.2 A special case – Ca^{2+} as necessary cofactor for closing

A radical version of Scheme 16, assuming that Ca^{2+} must bind and block the pore for a K or a Na channel to close (i.e. $K_C \gg K_O$), has been proposed by Armstrong and colleagues (Armstrong & Lopez-Barneo, 1987; Armstrong & Cota, 1991, 1999; Armstrong, 1999). Thus, Ca^{2+} is necessary for normal functioning, stabilizing the channel in its closed conformation. Their version can be stated in the following state diagram:

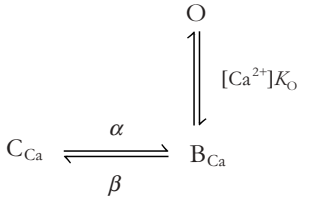

(Scheme 17)

As in Scheme 16, C_{Ca} is a closed state with a Ca^{2+} ion bound to the pore, B_{Ca} is an activated but blocked state – the main gate is open but the pore is blocked by a Ca^{2+} ion, and O is the

https://doi.org/10.1017/S0033583504003932 Published online by Cambridge University Press

open state. Binding is assumed to be much faster than the activation or deactivation. The fundamental feature of the model is that a Ca^{2+} ion has to block the pore to close the channel – Ca^{2+} functions as a gating particle. To get the Ca^{2+} effects on the closing time-course we reduce Scheme 17 to

$$C_{Ca} \underset{\beta/(1+1/([Ca^{2+}]K_O))}{\overset{\alpha}{\rightleftharpoons}} \{O + B_{Ca}\}, \qquad \text{(Scheme 18)}$$

where $\{O+B_{Ca}\}$ is the set of Ca^{2+} bound (closed) and unbound (open) activated states. Armstrong and colleagues (Armstrong & Cota, 1999; Armstrong, 1999) argue that this model better describes the closing process than other models. They support their arguments by experiments in which the specific pore blocker saxitoxin makes the gating currents insensitive to Ca^{2+}. Similarly, both saxitoxin and the related pore blocker tetrodotoxin displace a divalent cation from the external opening of the Na channel, thereby producing a voltage offset sensed by the channel-gating apparatus (Heggeness & Starkus, 1986). Taken together, this suggests that a pore site is important for the Ca^{2+}-induced effects on gating (Armstrong, 1999). Even though the saxitoxin-induced Ca^{2+} insensitivity is a strong argument for Scheme 18, this does not seem to be a general finding. For instance, the related pore blocker tetrodotoxin does not prevent Ca^{2+}-induced shifts of gating currents in Na channels (Hahin & Campbell, 1983). Pore block of Keag channels with TEA allows measurements of gating currents (Tang *et al.* 2000). Despite the pore block, $Q(V)$ is clearly shifted by Mg^{2+}. Also, contrary to the calculations presented by Armstrong & Cota (1999), a screening model not including pore block can be shown to increase the closing rate appropriately.

5.4.2.3 Expanding the basic model – Ca^{2+} affecting a voltage-independent step

The idea of Ca^{2+} as a necessary cofactor in K channel function has been advocated by Armstrong and colleagues in a number of studies (Armstrong & Matteson, 1986; Armstrong & Lopez-Barneo, 1987; Armstrong & Miller, 1990), even though a detailed reanalysis shows that Ca^{2+} binding to the pore is not necessary for closing K channels (Hong *et al.* 2001). Nevertheless, a follow-up study, investigating gating and ion currents in parallel, shows that Ca^{2+} speeds up the closing rate in a first voltage-sensor independent step (Gomez-Lagunas *et al.* 2003), thus in a way not explained by screening or direct voltage sensor models. In pore-block terms the suggested model can be seen as an extended version of Scheme 16:

$$\begin{array}{ccccc} C & \underset{\beta}{\overset{\alpha}{\rightleftharpoons}} & C_A & \underset{\lambda}{\overset{\kappa}{\rightleftharpoons}} & O \\ \Big\Updownarrow [Ca^{2+}]K_C f(V) & & \Big\Updownarrow [Ca^{2+}]K_C f(V) & & \Big\Updownarrow [Ca^{2+}]K_O f(V) \\ C_{Ca} & \underset{\beta}{\overset{\alpha}{\rightleftharpoons}} & C_{A,Ca} & \underset{\lambda^*_{Ca}}{\overset{\kappa^*_{Ca}}{\rightleftharpoons}} & B_{Ca} \end{array} \qquad \text{(Scheme 19)}$$

where C_A denotes a non-conducting state with the voltage sensor in an activated position. κ and λ are voltage-independent opening and closing rate constants, where $\lambda^*_{Ca} > \lambda$ and $\kappa > \kappa^*_{Ca}$. The block is state-dependent (as in Scheme 16) with the channel showing better affinity in

https://doi.org/10.1017/S0033583504003932 Published online by Cambridge University Press

the open state. The block is also voltage dependent [$f(V)$ from Eq. (15*a*)]. Scheme 19 can be reduced to the following three-state model:

$$\{C\} \underset{\beta}{\overset{\alpha}{\rightleftharpoons}} \{C_A\} \underset{\lambda_{Ca}}{\overset{\kappa_{Ca}}{\rightleftharpoons}} O + B_{Ca}, \qquad \text{(Scheme 20)}$$

where κ_{Ca} and λ_{Ca} are

$$\kappa_{Ca}(V) = (\kappa + [Ca^{2+}]K_C\kappa^*_{Ca}\exp(-V z_{Ca}\delta FR^{-1}T^{-1}))/(1 + [Ca^{2+}]K_C\exp(-V z_{Ca}\delta FR^{-1}T^{-1})), \qquad (20a)$$

$$\lambda_{Ca}(V) = (\lambda + [Ca^{2+}]K_C\lambda\kappa^*_{Ca}/\kappa\exp(-V z_{Ca}\delta FR^{-1}T^{-1}))/(1 + [Ca^{2+}]K_C\lambda\kappa^*_{Ca}/(\kappa\lambda^*_{Ca}) \exp(-V z_{Ca}\delta FR^{-1}T^{-1}). \qquad (20b)$$

Using reasonable parameters (e.g. $\lambda^*_{Ca} = 5\lambda$ and $\kappa^*_{Ca} = \kappa/5$ yielding 25 $K_O = K_C$; $\delta = 0{\cdot}3$) we can show that the Ca^{2+} at high concentrations clearly increases λ_{Ca} while κ_{Ca} is almost unchanged. The gating currents (generated by the voltage-dependent α/β transition) are unaffected. This model shows several similarities with the model presented by Gomez-Lagunas *et al.* (2003). The model also suggests an explanation to the reported behaviour of Ba^{2+} on K channels. Ba^{2+} destabilizes the open state and greatly slows down the opening (Armstrong & Taylor, 1980; Harris *et al.* 1998), and it is assumed to bind tightly in the channel pore, behind the slow inactivation gate (Basso *et al.* 1998; Harris *et al.* 1998; Jiang & MacKinnon, 2000). While the opening is greatly affected, the ON gating currents are hardly affected (Hurst *et al.* 1997). The open channel is blocked by Ba^{2+} at a return to negative voltages (voltage-dependent block). The Ba^{2+} ion now makes the OFF gating current much faster than if Ca^{2+} was present rather than Ba^{2+} (Hurst *et al.* 1997).

5.5 Summing up

In the aftermath of the work by Frankenhaeuser & Hodgkin (1957), it has become clear that most metal ions induce effects that can be described in terms of shifts of voltage-dependent parameters. The shifts may be ion specific and may differ for activation and inactivation parameters, and for different channels. We have discussed above principal mechanisms suggested in the literature explaining these effects. The models presented are summarized in Table 2.

The first mechanism described (Mechanism A) assumes electrostatic screening of fixed charges. The version discussed is the classical version of this mechanism, assuming that the fixed charges are distributed and can be approximated as a smeared layer. This version predicts equal shifts of all voltage-dependent parameters, the size of the shift depending on the fixed charge density, which differs for different channel types. This applies to the effect of group 2 ions like Mg^{2+} and Sr^{2+} on most channels.

The second mechanism discussed (Mechanism B) assumes binding and an accompanying electrostatic effect on the voltage sensor. We discussed both the classical approach, assuming distributed binding sites in a smeared layer and a one-binding-site model. Assuming binding to a smeared layer of charges predicts equal shifts of all parameters as in Mechanism A, but larger in magnitude. This version of Mechanism B explains the differential shifting by some group 2 ions and some transition metals. Assuming binding to a single site predicts different shifts of

https://doi.org/10.1017/S0033583504003932 Published online by Cambridge University Press

Table 3. *Summary of experimental data*

	c_{10} (mM)			A			K_d (mM)			
	Kv	Keag	Na	Kv	Keag	Na	Kv	Keag	Na	References
Group 2										
12. Mg^{2+}	16	2	8	1·0	30	1·1	⩾20			1–11
20. Ca^{2+}	9	1·8	4	1·0	1·0	1·0			35	1, 3, 7–24
38. Sr^{2+}	21*	2	7	1·0		1·1	⩾50	6·4	10	7, 10–12, 26, 38–40
56. Ba^{2+}	5	0·13	5			1·2	30	1·7	37	7, 8, 10, 11, 19, 26, 38, 43
Transition elements										
25. Mn^{2+}	4·5	0·3	2·0	1·2			⩾10	73	10	8, 10, 12, 19, 25–27
27. Co^{2+}	2·3	0·07	2·0	1·2	1·0	1·0	10[b]	20	13	1, 8, 10, 12, 18, 19, 25, 26, 28
28. Ni^{2+}	1·9	0·06	1·2	1·6		2	30		17	1, 8, 10, 12, 13, 19, 24, 25–26, 29
29. Cu^{2+}	0·1[a]		0·2	1·5		1·0	⩾0·1		⩾0·1	1, 16, 25
Group 12										
30. Zn^{2+}	0·03*	0·2	1·5*	3·1		1·5	0·25*	0·7	0·9*	1, 8, 10, 12, 13, 16, 19, 25–27, 30–37
48. Cd^{2+}	0·25	0·3	0·2	1·8			⩾1		0·9*	1, 8, 12, 16, 17, 19, 25, 27, 31, 34, 41, 42
Lanthanides										
57. La^{3+}	0·1*	0·0001	0·08	1·5	3	1·5	0·1*	>0·01	0·5	8, 11, 16, 18, 19, 38, 44–47
58. Ce^{3+}	0·02			2·2			0·028			44
59. Pr^{3+}	0·02						0·022			44
60. Nd^{3+}	0·02			3·1			0·011			44
62. Sm^{3+}				3·2			0·007			44
64. Gd^{3+}	0·001[c]		0·1	5		2·5	0·06		0·03	16, 44, 48, 49
66. Dy^{3+}	0·001			3·5			0·005			44
68. Er^{3+}	0·001			4			0·004			44, 50
70. Yb^{3+}				4			0·003			44
71. Lu^{3+}	0·001			4			0·003			44
82. Pb^{2+}	0·025						⩾0·1			16, 51, 52

Collected experimental data. c_{10} represents the concentration that shifts $G(V)$ with 10 mV. A represents the slowing factor for activation and deactivation curves. K_d is the concentration that blocks 50% of the current at 0 mV when corrections for the $G(V)$ shift have been made. Kv denotes voltage-gated K channels (cloned, Kv1–4, and native, delayed rectifier and A-type). Keag denotes ether-à-go-go-related K channels. Na denotes Na channels. The data are mean values from 1 to 13 investigations.

* Indicates that there is a large scatter in data, i.e. a factor >10 between the smallest and the biggest value. The table notes indicate that two very different values are found in the literature (in mM): [a] 0·004 and ⩾0·2; [b] 1 and ⩾10; [c] 0·00002 and 0·1.

References: 1, Agus *et al.* (1991); 2, Yao *et al.* (1995); 3, Brismar & Frankenhaeuser (1972); 4, Elinder & Århem (1998); 5, Elinder *et al.* (2001a); 6, Terlau *et al.* (1996); 7, Cukierman & Krueger (1990); 8, Hanck & Sheets (1992); 9, Hahin & Campbell (1983); 10, Hille *et al.* (1975); 11, Brismar (1980); 12, Paquette *et al.* (1998); 13, Arkett *et al.* (1994); 14, Brismar (1973); 15, Moore (1971); 16, Talukder & Harrison (1995); 17, Johnson *et al.* (1999); 18, Sanchez-Chapula & Sanguinetti (2000); 19, Sheets & Hanck (1992); 20, Armstrong & Cota (1991); 21, Armstrong & Cota (1999); 22, Boccaccio *et al.* (1998); 23, Chahine *et al.* (1992); 24, Hille (1968); 25, Århem (1980b); 26, Ho *et al.* (1999); 27, Visentin *et al.* (1990); 28, Fan & Hiraoka (1991); 29, Mozhayeva & Naumov (1970); 30, Boland *et al.* (1994); 31, Kuo & Chen (1999); 32, Kehl *et al.* (2002); 33, Harrison *et al.* (1993a, b); 34, Huang *et al.* (1993); 35, Spires & Begenisich (1994); 36, Stanfield (1975); 37, Anumonwo *et al.* (1999); 38, Århem (1980a); 39, Elinder *et al.* (1998); 40, Elinder *et al.* (1996); 41, Wickenden *et al.* (1999); 42, DiFrancesco *et al.* (1985); 43, Weerapura *et al.* (2000); 44, Enyeart *et al.* (1998); 45, Mozhayeva & Naumov (1973); 46, Armstrong & Cota (1990); 47, Neumcke & Stämpfli (1984); 48, Elinder & Århem (1994a); 49, Gui-Rong & Baumgarten (2001); 50, Starzak & Starzak (1978); 51, Madeja *et al.* (1997); 52, Madeja *et al.* (1995).

activation and deactivtion rate curves, as experimentally found for the transition metals Ni^{2+} and group 12 ions Zn^{2+} and Cd^{2+}. A special group of one-site-binding models, assumes binding to the pore, thereby blocking the ion permeation (Mechanism D). This mainly applies to Ca^{2+} (and Ba^{2+}), but has nevertheless been very influential in the field of modelling metal ion effects and has, therefore, been assigned a separate model in the present study.

Finally, we introduce a mechanism (Mechanism C) assuming binding and an accompanying non-electrostatic effect on the gating, either on the voltage sensor or on some other part of the gating mechanism. We argue that for the lanthanides La^{3+} and Gd^{3+} and possibly also Zn^{2+}, the one-site version of this mechanism has to be invoked in combination with an electrostatic mechanism (Mechanism B) to explain all the results. This last model is thus a hybrid model, combining mechanical and electrostatic action on the voltage sensor (Mechanisms B and C), and can be seen as a general model, explaining most experimental data covered in the present review. Specific models can be seen as special cases of this general model. This model thus provides the rationale for using the shift-and-scaling procedure in the following attempt to summarize the diverse experimental results into a common quantitative framework.

6. Quantifying the action: comparing the metal ions

The metal-ion-induced effects differ between ion species, between channels, and between parameters. The largest differences (a factor of $>10^5$, see Table 3) are found between the effects of different ion species, while the effects of a specific metal ion on different channels within the same family are in most cases within a factor of 10. The following comparative analysis of the effects will therefore be ion-species oriented. However, to simplify the analysis we will first consider the relation between effects on steady-state activation, $G(V)$, and on steady-state inactivation, $G(V_{PP})$.

6.1 Steady-state parameters are equally shifted

The shift of the $G(V)$ curve has been reported to be both larger than (Frankenhaeuser & Hodgkin, 1957; Hille, 1968; Vogel, 1974; Schauf, 1975) and equal to (Ohmori & Yoshii, 1977; Hahin & Campbell, 1983; Elinder & Århem, 1994a) that of the $G(V_{PP})$ curve. Figure 12 shows the results from a comparative analysis of the shifts of the $G(V)$ and $G(V_{PP})$ curves for different metal ions and different channels collected from 17 studies in the literature. Somewhat unexpectedly, there is a close to 1:1 relation, implying that the $G(V)$ and $G(V_{PP})$ curves are shifted equally and that that the reported differences are exaggerated. For some ion species even other parameters, such as the time constants for activation, deactivation, and inactivation are shifted equally to the steady-state parameters. This seems to be the case for ions such as Mg^{2+}, Sr^{2+}, and in some cases Ca^{2+} (Hahin & Campbell, 1983; Behrens *et al.* 1989; Elinder *et al.* 1996, 1998). Thus, we conclude that the shift effect is rather homogenous for $G(V)$ and $G(V_{PP})$, making the interesting differences dependent on ion species and channel type, rather than on kinetic parameters. In the quantitative evaluation of steady-state shifts below, we therefore found it appropriate to rely mainly on measurements of $G(V)$ curves.

In the quantitative comparison between the different metal ion species we have classified the channels in three main families: (1) Kv channels, comprising native delayed rectifier and A-type K channels, and cloned Kv1–4 K channels; (2) Keag channels, comprising cloned eag-type HERG and eag K channels; and (3) Na channels, comprising native and cloned Na

https://doi.org/10.1017/S0033583504003932 Published online by Cambridge University Press

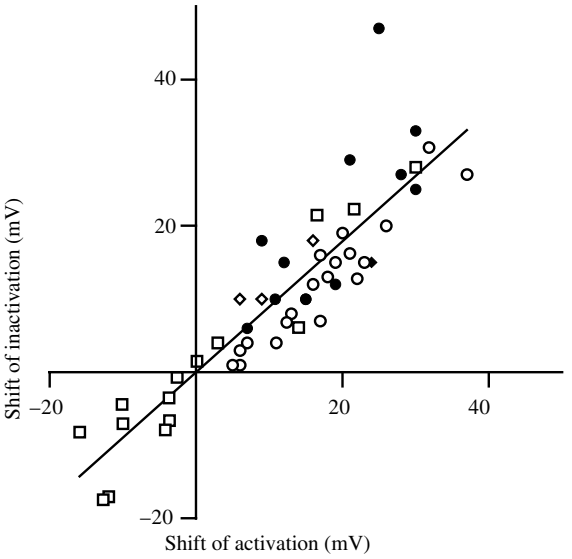

Fig. 12. Relation between experimental shifts of steady-state inactivation and steady-state activation curves for monovalent ions (squares), for divalent cations (circles), and for trivalent cations (diamonds). Open symbols indicate measurements on voltage-gated Na channels, and closed symbols on voltage-gated K channels. The least-squares fitted line has a slope of 0·89. (data taken from Chandler *et al.* 1965; Hille, 1968; Hille *et al.* 1975; Dani *et al.* 1983; Hahin & Campbell, 1983; Neumcke & Stämpfli, 1984; Rack & Woll, 1984; Rack & Drews, 1989; Lönnendonker *et al.* 1990; Visentin *et al.* 1990; Agus *et al.* 1991; Hanck & Sheets, 1992; Harrison *et al.* 1993a, b; Elinder & Århem, 1994a; Talukder & Harrison, 1995; Benitah *et al.* 1997; Elinder *et al.* 1998; Enyeart *et al.* 1998.)

channels from heart, muscle and nerve. The reason for separating Keag from Kv is that the two families demonstrate very different sensitivities to several metal ions. We have not included data for Ca channels in this comparison. The reason is that most studies dealing with metal ion effects on Ca channels focus on pore block, and it is difficult to extract data on gating effects from such studies. Ca channels are easily blocked by several di- and trivalent cations because of their high affinity for Ca^{2+} (exemplified by La^{3+}, having an IC_{50} value of 22 nM; Block *et al.* 1998). In Table 1, we present the 37 di- and trivalent metal ion species that should be possible to be investigated electrophysiologically. We have found useful data for 21 of them. Data from 52 studies are summarized in Table 3.

6.2 Different metal ions cause different shifts

To quantify the ability of metal ions to shift voltage-dependent parameters we have chosen to specify the concentration that, when *added* to the extracellular solution as a chloride salt, shifts the activation curve, $G(V)$, with +10 mV [or the inactivation curve, $G(V_{PP})$, if information for the activation curve is lacking]. This value we call c_{10}. If c_{10} was not possible to obtain by intrapolation, we extrapolated from values in the 5–30 mV range and assumed 22 mV shift per ten-fold concentration increase of a divalent ion, or 15 mV per ten-fold concentration increase of a trivalent ion (see Fig. 4*d*). In Fig. 13 we have plotted c_{10} for Na, Kv, and Keag channels against atomic number. A distinct pattern is evident. In general, the effects on the three channel families show a similar pattern, with Keag being the most sensitive and Kv the least.

https://doi.org/10.1017/S0033583504003932 Published online by Cambridge University Press

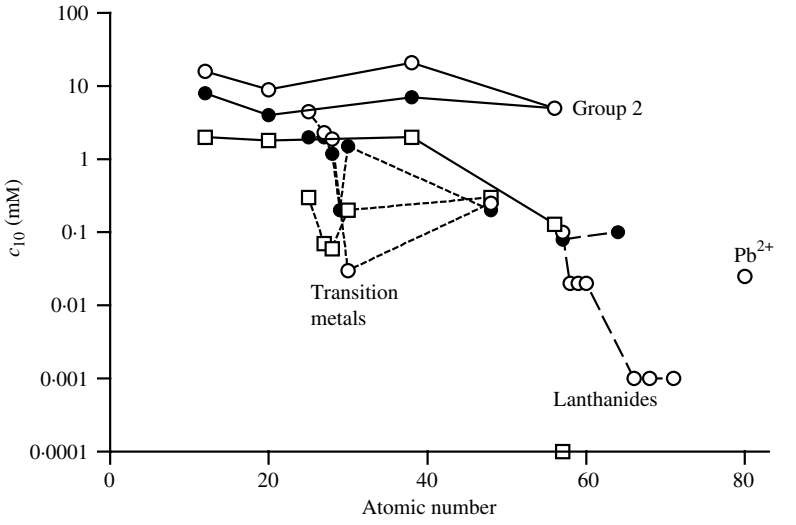

Fig. 13. Concentrations that shift steady-state $G(V)$ 10 mV (c_{10}) *versus* atomic number. Measurements on Na channels (filled circles), on Kv channels (open cirles), and on Keag channels (open squares). Values for group 2 ions are connected with continuous lines, for transition elements including Zn^{2+} and Cd^{2+} with short-dashed lines, and for lanthanides with long-dashed lines.

Concerning the efficacy of the ion species, group 2 ions induce the smallest shifts (continuous line, $c_{10} \approx 1$–10 mM), the transition and group 12 elements induce larger shifts (dotted line, $c_{10} \approx 0{\cdot}03$–3 mM), and the lanthanides the largest shifts (dashed line, $c_{10} \approx 0{\cdot}001$–0·1 mM). Pb^{2+} is the most effective divalent ion (0·03 mM). The results can be summarized in the following sequence:

Group 2 — Transition metals — Group 12 — Lanthanides — Pb^{2+}

$$\underline{Mg^{2+} = Sr^{2+} < Ba^{2+} = Ca^{2+}} < \underline{\mathbf{Mn^{2+} < Co^{2+} < Ni^{2+}}} < \underline{\mathbf{Zn}^{2+} = \mathit{Cd}^{2+}} = \underline{La^{3+} < \ldots < Lu^{3+}} > \underline{\mathbf{Pb}^{2+}}$$

The simplest explanation to the order of this sequence is that the lower ranked metals affect the channels by pure screening (Mechanism A described in Section 5) and that the higher ranked metals affect the channels also by binding (Mechanisms B and C), either close to the voltage sensor or in the pore (Mechanism D). The sequence closely follows the Irving–Williams series and the hard–soft characteristics of metal ions (mentioned in Section 3). These series reflect the tendency to form complexes for a given ligand. In the sequence above the hard–soft characteristics are indicated by different founts (hard in roman, **borderline** in bold, and *soft* in italicized style). The reason for the high potency of the lanthanides is probably partly due to their trivalency. If the effect only reflects a tendency for complex formation we would expect approximately the same order for different metal ions on the different channels. However, this is not the case for all metal ions.

For the *group 2* metal ions the effects are relatively similar within each channel family, and thus the relation between the channel families for specific ions are relatively fixed. The effect is mainly of electrostatic nature as expected from the hard characteristic of the ions in this group. The only exception from this is Ba^{2+} on the HERG channel that is unusually potent with a c_{10} of $\sim$100 μM (Weerapura *et al.* 2000). However, the concentration dependence is only $\sim$5 mV shift

https://doi.org/10.1017/S0033583504003932 Published online by Cambridge University Press

per decade, in contrast to 20–25 mV for most other ions. This may reflect another mechanism for Ba^{2+} on Keag than for the other ions. For the *transition* metal ions the relation between the ion channel families is relatively constant, but there is a clear trend in increased shift (i.e. lower c_{10}) with increased atomic number. Binding of borderline and soft ions probably depends on the orbital structure rather than charge. The binding is due to filled or half filled d-orbitals. For *group 12* metal ions the differences between the channel families seen for *group 2* metals and transition metals is radically different. Zn^{2+} is $\sim$100 times more effective in shifting $G(V)$ for Kv channels than for Na channels, whereas Cd^{2+} has similar effects on all channels seen in the present review. Furthermore, Zn^{2+} shows largest differences within each channel family – two Kv channels could have different sensitivity to Zn^{2+}. This suggests that some K channels have a specific Zn^{2+}-binding site, probably containing suitably located cysteines and histidines (see also Section 7). The *lanthanides*, with hard ion characteristics, show increasing shift effects with increasing atomic number. The reason for this is probably that the ions with the higher atom numbers have a smaller radius (the lanthanide contraction), thus making them bind stronger and closer to the site of action.

6.3 Different metal ions slow gating differently

Comparing experimental data in the literature we find that some ions greatly slow down the activation kinetics – much more than what is expected from the shift of $G(V)$. To get information on the underlying molecular mechanisms we quantified the effect by determining the slowing factor (A) for different ions from the experimental data described in the literature (see shift-and-scaling procedure in Section 5.3.1; Figs. 9 and 10; Elinder & Århem, 1994a, b). Because the A values are concentration-dependent we tried to obtain the A values at the highest possible concentrations.

The slowing effect differs very much for different metal ions. The *group 2* elements have values close to 1, indicating no or small affinity to the gating mechanism of the channel. The *transition* elements show slightly higher values (1·2–1·6 for Kv channels), and the Zn group (*group 12*) even larger (1·8 and 3·1). The highest values were shown by the lanthanides (1·5–5). Figure 14*a* shows the slowing factor A for several metal ions on Kv channels plotted against the number of electrons in the d- and f-shells respectively. For the transition elements the slowing factor increases abruptly at the end of the series. Zn^{2+} peaks with a value of 3·1. In contrast, the values for the lanthanides increase sharply at the beginning of the series (from 1·5 for La^{3+} to 3·1 for Nd^{3+}) to level out at $\sim$4. The A value is negatively correlated to the diameter of the ion as shown in Fig. 14*b*. An equation of the type $A = C/r^2$, where r is the radius and C is a constant, fits well with the experimental data (see Fig. 14*b*) suggesting that the surface area-to-charge ratio is important for the effects of the lanthanides. (Similarly, the rank order of efficacies of lanthanides to potentiate the GABA responses correlates inversely with the hydrated ionic radii; Ma & Narahashi, 1993.) There is also a clear relation between the shift and the slowing factor (Fig. 14*c*), suggesting a common site of action. Keag gating kinetics is extremely sensitive to divalent cations in the extracellular solution (Terlau *et al.* 1996). The series of efficacy is $Sr^{2+} < Ba^{2+} < Zn^{2+} < Mg^{2+} < Mn^{2+} < Co^{2+} < Ni^{2+}$, which approximately follows hydration enthalpy (Terlau *et al.* 1996). However, this series deviates from our series, primarily in the position of Zn^{2+}, suggesting that the eag binding site may be distinct from the slowing (and shifting) site on Kv channels.

https://doi.org/10.1017/S0033583504003932 Published online by Cambridge University Press

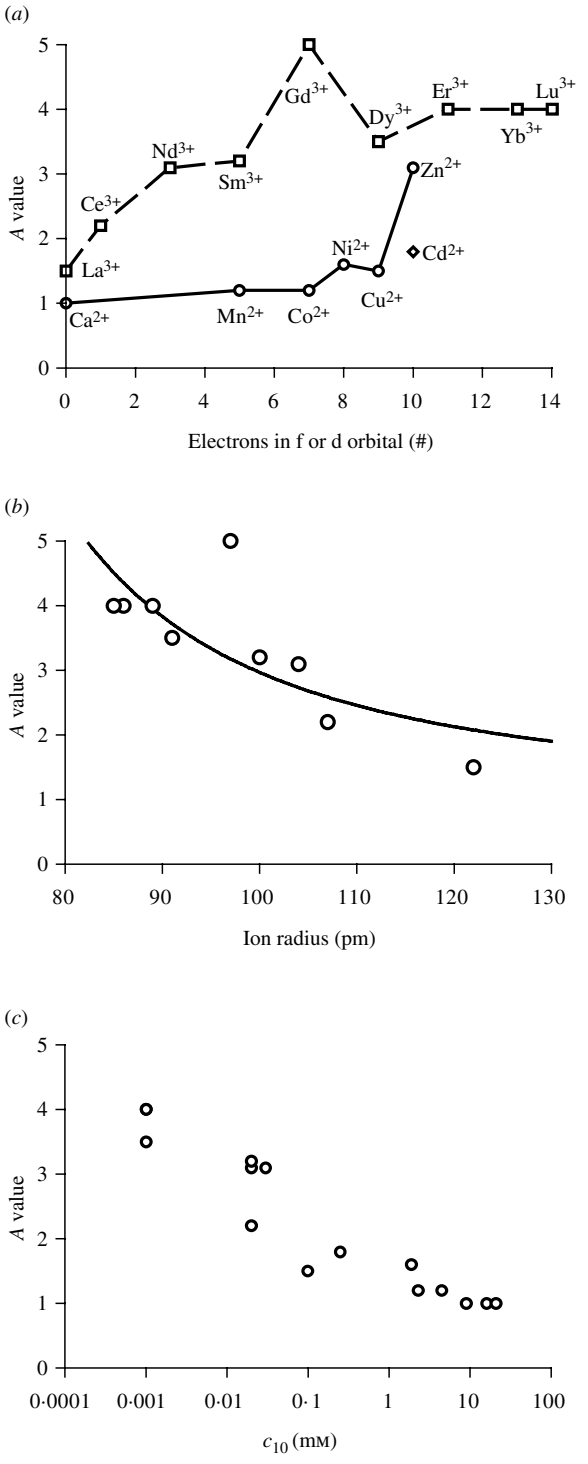

Fig. 14. Slowing factor (A) dependence on metal ion properties. Values derived from rate *versus* voltage curves of Kv channels. (*a*) Slowing factor *versus* electrons in f- or d-orbitals. Values from Table 3. (*b*) Slowing factor *versus* ion radius. Continuous line is $A = C/r^2$, where r is the radius and C is a constant = 10 900 pm^2. (*c*) Slowing factor *versus* c_{10}. Note the almost linear relation.

https://doi.org/10.1017/S0033583504003932 Published online by Cambridge University Press

6.4 Block of ion channels

Many metal ions also block the ion channels. Even though channel block as such is not a focus of the present review, we have included data in Table 3. For group 2, transition metals and group 12 ions, Kv channels (and Keag) need much higher concentrations to block the channels than to shift them (more than 100-fold), suggesting a lose connection, if any, between the block and the shift. For the same ions, the shift and block of Na channels shows a closer connection (less than 10-fold). This opens for the possibility that the pore block could cause part of the shift effect seen in Na channels. For lanthanides on Kv channels there is an even closer connection; the same concentration that shifts $G(V)$ by 10 mV also blocks the channel ~50%. Thus, the lanthanides, serving as 'super calcium', could also in part shift the $G(V)$ by blocking the channel. However, a strong correlation does necessarily imply a causal relation; it could also reflect a general propensity of the ion to bind to the channel protein.

7. Locating the sites of action

The screening (Mechanism A) and to some extent the binding (Mechanism B) models described above are based on the idea of the existence of fixed surface charges. Where are these critical charges located? Three types of groups have been at the centre of discussions (e.g. Green & Andersen, 1991): (1) charged phosphate groups either as phospholipids or as phosphorylated amino acids, (2) charged oligosaccharides (with sialic acid groups) fixed to the membrane lipids or to the channel protein, or (3) charged amino-acid residues of the channel protein itself. We will argue that charged amino-acid residues are the most important and we will focus our discussion on the role of specific residues. The reasons for not dealing with the other alternatives are as follows:

(i) If charged membrane phospholipids are the most important source for functional surface charges, then different channels in a specific expression system should be equally sensitive to a specific metal ion. This is not the case – approximately a 10 times higher concentration of Sr^{2+} is needed to shift the $G(V)$ curve for Kv3.4 equally as much as for Kv1.1, both heterologously expressed in oocytes from *Xenopus laevis* (Elinder *et al.* 1996). Other investigations, where the lipid bilayer has been changed (with respect to charge), also suggest that the lipid bilayer is of minor importance for the metal ion effect (Moczydlowski *et al.* 1985; Green *et al.* 1987; Cukierman *et al.* 1988; Cukierman, 1991). Phosphate groups on the intracellular side are little studied, but could play a role for the effect of intracellular metal ions, but not for the extracellular effects (Perozo & Bezanilla, 1990, 1991; see Fozzard & Hanck, 1996).

(ii) Most ion channels are glycosylated and comprise charged sialic acid groups. The contribution of sialic acids to surface-charge density, surface potential and Me^{n+}-induced $G(V)$ shifts varies from 0 to 50% in different studies. In Na channels, sialic acid residues on the N-linked carbohydrate side-chains contribute with a considerable fraction to the surface charge (Recio-Pinto *et al.* 1990; 25–50%). For K channels, the contribution is in most cases lower. For instance, site-directed mutagenesis studies have suggested that N-glycosylation exerts negligible effects on gating of Shaker K channels (Deal *et al.* 1994; Santacruz-Toloza *et al.* 1994), and the Kv1.6 channel, lacking putative N-glycosylation sites, is highly sensitive to Sr^{2+} (Elinder *et al.* 1996), suggesting that amino-acid residues are important. In contrast, N-glycosylation accounts for 40% of the surface-charge density in Kv1.1 channels (Watanabe *et al.* 2003).

https://doi.org/10.1017/S0033583504003932 Published online by Cambridge University Press

Thus, it seems likely that the critical charges are charged residues (the positive lysine, arginine, and histidine or the negative glutamate and aspartate) on the channel protein. In addition, cysteine has been shown to be important for binding some ion species.

7.1 Fixed surface charges involved in screening

To analyse the location of the critical charges for screening effects, it is natural to focus on ions exerting almost pure screening with minimal binding effects. For this reason we here chose the group 2 ions Mg^{2+} and Sr^{2+} (Hille *et al.* 1975; Cukierman & Krueger, 1990; Elinder *et al.* 1996, 1998; Elinder & Århem, 1998). Addition of 20 mM Mg^{2+} (+40 mM Cl^-) to Shaker K channels in a normal frog Ringer's solution shifts $G(V) \sim 14$ mV (Elinder *et al.* 2001a), implying that the surface potential around the voltage sensor is approximately −50 mV [Eq. (1) or (2)]. c_{10} values for Mg^{2+} and Sr^{2+} on a series of wild-type Kv channels expressed in *Xenopus* oocytes ranged from 6 to 100 mM (Elinder *et al.* 1996, 1998; Elinder & Århem, 1998). A correlation analysis, comparing experimentally estimated surface-charge densities with the number of charged residues in the extracellular linkers, suggested that the critical charges are located in the N-terminus of the extracellular S5-P loop. Special attention was paid to a conserved glutamate and its neighbour, at the extracellular end of S5, that varies in charge for different clones (Elinder & Århem, 1999; E418 and A419 in Shaker). Channels with a neutral residue in position 419 (Kv1) are highly sensitive to Mg^{2+} or Sr^{2+}, while the channels with a positive residue (Kv2 and Kv3) are less sensitive. In a mutational analysis we found that E418 adds −15 mV to the surface potential at the voltage sensor S4 and that a charge at 419 adds ±8 mV depending on the valence of the residue (Elinder *et al.* 2001a, b). Thus, 418 could explain 30% of the estimated surface potential, and consequently only 30% of the Me^{2+}-induced shift [see Eq. (2)]. Other studies have failed to find any charged residues affecting the voltage sensor (e.g. MacKinnon & Miller, 1989; Mathur *et al.* 1997; F. Elinder & H. P. Larsson, unpublished results). So, where are the charges contributing to the remaining 70% located?

There are several possible solutions to this paradoxical situation. One is that the negative surface potential is induced by mechanisms other than charged residues. The peptide bonds are polar (Åqvist *et al.* 1991) and are in most proteins oriented with the negative end to the exterior (Gunner *et al.* 2000). This could explain the positive shifts for all types of channels even though they have positively charged side-chains. Another possible solution is that the location of the extracellular charges depend on each other in a critical, self-regulatory way. Removing or neutralizing a charged residue in this model modifies the location so that the surface potential at the voltage sensor is compensated for; perhaps by decreasing the distance to the voltage sensor S4. Such a model would explain the finding that the extracellular linkers in Kv1.2 interact to induce a Mg^{2+}-dependent shift (M. Madeja, F. Elinder & P. Århem, unpublished observations).

7.2 Binding sites

Compared to the screening models (Mechanism A), binding models (Mechanism B) have been less investigated with respect to the molecular site of action. The group 2 ions and the transition elements mainly screen or bind to the fixed charges discussed above, and affect the voltage sensor by classical electrostatics. For some channels, however, Mg^{2+} seems to have additional direct (mechanistic) effects on the voltage sensor (Mechanism C), possibly by a tight binding close to the voltage sensor. Ca^{2+} and Ba^{2+} also form a special subgroup within group 2 by having

https://doi.org/10.1017/S0033583504003932 Published online by Cambridge University Press

binding sites inside the pore (Mechanism D). Otherwise, binding associated with direct, non-electrostatical effects (Mechanism C) on the voltage sensor, seems to be restricted to group 12 and the lanthanides. In spite of extensive investigations of metal-complex formation (especially Zn^{2+} complexes), relatively little is known about the molecular nature of these binding sites on ion channels. Overall, similar to other studies of toxin binding (French *et al.* 1996; Swartz & MacKinnon, 1997), the studies of metal binding suggest two critical locations, inside the channel pore (one binding site per channel) and in the neighbourhood of the voltage sensor (i.e. four binding sites per channel).

7.2.1 Group 2 ions

Both binding close to the voltage sensor and in the pore have been reported. In both cases negatively charged glutamate and aspartate residues are critical for binding. Mg^{2+} has a profound effect on Keag activation kinetics, but leaves the closing kinetics unaffected (Terlau *et al.* 1996; Tang *et al.* 2000). Negative charges unique to Keag family members, located in transmembrane segments S2 (287 in Shaker) and S3 (324 in Shaker), contribute to the Mg^{2+}-binding site (Silverman *et al.* 2000, 2003). These charges are close to the negative counter charges interacting with positive S4 charges. Binding thus affects S4 movement. This is a strong argument for a binding site outside the pore. A Ca^{2+}-binding site in the S4 region has been reported in the HERG channel. Residues in the S3–S4 loop are critical, the binding being stronger at closed states than at open (Johnson *et al.* 2001). A β-subunit in Ca channels is important for the sensitivity of modulatory effects of extracellular Ca^{2+} (Cens *et al.* 1998). Because this subunit is probably located in the periphery of the channel this also suggests that the voltage sensor is located in the periphery, as has been proposed (Elinder *et al.* 2001a; Broomand *et al.* 2003; Jiang *et al.* 2003a, b). Mg^{2+}, Ca^{2+} and Ba^{2+} all have binding sites in the pore. A glutamate in the pore of a Kir channel is critical for intracellular Mg^{2+} block (Lu & MacKinnon, 1994; equivalent to residue 470 in the Shaker K channel). Glutamate and aspartate residues inside the pores of Na, K and Ca channels are critical for Ca^{2+} binding (Heginbotham *et al.* 1992; Heinemann *et al.* 1992b; Root & MacKinnon, 1993, 1994; Eismann *et al.* 1994; Favre *et al.* 1995; Yang *et al.* 1995). Ba^{2+} strongly binds inside the pore of K channels by substituting for equally sized K^+ ions in the selectivity filter (Armstrong & Taylor, 1980; Hurst *et al.* 1995; Harris *et al.* 1998). It is not clear if any of the pore-binding sites affects gating and $G(V)$. Other binding sites on ion channels also exist. High-affinity Ca^{2+}-binding structures, such as EF-hands, have been located on the C-terminus of the α_{1C}-subunit in the L-type Ca channel, and have been suggested to be involved in the Ca^{2+}-dependent inactivation (de Leon *et al.* 1995).

7.2.2 Group 12 ions

Zn^{2+} and other members of *group 12* (i.e. Cd^{2+} and Hg^{2+}) are known to bind to cysteines, histidines and aspartates. Also for this group, sites close to the voltage sensor and sites in the pore have been suggested. In Scheme 12, Zn^{2+} is suggested to bind close to the voltage sensor (Gilly & Armstrong, 1982a, b). In the absence of cysteines and histidines, glutamate and aspartates can serve as sites of action. The mutation E454Q in Kv1.5 decreases the affinity for Zn^{2+} ten-fold (Talukder *et al.* 1995). E454 is homologous to E418 in Shaker, which is located close to the voltage sensor (Elinder *et al.* 2001b; Broomand *et al.* 2003). *Group 12* ions have also been suggested to bind within the pore. High sensitivity has been shown to be conferred by a cysteine

https://doi.org/10.1017/S0033583504003932 Published online by Cambridge University Press

residue in the selectivity filter of a Na channel (Schild & Moczydlowski, 1991; Backx *et al.* 1992; Heinemann *et al.* 1992a; Satin *et al.* 1992). The combination of critically located cysteines, histidines and aspartates creates a high-affinity site for Zn^{2+} in the Na channel pore (Favre *et al.* 1995). In a Kv1.5 channel, a histidine (equivalent to F425 in Shaker) and an arginine (equivalent to T449 in Shaker) are important for Zn-induced block (Kehl *et al.* 2002). Hg^{2+} binds irreversibly with high affinity ($K_D = 1$ μM) to rat muscle Na channel (hSkM1) pore, and the affinity depends on the number of cysteinyl groups in the pore (Hisatome *et al.* 2000). The coordinated binding between Hg^{2+} and ligands such as the sulfhydryl group exhibits the nature of a covalent bond rather than an ionic bond. In contrast, Cd^{2+} and Zn^{2+} bind to the free thiols semi-covalently (Benitah *et al.* 1996, 1997; Hisatome *et al.* 2000). It should be pointed out that a strong block is not necessarily associated with a shift of the $G(V)$ curve. Despite a strong binding of Hg^{2+} to the pore of a Na channel no $G(V)$ shift was seen (Hisatome *et al.* 2000), and the effects of certain amino-acid residues on the Zn^{2+}-induced block of a K channel did not affect $G(V)$ (Kehl *et al.* 2002).

8. Conclusions and perspectives

It has been stated that inorganic physiology is in its infancy (Finey & O'Halloran, 2003). In the present review we have tried to further the knowledge in this field by summarizing and analysing the effects of externally applied metal ions on voltage-gated ion channels to get a comprehensive view on mechanisms involved. We have tried to extract probable sites of action for different ion species and for different channel types. We have even tried to take some steps towards an atomic biology by relating the action of the ions to their atomic properties.

In conclusion, we have shown that it is possible to quantify most reported data by a simple shift-and-scaling procedure, i.e. a shift of voltage-dependent steady-state parameters (expressed by c_{10} in Table 3) along the voltage axis in combination with a down-scaling of the rate *versus* voltage curve, i.e. a slowing of the gating (expressed by the slowing factor A in Table 3). The relative success of this attempt implies that the metal ion action can be interpreted in terms of three basic mechanisms, represented in Fig. 4.

The first mechanism (A) assumes electrostatic screening of fixed surface charges. The classical version of this mechanism, assuming a smeared layer of distributed charges, predicts equal effects on all voltage-dependent parameters, and can be shown to account for the action of the *group 2* ions Mg^{2+}, Sr^{2+} and sometimes Ca^{2+} but not for the transition metals and the lanthanides. The c_{10} of Mg^{2+} and Sr^{2+} has a typical value of $\sim$10 mM. The critical fixed charges are located close to the voltage sensor. The second mechanism (B) assumes binding and a consequent electrostatic modulation of the voltage sensor motion. The one-site version of this mechanism explains much of the action of transition elements and the Zn group metals. The binding site may be either in the voltage sensor region or inside the pore (Mechanism D). The pore site of Ca^{2+} and Ba^{2+} has been extensively studied in K channels. The third mechanism (C) assumes binding and a non-electrostatic (allosteric) coupling to the gating machinery. The one-site version of this mechanism in combination with Mechanism B explains much of the action of the lanthanides. Most channels show similar ion-specific sensitivities. Deviating channels are HERG and eag, showing an unusual sensitivity to Mg^{2+} but also other metal ions.

A detailed understanding of the different metal ion species' action on voltage-gated ion channels will help us to understand the physiological role of metal ions, the

https://doi.org/10.1017/S0033583504003932 Published online by Cambridge University Press

'metallome' in normal cell physiology, and especially their role in normal neuron physiology. Metals of special interest here are Ca^{2+} and Zn^{2+}, the latter is suggested to act as a master hormone in many organisms (Fraústo da Silva & Williams, 2001). It will also help us to better understand the toxicological role of heavy-metal ions, notably Hg^{2+}, although direct conclusions from the presented data are, at present, impossible due to the many complicating factors involved when a metal ion is introduced into the organism. With the increasing knowledge about the detailed mechanisms of these processes, a further step has doubtless been taken towards a more fertile, and clinically and ecologically relevant, inorganic physiology.

9. Appendix

To quantify the metal-ion induced effects in the literature we used a shift-and-scaling procedure. If this procedure is adequate it implies that the mathematical expression of the rate constants in metal ion solution should be possible to be described in the form

$$\alpha_{\mathrm{Me}}(V) = \alpha(V + \Delta V_{G(V)})/A, \tag{A1a}$$

$$\beta_{\mathrm{Me}}(V) = \beta(V + \Delta V_{G(V)})/A, \tag{A1b}$$

where $\alpha(V)$ and $\beta(V)$ are the rate constants in control solution, $\Delta V_{G(V)}$ the shift of $G(V)$, and A the additional slowing factor of both the forward and the backward rates. Here we show that this is the case. We start with the basic one-site model (Scheme 8 in the main text)

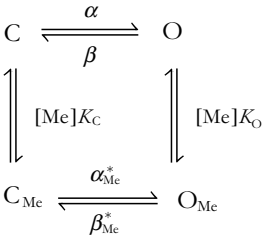

(Scheme A2)

where C and O are closed and open states respectively, K_C and K_O are binding constants, and [Me] is the metal ion concentration. The subscript Me denotes Me^{n+}-bound states. The voltage-dependent rate constants are expressed in terms of the transition-state theory (Glasstone *et al.* 1941) [Eqs. (6*a*, *b*) in the main text]

$$\alpha = k_{\mathrm{eq}} \exp((V - V_{\mathrm{eq}})z_\alpha FR^{-1}T^{-1}), \tag{A3a}$$

$$\beta = k_{\mathrm{eq}} \exp(-(V - V_{\mathrm{eq}})z_\beta FR^{-1}T^{-1}), \tag{A3b}$$

where k_{eq} is the rate constant of α and β, when $\alpha = \beta$, V the absolute membrane voltage, V_{eq} the membrane voltage when $\alpha = \beta$, z_α the gating valence for α and z_β the gating valence for β, and F, R and T have their normal thermodynamic significances. The metal-ion bound rate constants are [Eqs. (14*a*, *b*) in the main text]:

$$\alpha^*_{\mathrm{Me}} = (A^*)^{-1} k_{\mathrm{eq}} \exp((V - V_{\mathrm{eq}} - \Delta V^*_{\mathrm{Me}})z_\alpha FR^{-1}T^{-1}), \tag{A4a}$$

https://doi.org/10.1017/S0033583504003932 Published online by Cambridge University Press

$$\beta^*_{\mathrm{Me}} = (A^*)^{-1} k_{\mathrm{eq}} \exp(-(V - V_{\mathrm{eq}} - \Delta V^*_{\mathrm{Me}}) z_\beta F R^{-1} T^{-1}). \quad \text{(A 4}b\text{)}$$

A^* is a slowing factor [corresponding to adding an energy barrier of $\Delta W = kT \ln(A^*)$] introduced to account for mechanical effects of the bound metal ion (Elinder & Århem, 1994b). ΔV^*_{Me} is the effect on the electric field induced by one bound Me^{n+} ion. If the model is in thermodynamic equilibrium then

$$K_{\mathrm{O}} = K_{\mathrm{C}} \alpha^*_{\mathrm{Me}} \beta / (\alpha \beta^*_{\mathrm{Me}}). \quad \text{(A 5)}$$

Because the metal-binding transition is much faster than the channel gating, Scheme A 2 can be reduced to

$$\{\mathrm{C}\} \underset{\beta_{\mathrm{Me}}}{\overset{\alpha_{\mathrm{Me}}}{\rightleftharpoons}} \{\mathrm{O}\}, \quad \text{(Scheme A 6)}$$

where {C} denotes all closed states and {O} all open states, and where

$$\alpha_{\mathrm{Me}} = (\alpha + \alpha^*_{\mathrm{Me}} K_{\mathrm{C}} [\mathrm{Me}])/(1 + K_{\mathrm{C}} [\mathrm{Me}]), \quad \text{(A 6}a\text{)}$$

$$\beta_{\mathrm{Me}} = (\beta + \alpha^*_{\mathrm{Me}} K_{\mathrm{C}} [\mathrm{Me}] \beta \alpha^{-1})/(1 + \beta \alpha^*_{\mathrm{Me}} (\alpha \beta^*_{\mathrm{Me}})^{-1} K_{\mathrm{C}} [\mathrm{Me}]), \quad \text{(A 6}b\text{)}$$

Eqs. (A 6*a*) and (A 6*b*) can be expressed as [by Eqs. (A 3*a*, *b*) and (A 4*a*, *b*)]

$$\alpha_{\mathrm{Me}} = \alpha(1 + (A^*)^{-1} K_{\mathrm{C}} [\mathrm{Me}] \exp(-\Delta V^*_{\mathrm{Me}} z_\alpha F R^{-1} T^{-1}))/(1 + K_{\mathrm{C}} [\mathrm{Me}]), \quad \text{(A 7}a\text{)}$$

$$\begin{aligned} \beta_{\mathrm{Me}} = \beta(1 + (A^*)^{-1} K_{\mathrm{C}} [\mathrm{Me}] \exp(-\Delta V^*_{\mathrm{Me}} z_\alpha F R^{-1} T^{-1}))/ \\ (1 + K_{\mathrm{C}} [\mathrm{Me}] \exp(-\Delta V^*_{\mathrm{Me}} (z_\alpha + z_\beta) F R^{-1} T^{-1})). \end{aligned} \quad \text{(A 7}b\text{)}$$

The shifts of the $\alpha(V)$, $\beta(V)$, and $G(V)$ curves are then

$$\Delta V_{\alpha(V)} = RT/(z_\alpha F) \ln [(1 + K_{\mathrm{C}} [\mathrm{Me}])/(1 + (A^*)^{-1} K_{\mathrm{C}} [\mathrm{Me}] \exp(-\Delta V^*_{\mathrm{Me}} z_\alpha F R^{-1} T^{-1}))], \quad \text{(A 8}a\text{)}$$

$$\begin{aligned} \Delta V_{\beta(V)} = RT/(z_\beta F) \ln [(1 + (A^*)^{-1} K_{\mathrm{C}} [\mathrm{Me}] \exp(-\Delta V^*_{\mathrm{Me}} z_\alpha F R^{-1} T^{-1}))/ \\ (1 + K_{\mathrm{C}} [\mathrm{Me}] \exp(-\Delta V^*_{\mathrm{Me}} (z_\alpha + z_\beta) F R^{-1} T^{-1}))], \end{aligned} \quad \text{(A 8}b\text{)}$$

$$\Delta V_{G(V)} = RT/(F(z_\alpha + z_\beta)) \ln[(1 + K_{\mathrm{C}} [\mathrm{Me}])/(1 + K_{\mathrm{C}} [\mathrm{Me}] \exp(-\Delta V^*_{\mathrm{Me}} (z_\alpha + z_\beta) F R^{-1} T^{-1}))]. \quad \text{(A 8}c\text{)}$$

As stated above the shift-and-scaling procedure used in quantifying the metal ion effects implies that α_{Me} and β_{Me} should be able to be expressed in the form $\alpha(V + \Delta V_{G(V)})/A$ and $\beta(V + \Delta V_{G(V)})/A$. This is shown to be the case below, where Eqs. (A 7*a*) and (A 7*b*) are expressed as

$$\alpha_{\mathrm{Me}} = A^{-1} k_{\mathrm{eq}} \exp((V - V_{\mathrm{eq}} - \Delta V_{G(V)}) z_\alpha F R^{-1} T^{-1}), \quad \text{(A 9}a\text{)}$$

$$\beta_{\mathrm{Me}} = A^{-1} k_{\mathrm{eq}} \exp(-(V - V_{\mathrm{eq}} - \Delta V_{G(V)}) z_\beta F R^{-1} T^{-1}), \quad \text{(A 9}b\text{)}$$

https://doi.org/10.1017/S0033583504003932 Published online by Cambridge University Press

and where

$$\left.\begin{aligned} A = & \exp(-z_\alpha/(z_\beta+z_\alpha)\ln[(1+K_C[\mathrm{Me}]))/(1+K_C[\mathrm{Me}]\exp(-\Delta V^*_{\mathrm{Me}}(z_\alpha+z_\beta)FR^{-1}T^{-1}))]) \\ & (1+K_C[\mathrm{Me}])/(1+(A^*)^{-1}K_C[\mathrm{Me}]\exp(-\Delta V^*_{\mathrm{Me}}z_\alpha FR^{-1}T^{-1})) \\ = & (1+K_C[\mathrm{Me}])^{z_\beta/(z_\beta+z_\alpha)}(1+K_C[\mathrm{Me}]\exp(-\Delta V^*_{\mathrm{Me}}(z_\alpha+z_\beta)FR^{-1}T^{-1}))^{z_\alpha/(z_\beta+z_\alpha)}/ \\ & (1+(A^*)^{-1}K_C[\mathrm{Me}]\exp(-\Delta V^*_{\mathrm{Me}}z_\alpha FR^{-1}T^{-1})). \end{aligned}\right\} \quad (A10)$$

As seen, the relation between the experimentally obtained A and the theoretical A^* is not simple. Even if $A^*=1$ (i.e. Mechanism B), we will get a value of $A>1$.

10. Acknowledgements

We thank Peter Larsson and the Hille-book discussion group for comments on the manuscript. This study was supported by grants from the Swedish Research Council, Åke Wibergs Stiftelse, Magn. Bergvalls Stiftelse, and The Swedish Society of Medicine. F. Elinder has a junior research position at the Swedish Research Council.

11. References

Agus, Z. S., Dukes, I. D. & Morad, M. (1991). Divalent cations modulate the transient outward current in rat vetricular myocytes. *American Journal of Physiology* **261**, C310–C318.

Anumonwo, J. M. B., Horta, J., Delmar, M., Taffet, S. M. & Jalife, J. (1999). Proton and zinc effects on HERG currents. *Biophysical Journal* **77**, 282–298.

Åqvist, J., Luecke, H., Quiocho, F. A. & Warshel, A. (1991). Dipoles localized at helix termini of proteins stabilize charges. *Proceedings of the National Academy of Sciences USA* **88**, 2026–2030.

Araque, A., Cattaert, D. & Buño, W. (1995). Cd^{2+} regulation of the hyperpolarization-activated current I_{AB} in the crayfish muscle. *Journal of General Physiology* **105**, 725–744.

Århem, P. (1980a). Effects of rubidium, caesium, strontium, barium and lanthanum on ionic currents in myelinated nerve fibres from *Xenopus laevis*. *Acta Physiologica Scandinavica* **108**, 7–16.

Århem, P. (1980b). Effects of some heavy metal ions on the ionic currents of myelinated fibres from *Xenopus laevis*. *Journal of Physiology* **306**, 219–231.

Arkett, S. A., Dixon, S. J. & Sims, S. M. (1994). Effects of extracellular calcium and protons on osteoclast potassium currents. *Journal of Membrane Biology* **140**, 163–171.

Armstrong, C. M. (1966). Time course of TEA^+-induced anomalous rectification in squid giant axons. *Journal of General Physiology* **50**, 491–503.

Armstrong, C. M. (1971). Interaction of tetraethylammonium ion derivatives with the potassium channels of giant axons. *Journal of General Physiology* **58**, 493–437.

Armstrong, C. M. (1999). Distinguishing surface effects of calcium ion from pore-occupancy effects in Na^+ channels. *Proceedings of the National Academy of Sciences USA* **96**, 4158–4163.

Armstrong, C. M. (2003). Voltage-gated K channels. *Science's* STKE **188**, re10.

Armstrong, C. M. & Cota, G. (1990). Modification of sodium channel gating by lanthanum. Some effects that cannot be explained by surface charge theory. *Journal of General Physiology* **96**, 1129–1140.

Armstrong, C. M. & Cota, G. (1991). Calcium ion as a cofactor in Na channel gating. *Proceedings of the National Academy of Sciences USA* **88**, 6528–6531.

Armstrong, C. M. & Cota, G. (1999). Calcium block of Na^+ channels and its effect on closing rate. *Proceedings of the National Academy of Sciences USA* **96**, 4154–4157.

Armstrong, C. M. & Hille, B. (1998). Voltage-gated ion channels and electrical excitability. *Neuron* **20**, 371–380.

Armstrong, C. M. & Lopez-Barneo, J. (1987). External calcium ions are required for potassium channel gating in squid neurons. *Science* **236**, 712–714.

Armstrong, C. M. & Matteson, D. R. (1986). The role of calcium ions in the closing of K channels. *Journal of General Physiology* **87**, 817–832.

Armstrong, C. M. & Miller, C. (1990). Do voltage-dependent K^+ channels require Ca^{2+}? A critical test employing a heterologous expression system. *Proceedings of the National Academy of Sciences USA* **87**, 7579–7582.

Armstrong, C. M. & Taylor, S. R. (1980). Interaction of barium ions with potassium channels in squid giant axons. *Biophysical Journal* **30**, 473–488.

Assaf, S. Y. & Chung, S. H. (1984). Release of endogenous Zn^{2+} from brain tissue during activity. *Nature* **308**, 734–736.

Atkins, P. W. (1995). *The Periodic Kingdom*. New York: Basic Books.

Backx, P. H., Yue, D. T., Lawrence, J. H., Marban, E. & Tomaselli, G. F. (1992). Molecular localization of an ion binding site within the pore of mammalian sodium channels. *Science* **257**, 248–251.

Basso, C., Labarca, P., Stefani, E., Alvarez, O. & Latorre, R. (1998). Pore accessibility during C-type inactivation in Shaker K^+ channels. *FEBS Letters* **429**, 375–380.

Begenisich, T. & Lynch, C. (1974). Effects of internal divalent cations on voltage-clamped squid axons. *Journal of General Physiology* **63**, 675–689.

Behrens, M. I., Oberhauser, A., Bezanilla, F. & Latorre, R. (1989). Batrachotoxin-modified sodium channels from squid optic nerve in planar bilayers. Ion conduction and gating properties. *Journal of General Physiology* **93**, 23–41.

Benitah, J., Balser, J. R., Marban, E. & Tomaselli, G. F. (1997). Proton inhibition of sodium channels: mechanism of gating shifts and reduced conductance. *Journal of Membrane Biology* **155**, 121–131.

Benitah, J. P., Tomaselli, G. F. & Marban, E. (1996). Adjacent pore-lining residues within sodium channels identified by paired cysteine mutagenesis. *Proceedings of the National Academy of Sciences USA* **93**, 7392–7396.

Berridge, M. J., Bootman, M. D. & Lipp, P. (1998). Calcium – a life and death signal. *Nature* **395**, 645–648.

Berg, J. M. & Godwin, H. A. (1997). Lessons from zinc-binding peptides. *Annual Review of Biophysics and Biomolecular Structure* **26**, 357–371.

Bixby, K. A., Nanao, M. H., Shen, N. V., Kreusch, A., Bellamy, H., Pfaffinger, P. J. & Choe, S. (1999). Zn^{2+}-binding and molecular determinants of tetramerization in voltage-gated K^+ channels. *Nature Structural Biology* **6**, 38–43.

Bliss, T. V. & Collingridge, G. L. (1993). A synaptic model of memory: long-term potentiation in the hippocampus. *Nature* **361**, 31–39.

Block, B. M., Stacey, W. C. & Jones, S. W. (1998). Surface charge and lanthanum block of calcium current in bullfrog sympathetic neurons. *Biophysical Journal* **74**, 2278–2284.

Boccaccio, A., Moran, O. & Conti, F. (1998). Calcium dependent shifts of Na^+ channel activation correlated with the state dependence of calcium-binding to the pore. *European Biophysics Journal* **27**, 558–566.

Bokris, J. O'M. & Reddy, A. K. N. (1970). *Modern Electrochemistry*, vol. 2. New York: Plenum Press.

Boland, L. M., Jurman, M. E. & Yellen, G. (1994). Cysteines in the Shaker K^+ channel are not essential for channel activity or zinc modulation. *Biophysical Journal* **66**, 694–699.

Brehm, P. & Eckert, R. (1978). Calcium entry leads to inactivation of calcium channel in Paramecium. *Science* **202**, 1203–1206.

Brink, F. (1954). The role of calcium ions in neural processes. *Pharmacological Reviews* **6**, 243–298.

Brismar, T. (1973). Effects of ionic concentration on permeability properties of nodal membrane in myelinated nerve fibres of *Xenopus laevis*. Potential clamp experiments. *Acta Physiologica Scandinavica* **87**, 474–484.

Brismar, T. (1980). The effects of divalent and trivalent cations on the sodium permeability of myelinated nerve fibres of *Xenopus laevis*. *Acta Physiologica Scandinavica* **108**, 23–29.

Brismar, T. & Frankenhaeuser, B. (1972). The effect of calcium on the potassium permeability in the myelinated nerve fibre of *Xenopus laevis*. *Acta Physiologica Scandinavica* **85**, 237–241.

Broomand, A., Männikkö, R., Larsson, H. P. & Elinder, F. (2003). Molecular movement of the voltage sensor in a K channel. *Journal of General Physiology* **122**, 741–748.

Brown, R. H. (1974). Membrane surface charge: discrete and uniform modelling. *Progress in Biophysics and Molecular Biology* **28**, 341–370.

Bruland, K. W. (1983). Trace elements in sea water. In *Chemical Oceanography*, vol. 8 (eds J. P. Riley & R. Chester), chapter 45. London: Academic Press.

Bush, A. I., Pettingell, W. H., Multhaup, G., Paradis, M., Vonsattel, J. P., Gusella, J. F., Beyreuther, K., Masters, C. L. & Tanzi, R. E. (1994). Rapid induction of Alzheimer A beta amyloid formation by zinc. *Science* **265**, 1464–1467.

Cade, J. (1949). Lithium salts in the treatment of psychotic excitement. *Medical Journal of Australia* **2**, 349–352.

Catterall, W. A. (1986). Molecular properties of voltage-sensitive sodium channels. *Annual Review of Biochemistry* **55**, 953–985.

Cens, T., Dalle, C. & Charnet, P. (1998). Expression of β subunit modulates surface potential sensing by calcium channels. *European Journal of Physiology* **435**, 865–867.

Cevc, G. (1990). Membrane electrostatics. *Biochimica et Biophysica Acta* **1031**, 311–382.

Cha, A., Snyder, G. E., Selvin, P. R. & Bezanilla, F. (1999). Atomic scale movement of the voltage-sensing region in a potassium channel measured via spectroscopy. *Nature* **402**, 809–813.

Chahine, M., Chen, L. Q., Kallen, R. G., Barchi, R. L. & Horn, R. (1992). Expressed Na channel clones differ in their sensitivity to external calcium concentration. *Biophysical Journal* **62**, 37–40.

Chandler, W. K., Hodgkin, A. L. & Meves, H. (1965). The effect of changing the internal solution on sodium inactivation and related phenomena in giant axons. *Journal of Physiology* **180**, 821–836.

Chapman, D. L. (1913). A contribution to the theory of electrocapillarity. *Philosophical Magazine* **25**, 475–481.

Cherny, V. V. & DeCoursey, T. E. (1999). pH-dependent inhibition of voltage-gated H^+ currents in rat alveolar epithelial cells by Zn^{2+} and other divalent cations. *Journal of General Physiology* **114**, 819–838.

Choi, D. W. & Koh, J. Y. (1998). Zinc and brain injury. *Annual Review of Neuroscience* **21**, 347–375.

Christianson, D. W. & Alexander, R. S. (1989). Carboxylate-histidine-zinc interactions in protein structure and function. *Journal of the American Chemical Society* **111**, 6412–6419.

Coetzee, W. A., Amarillo, Y., Chiu, J., Chow, A., Lau, D., McCormack, T., Moreno, H., Nadal, M. S., Ozaita, A., Pountney, D., Saganich, M., Vega-Saenz De Miera, E. & Rudy, B. (1999). Molecular diversity of K^+ channels. *Annals of the New York Academy of Sciences* **868**, 233–285.

Cohen, B. E., Grabe, M. & Jan, L. Y. (2003). Answers and questions from the KvAP structures. *Neuron* **39**, 395–400.

Cole, K. S. (1969). Zeta potential and discrete vs. uniform surface charges. *Biophysical Journal* **9**, 465–469.

Cox, P. A. (1989). *The Elements*. Oxford: Oxford University Press.

Cox, P. A. (1995). *The Elements on Earth*. Oxford: Oxford University Press.

Cukierman, S. (1991). Asymmetric electrostatic effects on the gating of rat brain sodium channels in planar lipid membranes. *Biophysical Journal* **60**, 845–855.

Cukierman, S. (1993). Barium modulates the gating of batrachotoxin-treated Na^+ channels in high ionic strength solutions. *Biophysical Journal* **65**, 1168–1173.

Cukierman, S. & Krueger, B. K. (1990). Modulation of sodium channel gating by external divalent cations studied in planar lipid bilayers. Differential effects on opening and closing rates. *Pflügers Archiv* **416**, 360–367.

Cukierman, S. & Krueger, B. K. (1991). Effects of internal divalent cations on the gating of rat brain sodium channels reconstituted in planar lipid bilayers. *Pflügers Archiv* **419**, 559–566.

Cukierman, S., Zinkand, W. C., French, R. J. & Krueger, B. K. (1988). Effects of membrane surface charge and calcium on the gating of rat brain sodium channels in planar bilayers. *Journal of General Physiology* **92**, 431–447.

Dani, J. A., Sánchez, J. A. & Hille, B. (1983). Lyotropic anions. Na channel gating and Ca electrode response. *Journal of General Physiology* **81**, 255–281.

de Leon, M., Wang, Y., Jones, L., Perez-Reyes, E., Wei, X., Soong, T. W., Snutch, T. P. & Yue, D. T. (1995). Essential Ca^{2+}-binding motif for Ca^{2+}-sensitive inactivation of L-type Ca^{2+} channels. *Science* **270**, 1502–1506.

Deal, K. K., Lovinger, D. M. & Tamkun, M. M. (1994). The brain Kv1.1 potassium channel: in vitro and in vivo studies on subunit assembly and posttranslational processing. *Journal of Neuroscience* **14**, 1666–1676.

Deutsch, N., Matsuoka, S. & Weiss, J. N. (1994). Surface charge and properties of cardiac ATP-sensitive K^+ channels. *Journal of General Physiology* **104**, 773–800.

DiFrancesco, D., Ferroni, A., Visentin, S. & Zaza, A. (1985). Cadmium-induced blockade of the cardiac fast Na channels in calf Purkinje fibres. *Proceedings of the Royal Society of London Series B, Biological Sciences* **223**, 475–484.

Doyle, D. A., Cabral, J. M., Pfuetzner, R. A., Kuo, A., Gulbis, J. M., Cohen, S. L., Chait, B. T. & Mackinnon, R. (1998). The structure of the potassium channel: molecular basis of K^+ conduction and selectivity. *Science* **280**, 69–77.

Duchatelle-Gourdon, I., Hartzell, H. C. & Lagrutta, A. A. (1989). Modulation of the delayed rectifier potassium current in frog cardiomyocytes by beta-adrenergic agonists and magnesium. *Journal of Physiology* **415**, 251–274.

Eclampsia Trial Collaborative Group (1995). Which anticonvulsant for women with eclampsia? Evidence from the Collaborative Eclampsia Trial. *Lancet* **345**, 1455–1463. (Erratum. *Lancet* **346**, 258.)

Eismann, E., Müller, F., Heinemann, S. H. & Kaupp, U. B. (1994). A single negative charge within the pore region of a cGMP-gated channel controls rectification, Ca^{2+} blockage, and ionic selectivity. *Proceedings of the National Academy of Sciences USA* **91**, 1109–1113.

Elinder, F. & Århem, P. (1991). Properties of the leakage current pathway: effects of the gadolinium ion on myelinated axons. *Neuroreport* **2**, 685–687.

Elinder, F. & Århem, P. (1994a). Effects of gadolinium on ion channels in the myelinated axon of *Xenopus laevis*: four sites of action. *Biophysical Journal* **67**, 71–83.

Elinder, F. & Århem, P. (1994b). A modulatory site for the action of gadolinium on surface charges and channel gating. *Biophysical Journal* **67**, 84–90.

Elinder, F. & Århem, P. (1998). The functional surface charge density of a fast K channel in the myelinated axon of *Xenopus laevis*. *Journal of Membrane Biology* **165**, 175–181.

Elinder, F. & Århem, P. (1999). Role of individual surface charges of voltage-gated K channels. *Biophysical Journal* **77**, 1358–1362.

Elinder, F., Århem, P. & Larsson, H. P. (2001a). Localization of the extracellular end of the voltage sensor S4 in a potassium channel. *Biophysical Journal* **80**, 1802–1809.

Elinder, F., Liu, Y. & Århem, P. (1998). Divalent cation effects on the Shaker K channel suggest a pentapeptide sequence as determinant of functional surface charge density. *Journal of Membrane Biology* **165**, 183–189.

Elinder, F., Madeja, M. & Århem, P. (1996). Surface charges of K channels. Effects of strontium on five cloned channels expressed in *Xenopus* oocytes. *Journal of General Physiology* **108**, 325–332.

Elinder, F., Männikkö, R. & Larsson, H. P. (2001b). S4 charges move close to residues in the pore domain

during activation in a K channel. *Journal of General Physiology* **118**, 1–10.

Emsley, J. (1991). *The Elements*. Oxford: Clarendon Press.

Enos, B. E. & McQuarrie, D. A. (1981). The effect of discrete charges on the electrical properties of membranes. II. *Journal of Theoretical Biology* **93**, 499–522.

Enyeart, J. J., Xu, L., Gomora, J. C. & Enyeart, J. A. (1998). Modulation of I_A potassium current in adrenal cortical cells by a series of ten lanthanide elements. *Journal of Membrane Biology* **164**, 139–153.

Evans, C. H. (1990). *Biochemistry of the Lanthanides*. New York: Plenum Press.

Fan, Z. & Hiraoka, M. (1991). Depression of delayed outward K^+ current by Co^{2+} in guinea pig ventricular myocytes. *American Journal of Physiology* **261**, C23–31.

Favre, I., Moczydlowski, E. & Schild, L. (1995). Specificity for block by saxitoxin and divalent cations at a residue which determines sensitivity of sodium channel subtypes to guanidinium toxins. *Journal of General Physiology* **106**, 203–229.

Finey, L. A. & O'Halloran, T. V. (2003). Transition metal speciation in the cell: Insights from the chemistry of metal ion receptors. *Science* **300**, 931–936.

Fox, J. M., Rojas, E. & Stämpfli, R. (1974). Blocking of sodium and potassium conductance by internal application of Zn^{2+} in the node of Ranvier. *Pflügers Archiv* **351**, 271–274.

Fozzard, H. A. & Hanck, D. A. (1996). Structure and function of voltage-dependent sodium channels: comparison of brain II and cardiac isoforms. *Physiological Reviews* **76**, 887–926.

Frankenhaeuser, B. (1957). The effect of calcium on the myelinated nerve fibre. *Journal of Physiology* **137**, 245–260.

Frankenhaeuser, B. & Hodgkin, A. L. (1957). The action of calcium on the electrical properties of squid axons. *Journal of Physiology* **137**, 218–244.

Fraústo Da Silva, J. J. R. & Williams, R. J. P. (2001). *The Biological Chemistry of the Elements*, 2nd edn. Oxford: Oxford University Press.

Frederickson, C. J. (1989). Neurobiology of zinc and zinc-containing neurons. *International Review of Neurobiology* **31**, 145–238.

French, R. J., Prusak-Sochaczewski, E., Zamponi, G. W., Becker, S., Kularatna, A. S. & Horn, R. (1996). Interactions between a pore-blocking peptide and the voltage sensor of the sodium channel: an electrostatic approach to channel geometry. *Neuron* **16**, 407–413.

Friberg, L., Nordberg, G. F. & Vouk, V. B. (1986a). *Handbook on the Toxicology of Metals*, vol. I, *General Aspects*, 2nd edn. Amsterdam: Elsevier Science Publishers B.V.

Friberg, L., Nordberg, G. F. & Vouk, V. B. (1986b). *Handbook on the Toxicology of Metals*, vol. II, *Specific Metals*, 2nd edn. Amsterdam: Elsevier Science Publishers B.V.

Gandhi, C. S. & Isacoff, E. Y. (2002). Molecular models of voltage sensing. *Journal of General Physiology* **120**, 455–463.

Gárdos, G. (1958). The function of calcium in the potassium permeability of human erythrocytes. *Biochimica Biophysica Acta* **30**, 653–654.

Gilbert, D. L. (1971). Fixed surface charges. In *Biophysics and Physiology of Excitable Membranes* (ed. W. J. Adelman), pp. 359–378. Princeton: Van Nostrand-Reinhold.

Gilbert, D. L. & Ehrenstein, G. (1969). Effect of divalent cations on potassium conductance of squid axons: determination of surface charge. *Biophysical Journal* **9**, 447–463.

Gilbert, D. L. & Ehrenstein, G. (1970). Use of a fixed charge model to determine the pK of the negative sites on the external membrane surface. *Journal of General Physiology* **55**, 822–825.

Gilbert, D. L. & Ehrenstein, G. (1984). Membrane surface charge. *Current Topics in Membrane Transport* **22**, 407–421.

Gilly, W. F. & Armstrong, C. M. (1982a). Divalent cations and the activation kinetics of potassium channels in squid giant axons. *Journal of General Physiology* **79**, 965–996.

Gilly, W. F. & Armstrong, C. M. (1982b). Slowing of sodium channel opening kinetics in squid axon by extracellular zinc. *Journal of General Physiology* **79**, 935–964.

Glasstone, S., Laidler, K. J. & Eyring, H. (1941). *The Theory of Rate Processes*. New York: McGraw-Hill.

Goldman, R. S. & Finkbeiner, S. M. (1988). Therapeutic use of magnesium sulfate in selected cases of cerebral ischemia and seizures. *New England Journal of Medicine* **319**, 1224–1225.

Goldwater, L. J. (1972). *Mercury. A History of Quicksilver*. Baltimore: York Press.

Gomez-Lagunas, F., Melishchuk, A. & Armstrong, C. M. (2003). Block of Shaker potassium channels by external calcium ions. *Proceedings of the National Academy of Sciences USA* **100**, 347–351.

Gordon, H. T. & Welsh, J. H. (1948). The role of ions in axon surface reactions to toxic organic compounds. *Journal of Cellular and Comparative Physiology* **31**, 395–419.

Gordon, S. E. & Zagotta, W. N. (1995). A histidine residue associated with the gate of the cyclic nucleotide-activated channels in rod photoreceptors. *Neuron* **14**, 177–183.

Gouy, G. (1910). Sur la constitution de la charge électrique à la surface d'un électrolyte. *Journal de Physique et le Radium* (*Paris*) **9**, 457–468.

Grahame, D. C. (1947). The electrical double layer and the theory of electrocapillarity. *Chemical Reviews* **41**, 441–501.

Green, W. N. & Andersen, O. S. (1991). Surface charges and ion channel function. *Annual Review of Physiology* **53**, 341–359.

Green, W. N., Weiss, L. B. & Andersen, O. S. (1987). Batrachotoxin-modified sodium channels in planar lipid bilayers. Ion permeation and block. *Journal of General Physiology* **89**, 841–872.

Gui-Rong, L. & Baumgarten, C. M. (2001). Modulation of cardiac Na^+ current by gadolinium, a blocker of stretch-induced arrhythmias. *American Journal of Physiology* **280**, H272–H279.

Gunner, M. R., Saleh, M. A., Cross, E., Ud-Doula, A. & Wise, M. (2000). Backbone dipoles generate positive potentials in all proteins: Origins and implications of the effect. *Biophysical Journal* **78**, 1126–1144.

Guy, H. R. & Seetharamulu, P. (1986). Molecular model of the action potential sodium channel. *Proceedings of the National Academy of Sciences USA* **83**, 508–512.

Hahin, R. & Campbell, D. T. (1983). Simple shifts in the voltage dependence of sodium channel gating caused by divalent cations. *Journal of General Physiology* **82**, 785–802.

Haley, J. T. (1965). Pharmacology and toxicology of rare earth elements. *Journal of Pharmacological Sciences* **54**, 663–670.

Hamill, O. P. & McBride, Jr. D. W. (1996). The pharmacology of mechanogated membrane ion channels. *Pharmacological Reviews* **48**, 231–252.

Hanck, D. A. & Sheets, M. F. (1992). Extracellular divalent and trivalent cation effects on sodium current kinetics in single canine cardiac purkinje cells. *Journal of Physiology* **454**, 267–298.

Harris, R. E., Larsson, H. P. & Isacoff, E. Y. (1998). A permanent ion binding site located between two gates of the Shaker K^+ channel. *Biophysical Journal* **74**, 1808–1820.

Harrison, N. L., Radke, H. K., Tamkun, M. M. & Lovinger, D. M. (1993a). Modulation of gating of cloned rat and human K^+ channels by micromolar Zn^{2+}. *Molecular Pharmacology* **43**, 482–486.

Harrison, N. L., Radke, H. K., Talukder, G. & Ffrench-Mullen, J. M. (1993b). Zinc modulates transient outward current gating in hippocampal neurons. *Receptors and Channels* **1**, 153–163.

Heggeness, S. T. & Starkus, J. G. (1986). Saxitoxin and tetrodotoxin. Electrostatic effects on sodium channel gating current in crayfish axons. *Biophysical Journal* **49**, 629–643.

Heginbotham, L., Abramson, T. & Mackinnon, R. (1992). A functional connection between the pores of distantly related ion channels as revealed by mutant K^+ channels. *Science* **258**, 1152–1155.

Heilbrunn, L. V. & Wiercinski, F. J. (1947). The action of various cations on muscle protoplasm. *Journal of Cellular and Comparative Physiology* **29**, 15–32.

Heinemann, S. H., Terlau, H. & Imoto, K. (1992a). Molecular basis for pharmacological differences between brain and cardiac sodium channels. *Pflügers Archiv* **422**, 90–92.

Heinemann, S. H., Terlau, H., Stühmer, W., Imoto, K. & Numa, A. (1992b). Calcium channel characteristics conferred on the sodium channel by single mutations. *Nature* **356**, 441–443.

Hille, B. (1968). Charges and potentials at the nerve surface. Divalent ions and pH. *Journal of General Physiology* **51**, 221–236.

Hille, B. (2001). *Ion Channels of Excitable Membranes*. Sunderland: Sinauer.

Hille, B., Woodhull, A. M. & Shapiro, B. I. (1975). Negative surface charge near sodium channels of nerve: divalent ions, monovalent ions, and pH. *Philosophical Transactions of the Royal Society of London Series B, Biological Sciences* **270**, 301–318.

Hisatome, I., Kurata, Y., Sasaki, N., Morisaki, T., Morisaki, H., Tanaka, Y., Urashima, T., Yasuhashi, T., Tsuboi, M., Kitamura, F., Miake, J., Takeda, S.-I., Taniguchi, S. I., Ogino, K., Igawa, O., Yoshida, A., Sato, R., Makita, N. & Shigemasa, C. (2000). Block of sodium channels by divalent mercury: role of specific cysteinyl residues in the P-loop region. *Biophysical Journal* **79**, 1336–1345.

Ho, W. K., Kim, I., Lee, C. O., Youm, J. B., Lee, S. H. & Earm, Y. E. (1999). Blockade of HERG channels expressed in *Xenopus laevis* oocytes by external divalent cations. *Biophysical Journal* **76**, 1959–1971.

Hodgkin, A. L. (1976). Chance and design in electrophysiology: an informal account of certain experiments on nerve carried out between 1934 and 1952. *Journal of Physiology* **263**, 1–21.

Hodgkin, A. L. & Huxley, A. F. (1952). A quantitative description of membrane current and its application to conduction and excitation in nerve. *Journal of Physiology* **117**, 500–544.

Hodgkin, A. L. & Katz, B. (1949). The effect of sodium ions on the electrical activity of the giant axon of the squid. *Journal of Physiology* **108**, 37–77.

Hong, K. H., Armstrong, C. M. & Miller, C. (2001). Revisiting the role of Ca^{2+} in Shaker K^+ channel gating. *Biophysical Journal* **80**, 2216–2220.

Honig, B. H., Hubbell, W. L. & Flewelling, R. F. (1986). Electrostatic interactions in membranes and proteins. *Annual Review of Biophysics and Biophysical Chemistry* **15**, 163–193.

Horn, R. (1999). The dual role of calcium: Pore blocker and modulator of gating. *Proceedings of the National Academy of Sciences USA* **96**, 3331–3332.

Housecroft, C. E. (1999). *The Heavier d-Block Metals*. Oxford: Oxford University Press.

Huang, R. C., Peng, Y. W. & Yau, K. W. (1993). Zinc modulation of a transient potassium current and histochemical localization of the metal in neurons of the suprachiasmatic nucleus. *Proceedings of the National Academy of Sciences USA* **90**, 11806–11810.

Hurst, R. S., Latorre, R., Toro, L. & Stefani, E. (1995). External barium block of Shaker potassium channels:

evidence for two binding sites. *Journal of General Physiology* **106**, 1069–1087.

Hurst, R. S., Roux, M. J., Toro, L. & Stefani, E. (1997). External barium influences the gating charge movement of Shaker potassium channels. *Biophysical Journal* **72**, 77–84.

Huxley, A. F. (1959). Ion movements during nerve activity. *Annals of the New York Academy of Sciences* **81**, 221–246.

Jiang, Y., Lee, A., Chen, J., Cadene, M., Chait, B. T. & MacKinnon, R. (2002). Crystal structure and mechanism of a calcium-gated potassium channel. *Nature* **417**, 515–522.

Jiang, Y., Lee, A., Chen, J., Ruta, V., Cadene, M., Chait, B. T. & MacKinnon, R. (2003a). X-ray structure of a voltage-dependent K^+ channel. *Nature* **423**, 33–41.

Jiang, Y. & MacKinnon, R. (2000). The barium in a potassium channel by X-ray crystallography. *Journal of General Physiology* **115**, 269–272.

Jiang, Y., Ruta, V., Chen, J., Lee, A. & MacKinnon, R. (2003b). The principles of gating charge movement in a voltage-dependent K^+ channel. *Nature* **423**, 42–48.

Johnson, J. P., Balser, J. R. & Bennett, P. B. (2001). A novel extracellular calcium sensing mechanism in voltage-gated potassium ion channels. *Journal of Neuroscience* **21**, 4143–4153.

Johnson, J. P., Mullins, F. M. & Bennett, P. B. (1999). Human ether-a-go-go-related gene K^+ channel gating probed with extracellular Ca^{2+}. Evidence for two distinct voltage sensors. *Journal of General Physiology* **113**, 565–580.

Karpen, J. W., Brown, R. L., Stryer, L. & Baylor, D. A. (1993). Interactions between divalent cations and the gating machinery of cyclic GMP-activated channels in salamander retinal rods. *Journal of General Physiology* **101**, 1–25.

Katz, B. (1936). Multiple response to constant current in frog's medullated nerves. *Journal of Physiology* (*London*) **88**, 239–255.

Katz, B. (1969). *The Release of Neural Transmitter Substances*. Liverpool: Liverpool University Press.

Kehl, S. J., Eduljee, C., Kwan, D. C. H., Zhang, S. & Fedida, D. (2002). Molecular determinants of the inhibition of human Kv1.5 potassium currents by external protons and Zn^{2+}. *Journal of Physiology* **541**, 9–24.

Keynes, R. D. & Elinder, F. (1999). The screw-helical voltage gating of ion channels. *Proceedings of the Royal Society of London Series B, Biological Sciences* **266**, 843–852.

Kinter, N. B. & Pritchard, U. B. (1977). Altered permeability of cell membranes. In *Handbook of Physiology. Reactions to Environmental Agents*. Washington, DC: American Physiological Society.

Kiss, T. & Osipenko, O. (1994). Metal ion-induced permeability changes in cell membranes: a minireview. *Cellular and Molecular Neurobiology* **14**, 781–789.

Koh, J. Y. (2001). Zinc and disease of the brain. *Molecular Neurobiology* **24**, 99–106.

Kostyuk, P. G. (1992). *Calcium Ions in Nerve Cell Function*. Oxford: Oxford University Press.

Kretsinger, R. H. (1972). Gene triplication deduced from the tertiary structure of a muscle calcium binding protein. *Nature New Biology* **240**, 85–88.

Kuo, C. C. & Chen, F. P. (1999). Zn^{2+} modulation of neuronal transient K^+ current: fast and selective binding to the deactivated channels. *Biophysical Journal* **77**, 2552–2562.

Lakshminarayanaiah, N. (1976). Surface charges on membranes. *Journal of Membrane Biology* **22**, 243–253.

Lakshminarayanaiah, N. (1977). Evaluation of membrane surface charge density: a discussion of some models. *Bulletin of Mathematical Biology* **39**, 643–662.

Lane, T. W. & Morel, F. M. M. (2000). A biological function for cadmium in marine diatoms. *Proceedings of the National Academy of Sciences USA* **97**, 4627–4631.

Larsen, E. M. (1965). *Transitional Elements*. New York: W. A. Benjamin, Inc.

Lecar, H., Larsson, H. P. & Grabe, M. (2003). Electrostatic model of S4 motion in voltage-gated ion channels. *Biophysical Journal* **85**, 2854–2864.

Lehrmann, R. & Seelig, J. (1994). Adsorption of Ca^{2+} and La^{3+} to bilayer membranes: measurement of the adsorption enthalpy and binding constant with titration calorimetry. *Biochimica et Biophysica Acta* **1189**, 89–95.

Lettvin, J. Y., Pickard, W. F., McCulloch, W. S. & Pitts, W. (1964). A theory of passive ion flux through axon membranes. *Nature* **202**, 1338–1339.

Li, C., Peoples, R. W., Li, Z. & Weight, F. F. (1993). Zn^{2+} potentiates excitatory action of ATP on mammalian neurons. *Proceedings of the National Academy of Sciences USA* **90**, 8264–8267.

Loeb, J. (1901). On an apparently new form of muscular irritability (contact irritability?) produced by solutions of salts (preferably sodium salts) whose anions are liable to form insoluble calcium compounds. *American Journal of Physiology* **5**, 362–373.

Lönnendonker, U., Neumcke, B. & Stämpfli, R. (1990). Interaction of monovalent cations with tetrodotoxin and saxitoxin binding at sodium channels of frog myelinated nerve. *Pflügers Archiv* **416**, 750–757.

Lu, Z. & MacKinnon, R. (1994). Electrostatic tuning of Mg^{2+} affinity in an inward-rectifier K^+ channel. *Nature* **371**, 243–246.

Ma, J. Y. & Narahashi, T. (1993). Enhancement of γ-aminobutyric acid-activated chloride channel currents by lanthanides in rat dorsal root ganglion neurons. *Journal of Neuroscience* **13**, 4872–4879.

MacKinnon, R. & Miller, C. (1989). Mutant potassium channels with altered binding of charybdotoxin, a pore-blocking peptide inhibitor. *Science* **245**, 1382–1385.

Madeja, M., Binding, N., Musshoff, U., Pongs, O., Witting, U. & Speckmann, E. J. (1995). Effects of lead

on cloned voltage-operated neuronal potassium channels. *Naunyn-Schmiedeberg's Archives of Pharmacology* **351**, 320–327.

Madeja, M., Musshoff, U., Binding, N., Witting, U. & Speckmann, E. J. (1997). Effects of Pb^{2+} on delayed-rectifier potassium channels in acutely isolated hippocampal neurons. *Journal of Neurophysiology* **78**, 2649–2654.

Männikkö, R., Elinder, F. & Larsson, H. P. (2002). Voltage-sensing mechanism is conserved among ion channels gated by opposite voltages. *Nature* **419**, 837–841.

Martin, R. B. (1988). pH as a variable in free zinc ion concentration from zinc-containing lozenges. *Antimicrobial Agents and Chemotherapy* **32**, 608–609.

Martin, R. B. & Richardson, F. S. (1979). Lanthanides as probes for calcium in biological systems. *Quarterly Reviews of Biophysics* **12**, 181–209.

Mathias, R. T., Baldo, G. J., Manivannan, K. & McLaughlin, S. (1992). Discrete charges on biological membranes. In *Electrified Interfaces in Physics, Chemistry and Biology* (ed. R. Guidelli), pp. 473–490. Dordrecht: Kluwer Academic Publishers.

Mathur, R., Zheng, J., Yan, Y. & Sigworth, F. J. (1997). Role of the S3-S4 linker in Shaker potassium channel activation. *Journal of General Physiology* **109**, 191–199.

Matsuda, H., Saigusa, A. & Irisawa, H. (1987). Ohmic conductance through the inwardly rectifying K channel and blocking by internal Mg^{2+}. *Nature* **325**, 156–159.

Mayer, M. L., Westbrook, G. L. & Guthrie, P. B. (1984). Voltage-dependent block by Mg^{2+} of NMDA responses in spinal cord neurones. *Nature* **309**, 261–263.

McCleverty, J. (1999). *Chemistry of the First-row Transition Metals*. Oxford: Oxford University Press.

McLarnon, J. G. & Sawyer, D. (1993). Effects of divalent cations on the activation of a calcium-dependent potassium channel in hippocampal neurons. *Pflügers Archiv* **424**, 1–8.

McLaughlin, S. (1977). Electrostatic potentials at membrane solution interfaces. *Current Topics in Membrane Transport* **9**, 71–144.

McLaughlin, S. (1989). The electrostatic properties of membranes. *Annual Review of Biophysics and Biophysical Chemistry* **18**, 113–136.

McLaughlin, S. G. A., Szabo, G. & Eisenman, G. (1971). Divalent ions and surface potential of charged phospholipid membranes. *Journal of General Physiology* **58**, 667–687.

Means, A. R., Tash, J. S. & Chafouleas, J. G. (1982). Physiological implications of the presene, distribution, and regulation of calmodulin in eukaryotic cells. *Physiological Reviews* **62**, 1–39.

Miller, G. (2003). The puzzling portrait of the pore. *Science* **300**, 2020–2022.

Miller, J., McLachlan, A. D. & Klug, A. (1985). Repetitive zinc-binding domains in the protein transcription factor IIIA from *Xenopus* oocytes. *EMBO Journal* **4**, 1609–1614.

Moczydlowski, E., Alvarez, O., Vergara, C. & Latorre, R. (1985). Effect of phospholipid surface charge on the conductance and gating of a Ca^{2+}-activated K^+ channel in planar lipid bilayers. *Journal of Membrane Biology* **83**, 273–282.

Moeller, T., Martin, D. F., Thompson, L. C., Ferrús, R., Feistel, G. R. & Randall, W. J. (1965). The coordination chemistry of yttrium and the rare earth metal ions. *Chemical Reviews* **65**, 1–50.

Moore, L. E. (1971). Effect of temperature and calcium ions on rate constants of myelinated nerve. *American Journal of Physiology* **221**, 131–137.

Mozhayeva, G. N. & Naumov, A. P. (1970). Effect of surface charge on the steady-state potassium conductance of nodal membrane. *Nature* **228**, 164–165.

Mozhayeva, G. N. & Naumov, A. P. (1973). Potassium conductance of the ranvier node membrane in the presence of La^{3+}, Zn^{2+} and Cu^{2+} ions in the media. *Cytology* **15**, 1431–1435.

Mozhayeva, G. N., Naumov, A. P. & Nosyreva, E. D. (1985). Potential-dependent calcium blockage of normal and aconitine-modified sodium channels in frog node of Ranvier. *General Physiology and Biophysics* **4**, 425–427.

Nelson, A. P. & McQuarrie, D. A. (1975). The effect of discrete charges on the electrical properties of a membrane. *Journal of Theoretical Biology* **55**, 13–27.

Neumcke, B. & Stämpfli, R. (1984). Heterogeneity of external surface charges near sodium channels in the nodal membrane of frog nerve. *Pflügers Archiv* **401**, 125–131.

Nowak, L., Bregestovski, P., Ascher, P., Herbert, A. & Prochiantz, A. (1984). Magnesium gates glutamate-activated channels in mouse central neurones. *Nature* **307**, 462–465.

Ohmori, H. & Yoshii, M. (1977). Surface potential reflected in both gating and permeation mechanisms of sodium and calcium channels of the tunicate egg cell membrane. *Journal of Physiology* **267**, 429–463.

Overton, C. E. (1902). Beiträge zur allgemeine Muskel und Nervenphysiologie. II. Mitt. Über die Unentbehrlichkeit von Natrium (oder Lithium) Ionen für den Kontraktionsakt des Muskels. *Pflügers Archiv* **92**, 345–386.

Papazian, D. M. & Bezanilla, F. (1997). How does an ion channel sense voltage? *News in Physiological Sciences* **12**, 203–210.

Papazian, D. M., Timpe, L. C., Jan, Y. N. & Jan, L. Y. (1991). Alteration of voltage-dependence of Shaker potassium channel by mutations in the S4 sequence. *Nature* **349**, 305–310.

Paquette, T., Clay, J. R., Ogbaghebriel, A. & Shrier, A. (1998). Effects of divalent cations on the

E-4031-sensitive repolarization current, I(Kr), in rabbit ventricular myocytes. *Biophysical Journal* **74**, 1278–1285.

Passow, H., Rothstein, A. & Clarkson, T. W. (1961). The general pharmacology of the heavy metals. *Pharmacological Reviews* **13**, 185–224.

Pearson, R. G. (1963). Hard and soft acids and bases. *Journal of the American Chemical Society* **85**, 3533–3539.

Peitzsch, R. M., Eisenberg, M., Sharp, K. A. & McLaughlin, S. (1995). Calculation of the electrostatic potential adjacent to model phospholipid bilayers. *Biophysical Journal* **68**, 729–738.

Perozo, E. & Bezanilla, F. (1990). Phosphorylation affects voltage gating of the delayed rectifier K^+ channel by electrostatic interactions. *Neuron* **5**, 685–690.

Perozo, E. & Bezanilla, F. (1991). Phosphorylation of K^+ channels in the squid giant axon. A mechanistic analysis. *Journal of Bioenergetics and Biomembranes* **23**, 599–613.

Peters, S., Koh, J. & Choi, D. W. (1987). Zinc selectively blocks the action of N-methyl-D-aspartate on cortical neurons. *Science* **236**, 589–593.

Pusch, M. (1990). Divalent cations as probes for structure-function relationships of cloned voltage-dependent sodium channels. *European Biophysics Journal* **18**, 327–333.

Rack, M. & Drews, G. (1989). Effects of a synthetic cationic polymer on sodium and potassium currents of frog nerve fibres. *Pflügers Archiv* **413**, 610–615.

Rack, M. & Woll, K.-H. (1984). Effects of chemical modification of carboxyl groups on the voltage-clamped nerve fiber of the frog. *Journal of Membrane Biology* **82**, 41–48.

Recio-Pinto, E., Thornhill, W. B., Duch, S., Levinson, S. R. & Urban, B. W. (1990). Neuraminidase treatment modifies the function of electroplax sodium channels in planar lipid bilayers. *Neuron* **5**, 675–684.

Ringer, S. (1883). A further contribution regarding the influence of the different constituents of the blood on the contraction of the heart. *Journal of Physiology* **4**, 29–42.

Root, M. J. & MacKinnon, R. (1993). Identification of an external divalent cation-binding site in the pore of a cGMP-activated channel. *Neuron* **11**, 459–66.

Root, M. J. & MacKinnon, R. (1994). Two identical noninteracting sites in an ion channel revealed by proton transfer. *Science* **265**, 1852–1856.

Sanchez-Chapula, J. A. & Sanguinetti, M. C. (2000). Altered gating of HERG potassium channels by cobalt and lanthanum. *Pflügers Archiv* **440**, 264–274.

Santacruz-Toloza, L., Huang, Y., John, S. A. & Papazian, D. M. (1994). Glycosylation of Shaker potassium channel protein in insect cell culture and in *Xenopus* oocytes. *Biochemistry* **33**, 5607–5613.

Satin, J., Kyle, J. W., Chen, M., Bell, P., Cribbs, L. L., Fozzard, H. A. & Rogart, R. B. (1992). A mutant of TTX-resistant cardiac sodium channels with TTX-sensitive properties. *Science* **256**, 1202–1205.

Sauve, R. & Ohki, S. (1979). Interactions of divalent cations with negatively charged membrane surfaces. I. Discrete charge potential. *Journal of Theoretical Biology* **81**, 157–179.

Schauf, C. L. (1975). The interactions of calcium with Myxicola giant axons and a description in terms of a simple surface charge model. *Journal of Physiology* **248**, 613–624.

Schauf, C. L. (1983). Evidence for negative gating charges in Myxicola axons. *Biophysical Journal* **42**, 225–231.

Schild, L. & Moczydlowski, E. (1991). Competitive binding interaction between Zn^{2+} and saxitoxin in cardiac Na^+ channels. Evidence for a sulfhydryl group in the Zn^{2+}/saxitoxin binding site. *Biophysical Journal* **59**, 523–537.

Schoppa, N. E., McCormack, K., Tanouye, M. A. & Sigworth, F. J. (1992). The size of gating charge in wild-type and mutant Shaker potassium channels. *Science* **255**, 1712–1715.

Sheets, M. F. & Hanck, D. F. (1992). Mechanisms of extracellular divalent and trivalent cation block of the sodium current in canine cardiac purkinje cells. *Journal of Physiology* **454**, 299–320.

Sherman, S. J., Chrivia, J. & Catterall, W. A. (1985). Cyclic adenosine 3′,5′-monophosphate and cytosolic calcium exert opposing effects on biosynthesis of tetrodotoxin-sensitive sodium channels in rat muscle cells. *Journal of Neuroscience* **5**, 1570–1576.

Shrager, P. (1974). Ionic conductance changes in voltage clamped crayfish axons at low pH. *Journal of General Physiology* **64**, 666–690.

Sigg, D. & Bezanilla, F. (2003). A physical model of potassium channel activation: from energy landscape to gating kinetics. *Journal of General Physiology* **84**, 3703–3716.

Sillén, L. G. & Martell, A. E. (1971). *Stability Constants, Supplement No. 1*. Oxford: Alden Press.

Silverman, W. R., Roux, B. & Papazian, D. M. (2003). Structural basis of two-stage voltage-dependent activation in K^+ channels. *Proceedings of the National Academy of Sciences USA* **100**, 2935–2940.

Silverman, W. R., Tang, C. Y., Mock, A. F., Huh, K. B. & Papazian, D. M. (2000). Mg^{2+} modulates voltage-dependent activation in ether-a-go-go potassium channels by binding between transmembrane segments S2 and S3. *Journal of General Physiology* **116**, 663–678.

Sinha, S. P. (1976). *Structure and Bonding* **25**, 69–145.

Skriver, H. (1983). *Systematics and Properties of the Lanthanides* (ed. S. P. Sinha), pp. 213–254. Dordrecht: Reidel.

Smart, T. G., Xie, X. & Krishek, B. J. (1994). Modulation of inhibitory and excitatory amino acid receptor ion channels by zinc. *Progress in Neurobiology* **42**, 393–441.

Spires, S. & Begenisich, T. (1994). Modulation of potassium channel gating by external divalent cations. *Journal of General Physiology* **104**, 675–692.

Spyropoulus, C. S. & Brady, R. O. (1959). Prolongation of response of node of Ranvier by metal ions. *Science* **129**, 1366–1367.

Stanfield, P. R. (1975). The effect of zinc ions on the gating of the delayed potassium conductance of frog sartorius muscle. *Journal of Physiology* **251**, 711–735.

Starzak, M. E. & Starzak, R. J. (1978). The compensation of potential changes produced by trivalent erbium ion in squid giant axon with applied potentials. *Biophysical Journal* **24**, 555–560.

Stern, O. (1924). Zur Theorie der elektrolytischen Doppelschicht. *Zeitschrift für Elektrochemie* **30**, 508–516.

Swartz, K. J. & MacKinnon, R. (1997). Mapping the receptor site for hanatoxin, a gating modifier of voltage-dependent K^+ channels. *Neuron* **18**, 675–682.

Swenson, Jr. R. P. & Armstrong, C. M. (1981). K^+ channels close more slowly in the presence of external K^+ and Rb^+. *Nature* **291**, 427–429.

Takata, M., Pickard, W. F., Lettvin, J. Y. & Moore, J. W. (1966). Ionic conductance changes in lobster axon membranes when lanthanum is substituted for calcium. *Journal of General Physiology* **50**, 461–472.

Talukder, G. & Harrison, N. L. (1995). On the mechanism of modulation of transient outward current in cultured rat hippocampal neurons by di- and trivalent cations. *Journal of Neurophysiology* **73**, 73–79.

Talukder, G., Tamkun, M. M. & Harrison, N. L. (1995). A role for the 'pre-pore' region of voltage-dependent K^+ channels in gating and zinc modulation. *Society for Neuroscience Abstracts* **21**, 1033.

Tang, C.-Y., Bezanilla, F. & Papazian, D. M. (2000). Extracellular Mg^{2+} modulates slow gating transitions and the opening of *Drosophila* ether-a-go-go potassium channels. *Journal of General Physiology* **115**, 319–337.

Tarr, M., Trank, J. W. & Goertz, K. K. (1989). Intracellular magnesium affects I(K) in single frog atrial cells. *American Journal of Physiology* **257**, H1663–1669.

Tarras-Wahlberg, N. H., Flachier, A., Lane, S. N. & Sangfors, O. (2001). Environmental impacts and metal exposure of aquatic ecosystems in rivers contaminated by small scale gold mining: the Puyango River basin, southern Ecuador. *The Science of the Total Environment* **278**, 239–261.

Teorell, T. (1953). Transport processes and electrical phenomena in ionic membranes. *Progress in Biophysics* **3**, 305–369.

Terlau, H., Ludwig, J., Steffan, R., Pongs, O., Stühmer, W. & Heinemann, S. H. (1996). Extracellular Mg^{2+} regulates activation of rat eag potassium channel. *Pflügers Archiv* **432**, 301–312.

Vallee, B. L. & Falchuk, K. H. (1993). The biochemical basis of zinc physiology. *Physiological Reviews* **73**, 79–118.

Van Helden, D., Hamill, O. P. & Gage, P. W. (1977). Permeant ions alter endplate channel characteristics. *Nature* **269**, 711–712.

Venugopal, B. & Luckey, T. D. (1978). Toxicity of group III metals. In *Metal Toxicity in Mammals*, pp. 127–157. New York: Plenum.

Verwey, E. J. W. & Overbeek, J. T. G. (1948). *Theory of the Stability of Lyophobic Colloids*. Amsterdam: Elsevier.

Visentin, S., Zaza, A., Ferroni, A., Tromba, C. & DiFrancesco, D. (1990). Sodium current block caused by group IIb cations in calf Purkinje fibres and in guinea-pig ventricular myocytes. *Pflügers Archiv* **417**, 213–222.

Vogel, W. (1974). Calcium and lanthanum effects at the nodal membrane. *Pflügers Archiv* **350**, 25–39.

Watanabe, I., Wang, H.-G., Sutachan, J. J., Zhu, J., Recio-Pinto, E. & Thornhill, W. B. (2003). Glycosylation affects rat Kv1.1 potassium channel gating by a combined surface potential and cooperative subunit interaction mechanism. *Journal of Physiology* **550**, 51–66.

Weerapura, M., Nattel, S., Courtemanche, M., Doern, D., Ethier, N. & Hébert, T. E. (2000). State-dependent barium block of wild-type and inactivation-deficient HERG channels in *Xenopus* oocytes. *Journal of Physiology* **526**, 265–278.

Wei, A., Jegla, T. & Salkoff, L. (1996). Eight potassium channel families revealed by the *C. elegans* genome project. *Neuropharmacology* **35**, 805–829.

Westbrook, G. L. & Mayer, M. L. (1987). Micromolar concentrations of zinc antagonize NMDA and GABA responses in hippocampal neurons. *Nature* **328**, 640–643.

Wickenden, A. D., Tsushima, R. G., Losito, V. A., Kaprielian, R. & Backx, P. H. (1999). Effect of Cd^{2+} on Kv4.2 and Kv1.4 expressed in *Xenopus* oocytes and on the transient outward currents in rat and rabbit ventricular myocytes. *Cellular Physiology and Biochemistry* **9**, 11–28.

Wilson, G. G., Pascual, J. M., Brooijmans, N., Murray, D. & Karlin, A. (2000). The intrinsic electrostatic potential and the intermediate ring of charge in the acetylcholine receptor channel. *Journal of General Physiology* **115**, 93–106.

Winegar, B. D., Kelly, R. & Lansman, J. B. (1991). Block of current through single calcium channels by Fe, Co, and Ni. Location of the transition metal binding site in the pore. *Journal of General Physiology* **97**, 351–367.

Winiski, A. P., McLaughlin, A. C., McDaniel, R. V., Eisenberg, M. & McLaughlin, S. (1986). An experimental test of the discreteness-of-charge effect in positive and negative lipid bilayers. *Biochemistry* **25**, 8206–8214.

Woodhull, A. M. (1973). Ionic blockage of sodium channels in nerve. *Journal of General Physiology* **61**, 687–708.

Xie, X. & Smart, T. G. (1991). A physiological role for endogenous zinc in rat hippocampal synaptic neurotransmission. *Nature* **349**, 521–524.

Yamamoto, D., Yeh, J. Z. & Narahashi, T. (1984). Voltage-dependent calcium block of normal and tetramethrin-modified single sodium channels. *Biophysical Journal* **45**, 337–344.

Yang, J., Ellinor, P. T., Sather, W. A., Zhang, J. F. & Tsien, R. W. (1993). Molecular determinants of Ca^{2+} selectivity and ion permeation in L-type Ca^{2+} channels. *Nature* **366**, 158–161.

Yang, X. C. & Sachs, F. (1989). Block of stretch-activated ion channels in *Xenopus* oocytes by gadolinium and calcium ions. *Science* **243**, 1068–1071.

Yao, J. A., Saxena, N. C., Ziai, M. R., Ling, S. & Tseng, G. N. (1995). Effects of n-dodecylguanidine on A-type potassium channels: role of external surface charges in channel gating. *Molecular Pharmacology* **48**, 160–171.

Yellen, G. (1998). The moving parts of voltage-gated ion channels. *Quarterly Reviews of Biophysics* **31**, 239–295.

Zheng, F., Erreger, K., Low, C.-M., Banke, T., Lee, C. J., Conn, P. J. & Traynelis, S. F. (2001). Allosteric interaction between the amino terminal domain and the ligand binding domain of NR2A. *Nature Neuroscience* **4**, 894–901.

Zimmerman, A. N. E. & Hulsmann, W. C. (1966). Paradoxical influence of calcium ions on the permeability of the cell membranes of isolated rat hearts. *Nature* **211**, 646–647.